# Chapter 14
# Microbial Metabolism of Nickel


**Robert P. Hausinger**

**Abstract** This chapter summarizes the multiple processes that microorganisms use to metabolize nickel ions and describes nickel-dependent enzymatic transformations. A wide variety of microbial species sense and respond to nickel ion concentrations by synthesizing nickel-specific transcription factors, and a few possess nickel-responsive riboswitches. During nickel deficiency, some microbes are capable of taking up this micronutrient using influx systems that include ATP binding cassette transporters and secondary transporters such as permeases. Certain microorganisms eliminate excess concentrations of internal nickel ions by using nickel-specific cation diffusion facilitators, major facilitator protein superfamily members, P-type ATPases, and other efflux systems. The basis of nickel toxicity and several mechanisms of nickel resistance also are described in this chapter. Many microorganisms utilize nickel, variously incorporating it into glyoxalase I, acireductone dioxygenase, quercetin 2,4-dioxygenase, superoxide dismutase, urease, [NiFe] hydrogenase, carbon monoxide dehydrogenase, the acetyl-coenzyme A synthase/decarbonylase complex, 2-hydroxyacid racemases and epimerases, and methyl-*S*-coenzyme M reductase. Auxiliary proteins often function during the biosynthesis of nickel enzymes by delivering the nickel ion, synthesizing a nickel-containing organometallic cofactor, coupling the energy of nucleotide hydrolysis to the metal incorporation, or acting in other ways. Nickel storage proteins are present in some microorganisms. In sum, the microbial metabolism of nickel involves a rich landscape of biological processes.

R. P. Hausinger (✉)
Microbiology and Molecular Genetics, Biomedical Physical Sciences, Michigan State University, East Lansing, MI, USA
e-mail: hausinge@msu.edu



C. J. Hurst (ed.), *Microbial Metabolism of Metals and Metalloids*, Advances in Environmental Microbiology 10, https://doi.org/10.1007/978-3-030-97185-4_14

## 14.1 Introduction: Nickel in the Environment

Nickel is the fifth most abundant element on earth, although much of it is concentrated in the earth's core where it is second most in abundance at 8.5% (Zamble et al. 2017). The earth's crust contains 0.009% nickel, placing it among the top 25 most prevalent elements. The nickel content of soils ranges from 3 to over 1000 ppm (μg/g) depending on the origin of the parent rock, with an average of ~16 ppm (Iyaka 2011). In an extreme natural case, nickel is present at >1 mg/g in serpentine soils. The nickel content of lakes and rivers averages about 1 ppm, but varies widely depending on the type of soil associated with the watershed of interest (Nriagu 1980). In the ocean, the nickel concentration is quite uniform at the surface (2–4 nM), increasing at greater depth to 10 nM in the Pacific and 6 nM in Atlantic (Glass and Dupont 2017). Anthropogenic sources of nickel include mining of nickel ores and certain industrial processes that can lead to local areas of very high nickel concentrations. Regardless of the source of nickel or the properties of diverse environments, the biologically relevant form of the metal typically occurs as the dication ($Ni^{2+}$).

Nickel may have beneficial or toxic effects depending on the microbial species and the metal ion concentration. Importantly, the availability of nickel depends on factors other than just its concentration: this metal ion forms complexes with inorganic matrices such as sulfides and iron oxyhydroxides or with organic compounds such as humic and fulvic acids. These anionic substances reduce the effective nickel concentration by sequestration. A growth requirement for nickel was first reported in 1965 for two strains of hydrogen-oxidizing bacteria (Bartha and Ordal 1965) and this metal ion has since been shown to be essential for multiple microorganisms. Negative effects of nickel on microorganisms also have long been established (Babich and Stotzky 1983).

This chapter surveys the metabolism of nickel by microorganisms. It starts by describing homeostasis mechanisms by which microbes sense the intracellular (or periplasmic) concentration of this metal and use various mechanisms to facilitate either its import or efflux, depending on whether the available levels of this nutrient are inadequate or if in excess as a toxicant. The chapter then explains the basis for nickel toxicity and describes how microorganisms circumvent this damage. Next, the nickel-containing enzymes are highlighted including their biosynthetic pathways that sometimes use nickel storage and delivery proteins, nucleotide hydrolyzing enzymes, and other components.

## 14.2 Nickel Homeostasis

Many microorganisms contain elaborate systems to sense the cytoplasmic (or periplasmic) concentration of nickel, turn on nickel-specific uptake transporters when the metal ion is limiting, and increase levels of nickel-specific efflux systems

**Table 14.1** Summary of selected nickel-dependent transcriptional regulators (sensors) and their associated nickel transport systems.

| Microorganism | Sensor | Transporter (type)[a] | References |
|---|---|---|---|
| *Agrobacterium tumefaciens* | DmeR | DmeF (CDF exporter) | Dokpikul et al. (2016) |
| *Brucella abortus* | NikR | NikABCDE (ABC-type importer) | Budnick et al. (2018) |
| *Escherichia coli* | NikR | NikABCDE (ABC-type importer) | de Pina et al. (1999) and Navarro et al. (1993) |
| | RcnR | RcnA (efflux pump) | Koch et al. (2007) |
| *Cupriavidus metallidurans* CH34 | CnrYXH | CnrCBA (RND efflux pump) | Grass et al. (2000) and Tibazarwa et al. (2000) |
| *Geobacter uraniireducens* | NikR | Nik(MN)1 and Nik(MN)2-NikQO (ECF-type importer components) | Benanti and Chivers (2010) |
| *Haemophilus influenzae* | NimR | NikKLMQO (ECF-type ABC importer) | Kidd et al. (2011) |
| *Helicobacter hepaticus* | NikR | NikABDE (ABC-type importer) and HH0418 (OM transporter) | Benoit et al. (2013) |
| *Helicobacter pylori* | NikR | NixA (uptake permease), HP1515 (OM importer), TonB-ExbB-ExbD (OM energizer), NiuBDE (ABC-type transporter), and CeuE (another periplasmic Ni-binding protein) | Contreras et al. (2003), Davis et al. (2006), Ernst et al. (2005), Ernst et al. (2006), Fischer et al. (2016), Jones et al. (2015), and Wolfram et al. (2006) |
| *Leptospirillum ferriphilum* | NcrB | NcrAC (efflux pump) | Tian et al. (2007) and Zhu et al. (2011) |
| *Mycobacterium tuberculosis* | NmtR | NmtA (P-type ATPase) | Cavet et al. (2002) |
| | KmtR | Rv2025c (CDF exporter) | Campbell et al. (2007) |
| *Rhizobium leguminosarum* | DmeR | DmeF (CDF exporter) | Rubio-Sanz et al. (2013) |
| *Streptomyces coelicolor* | Nur | NikABCDE and NikMNOQ (ABC-type uptake systems) | Ahn et al. (2006) and An et al. (2009) |
| | NmtR | NmtA (P-type ATPase for efflux) | Kim et al. (2015) |
| *Synechocystis* sp. PCC 6803 | InrS | NrsD (efflux permease) | Foster et al. (2012) |
| | NrsRS | NrsBACD (RND exporter) | Garcia-Dominguez et al. (2000) and Lopez-Maury et al. (2002) |

[a] The abbreviations are defined in the text sections related to each topic

when the metal is in excess (Table 14.1). Numerous excellent reviews covering these homeostatic process are available for those interested in more extensive treatment of this topic (Chivers 2017; Higgins 2019; Higgins et al. 2012a; Iwig and Chivers 2010;

Li and Zamble 2009; Musiani et al. 2015; Rodrigue et al. 2017; Zeer-Wanklyn and Zamble 2017). The highlights of the better-studied systems are described here.

A few general comments about cellular nickel concentrations are worth mentioning. Unless located in a nickel-rich environment, microorganisms tend to concentrate the metal ion to levels exceeding that found in their external milieu. For example, *Escherichia coli* concentrates this metal ion from minimal or LB media (where nickel is present at ~$10^{-8}$ M and ~$10^{-7}$ M, respectively) to greater than $10^{-6}$ M in the cell (Outten and O'Halloran 2001). One can calculate that a single atom of nickel in an *E. coli* cell (~2 μm in length and ~0.5 μm in diameter or ~$4 \times 10^{-16}$ L) yields a concentration of approximately 4 nM ($4 \times 10^{-9}$ M). This value is of interest when considering the measured dissociation constants ($K_d$) for nickel-binding sensors such as NikR of *E. coli* (described in greater detail below) with a value of less than 1 pM ($10^{-12}$ M)—nearly three orders of magnitude less than one per cell (Chivers and Sauer 2002; Wang et al. 2004). This apparent discrepancy arises because the measured concentration of nickel within cells does not equate to the level of free or available nickel ion—much of it is found dynamically associated with cytoplasmic components (thiols, polynucleotides, amino acids, etc.). The nickel sensors assure that an ideal regulatory balance of nickel import and export exists to provide optimal metal levels for cellular growth. Selected examples of nickel sensing transcriptional regulators are described in Sect. 14.2.1. That section is followed by discussions of the systems controlled by these sensors: nickel uptake (Sect. 14.2.2) and nickel efflux (Sect. 14.2.3).

### *14.2.1 Nickel-Sensing Transcription Factors*

Metalloregulatory transcription factors undergo protein conformational changes upon binding their cognate metal ions, with consequent modification of their transcriptional regulatory properties. Figure 14.1 depicts four highly simplified mechanisms for transcription factor regulation by metal ions, but it is important to note that many other options exist. In the first case, a metal-repressor complex (co-repressor) binds to the operator region of a gene to prevent transcription, whereas the apoprotein form of the transcription factor is non-functional as a repressor. The opposite situation occurs when the apoprotein of the transcription factor directly represses transcription, with metal binding leading to de-repression that allows the gene to be transcribed. The third option parallels the first in that only the metal-bound transcription factor binds to DNA, but in this case the complex (co-activator) interacts with RNA polymerase to enhance gene expression. A final option occurs when the apoprotein of the transcription factor functions as the activator, with metal binding leading to loss of activation capability. As described below, all of these mechanisms, at least in modified forms, apply to nickel-sensing transcription factors.

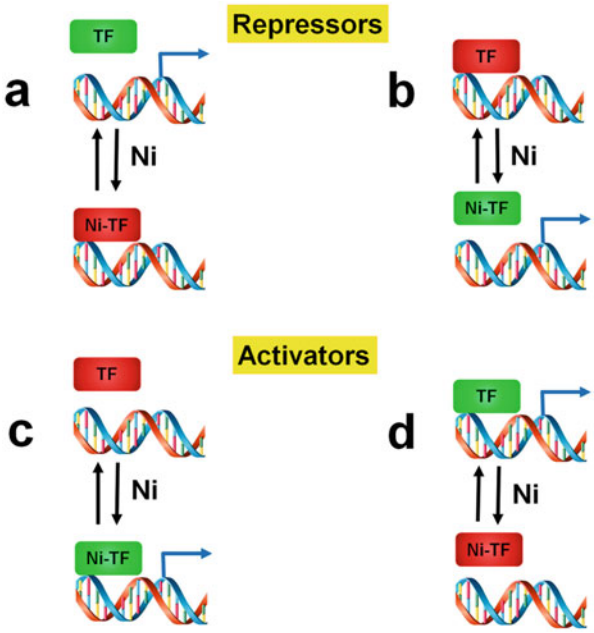


**Fig. 14.1** Four potential roles for nickel-dependent transcriptional regulatory factors. (**a**) Co-repression of a gene by the complex of nickel bound to the transcription factor (Ni-TF). (**b**) Loss of repressor function induced by the binding of nickel. (**c**) Co-activation of a gene by the nickel-transcription factor complex. (**d**) Loss of activator function caused by the binding of nickel

#### 14.2.1.1 NikR

*E. coli* NikR nicely illustrates the metalloregulatory mechanism shown in Fig. 14.1a. When nickel binds to this protein (subunit size of 15-kDa) it functions as a repressor of the *nikABCDE* operon encoding an ATP-binding cassette (ABC) nickel-uptake system located in the cytoplasmic membrane (de Pina et al. 1999). Mutants affecting *nikR* lead to constitutive expression of the *nik* operon. The nickel-bound repressor binds to an operator site consisting of dyad-symmetric 6-base pair recognition sequences (GTATGA) separated by 16 base pairs (Chivers and Sauer 2000). A high affinity nickel-binding site ($K_d$ measured in the pM range except for one report of a sub-μM value) must be occupied for NikR to bind DNA, but tighter interaction with DNA ($K_d$ ~ 20 pM) occurs when additional nickel is bound to a poorly characterized lower affinity site on NikR ($K_d$ ranging from 30 nM to 30 μM) (Bloom and Zamble 2004; Chivers and Sauer 2002; Diederix et al. 2008; Wang et al. 2010a). Potassium also must bind to NikR for effective interaction with DNA (Wang et al. 2010b).

A series of crystal structures provides important insights into how *E. coli* NikR functions as a transcription factor. The tetrameric apoprotein possesses two dimeric ribbon-helix-helix DNA-binding regions separated by a nickel-binding regulatory domain (Schreiter et al. 2003). The structurally-characterized C-terminal domain is a tetramer that binds four nickel atoms at high-affinity square-planar sites using His87, His89, and Cys95 from one subunit along with His76′ from another subunit

(Schreiter et al. 2003). The structure of the full-length NikR holoprotein reveals that nickel addition results in a protein conformational change affecting the relative orientations of the DNA-binding regions (Schreiter et al. 2006). A further change occurs when the nickel-NikR complex binds to operator DNA (Fig. 14.2a) (Schreiter et al. 2006). In particular, the DNA-binding regions rotate to allow both to bind to the DNA simultaneously, leading to a bend in the operator region. Co-repressor binding to this region prevents its interaction with RNA polymerase, thus leading to cessation of transcription. This structure also identifies how potassium is coordinated; i.e. via bidentate Glu30, bidentate Asp34, and backbone carbonyls of Ile116, Gln118, and Val121. Additional structural studies have probed the basis for the metal-binding specificity of *E. coli* NikR by identifying sites for binding other metals (Phillips et al. 2008) and analyzed low-affinity binding sites for nickel (Phillips et al. 2010). Despite its ability to bind other metals, the cellular response of NikR as a transcriptional regulator is specific to nickel.

NikR in *Helicobacter pylori* exhibits several intriguing differences from the protein described above. Like *E. coli* NikR, the nickel-bound *H. pylori* NikR functions as a co-repressor (Fig. 14.1a) of a cytoplasmic membrane-associated nickel import system; however, this NikR-dependent regulation primarily involves *nixA* encoding a single-component secondary or permease-type transporter (Contreras et al. 2003; Ernst et al. 2005; Wolfram et al. 2006). Another NikR target is *fecDE* (Jones et al. 2015), a cluster that was later expanded, renamed, and shown to encode the NiuBDE ABC-type nickel uptake system (Fischer et al. 2016). Various strains of *H. pylori* contain periplasmic components of the ABC-type uptake system (comparable to NikA) known as NiuB1, NiuB2, and CeuE, with the latter also regulated by NikR (Jones et al. 2015). Of further interest, *ceuE* and *fecDE* encode an ABC-type transporter in *Helicobacter mustelae* (Stoof et al. 2010a). NikR of *H. pylori* also regulates production of a system for nickel transport across the outer membrane (OM) involving the OM protein HP1512 and the ExbB-ExbD-TonB cross-periplasm energizer (Davis et al. 2006; Ernst et al. 2006). In addition, the nickel-bound form of *H. pylori* NikR functions as a co-activator (Fig. 14.1c) of the gene cluster encoding urease, a nickel-containing enzyme (van Vliet et al. 2002), and it modulates several other nickel-repressed or nickel-activated genes (Contreras et al. 2003; Ernst et al. 2006; Vannini et al. 2017). The operator region recognized by *H. pylori* NikR differs from that bound by the *E. coli* protein and has poorly conserved inverted repeats (Delany et al. 2005). Additional changes in regulatory properties relate to pH-dependent effects (Bury-Moné et al. 2004; Jones and Zamble 2018; van Vliet et al. 2004) and hierarchical effects that provide an order to gene regulation (Dosanjh et al. 2009; Muller et al. 2011). Nickel binding to the *H. pylori* tetrameric protein also differs from that for the *E. coli* protein; two nickel are bound with greater affinity ($K_d \sim 10$ nM), two with less affinity ($K_d \sim 100$ nM), and others with weak affinity ($K_d \sim \mu M$) (Zambelli et al. 2007a). Crystal structures are reported for the *H. pylori* NikR apoprotein and several holoprotein forms (Benini et al. 2011; Dian et al. 2006; West et al. 2010). The overall structures closely resemble that of the *E. coli* protein with some differences noted for nickel sites in the holoproteins, but all

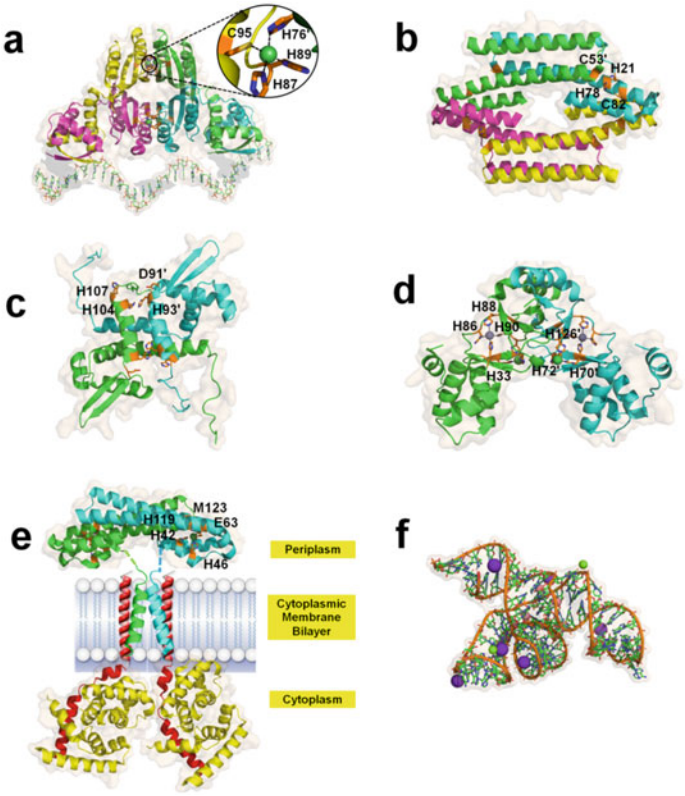


**Fig. 14.2** Selected structures of nickel-dependent transcription regulatory factors. (**a**) *Escherichia coli* NikR homotetramer in complex with nickel and bound to DNA (PDB ID 2hzv). The inset reveals one of the four nickel-binding sites with its ligands. (**b**) *Synechocystis* sp. PCC 6803 InrS homotetrameric transcription factor in its apoprotein form (PDB ID 5fmn) with the four residues likely to coordinate one of the four metal-binding sites indicated. (**c**) Homodimeric *Mycobacterium tuberculosis* NmtR transcription factor apoprotein (PDB ID 2lkp). Four likely coordinating residues, with two others not yet identified, are shown for one of the two sites. (**d**) Homodimeric *Streptomyces coelicolor* Nur transcription factor (PDB ID 3eyy). Two types of metal sites are shown (gray and green spheres). (**e**) *Cupriavidus metallidurans* CH34 CnrX-CnrY-CnrH tripartite nickel sensor with its periplasmic CnrX homodimer (cyan and green; residues 39–148 are from PDB ID 2y39 and the membrane-bound amino-terminal region is modeled) and a complex (PDB ID 4cxf) between the transmembrane CnrY (red; residues 2–30 are from the structure and a membrane-localized helix is modeled) and cytoplasmic CnrH (yellow). The metal sites in CnrX are indicated. Nickel binding to CnrX results in release of the sigma factor CnrH for interaction with RNA polymerase. (**f**) NiCo riboswitch from *Erysipelotrichaceae bacterium*. The riboswitch RNA structure (PDB ID 4rum) contains four cobalt (brown spheres, likely equivalent to the nickel-binding sites), two magnesium (green spheres), and seven potassium atoms (purple spheres). For all panels, the proteins are illustrated in cartoon mode with partially transparent surfaces, and individual subunits are in different colors. DNA and RNA are shown as sticks with RNA also depicted as wires. Residues of interest are shown in stick mode with orange carbon atoms. When bound, nickel is shown as green spheres

showing at least one of the familiar square-planar site (His99, His101, and Cys107 from one subunit with His88′ from a second subunit).

Several other NikR proteins are characterized to various extents, with four examples cited here. In *Helicobacter hepaticus*, NikR-dependent regulation resembles features of the *H. pylori* and *E. coli* systems. This NikR controls the levels of a putative inner-membrane ABC-type nickel transporter (encoded by *nikABDE*) and a possible OM nickel transporter (using *hh0418*), along with affecting levels of nickel-dependent urease and [NiFe] hydrogenase activities (Benoit et al. 2013). The situation in *Brucella abortus* is comparable to that in *E. coli*, with NikR serving as a transcriptional regulator of *nikABCDE* (Budnick et al. 2018). NikR from *Geobacter uraniireducens* binds cooperatively to promoter regions of *nik(MN)1* and *nik(MN)2*, components of ABC-type transporters (Benanti and Chivers 2010). Finally, NikR from *Pyrococcus horikoshii*, for which the transcriptional target has not been reported, is notable because crystal structures were determined for its apoprotein and four nickel-bound conformations (Chivers and Tahirov 2005). The overall tetrameric structures closely resemble those cited above, with the DNA-binding domains undergoing bending and rotational changes in conformation. The high affinity nickel-binding site is square planar and utilizes His89, His91, and Cys97 from one subunit along with His78′ from a second subunit, thus creating a situation essentially identical to the other NikR nickel sites.

#### 14.2.1.2 RcnR/InrS/DmeR/NcrB

The *E. coli* RcnR nickel and cobalt sensor operates by metal-dependent de-repression or release of the regulatory protein from the DNA (Fig. 14.1b), resulting in up-regulation of *rcnA* encoding a nickel/cobalt efflux system (Iwig et al. 2006; Koch et al. 2007). The designation *rcn* is named for *r*esistance to *c*obalt and *n*ickel, with increased sensitivity to these metals noted when *rcnA* is deleted (Rodrigue et al. 2005) and decreased metal sensitivity for the case of *rcnR* deletion (Koch et al. 2007). The 40-kDa homotetrameric RcnR sensor apoprotein binds to a TACT-$G_6$-N-AGTA motif between the divergently transcribed *rcnR* and *rcnA* genes (Iwig et al. 2006; Iwig and Chivers 2009). Dissociation from the DNA occurs upon binding one cobalt or nickel ion per 89-residue subunit, with the metals exhibiting nM affinity (Iwig et al. 2008). X-ray absorption spectroscopy (XAS) provides evidence for partial thiolate ligation of the metals, which are 6-coordinate (Iwig et al. 2008). This technique was combined with mutagenesis methods and modeling studies (using the structure of the copper-sensor CsoR as a template) to propose the nickel is bound by the amino-terminal amine, Glu63, and His64 of one subunit along with Cys35′ of another subunit (Carr et al. 2017b; Higgins et al. 2012b; Iwig et al. 2008; Musiani et al. 2015). Crystals of the RcnR-DNA complex were reported (Li et al. 2020), but no structure is yet available.

*Synechocystis* sp. PCC 6803 contains the nickel-responsive regulatory protein InrS (named for *i*nternal *n*ickel *r*esponsive *s*ensor) that belongs to the same protein family as RcnR and CsoR (Foster et al. 2012). The tetrameric cyanobacterial

protein is a repressor of *nrsD* (Fig. 14.1b), encoding a nickel efflux pump, and the repression is relieved by nickel binding (one metal ion per subunit) with an estimated $K_d$ of $2 \times 10^{-14}$ M (Foster et al. 2012). Mutagenesis studies indicate that nickel binds to the protein using Cys53, His78, and Cys82 ligands, perhaps also including His21 (Foster et al. 2014). A crystal structure of the InrS apoprotein (Fig. 14.2b) is consistent with this same set of coordinating residues, where Cys53 from one subunit partners with the other three residues from a second subunit (Foster et al. 2017). XAS analysis of nickel-bound InrS was consistent with a square-planar Ni $(His)_2(Cys)_2$ site (Carr et al. 2017a). The protein can also bind copper or cobalt, but its physiological function is specific to nickel.

*Rhizobium leguminosarum* also possesses an RcnR-like protein that is denoted DmeR for *d*ivalent *m*etal *e*fflux *r*epressor (Rubio-Sanz et al. 2013). The apoprotein form of DmeR represses *dmeF*, encoding a cation diffusion facilitator (CDF) efflux transporter, and repression is alleviated by nickel or cobalt (Fig. 14.1b). A similar *dmeRF* gene cluster is responsible for nickel (or cobalt)-dependent regulation and export in *Agrobacterium tumefaciens* (Dokpikul et al. 2016). Structural characterization has not been reported for any DmeR.

Another sequence-related family member is NcrB from *Leptospirillum ferriphilum* strain UBK03, an iron-oxidizing, metal-resistant bacterium containing the *ncrABC* gene cluster that confers resistance to nickel (Tian et al. 2007). NcrB is a histidine-rich, 89-residue protein that functions as a repressor of the gene cluster in its apoprotein form, but the regulation is derepressed by nickel binding to the protein (Fig. 14.1b) leading to synthesis of the NcrAC efflux pump (Zhu et al. 2011). The structure of NcrB has not been determined.

#### 14.2.1.3 NmtR/KmtR

Examples of repressors that dissociate from the DNA upon binding nickel (Fig. 14.1b), yet are unrelated to those just described, include NmtR and KmtR from *Mycobacterium tuberculosis* (Campbell et al. 2007; Cavet et al. 2002). These proteins are members of the ArsR/SmtB family of transcriptional regulatory proteins (Busenlehner et al. 2003). The apoprotein forms of NmtR and KmtR bind to operator-promoter sites upstream of *nmtA* and *cdf*, encoding a P-type ATPase efflux pump and a CDF protein, respectively. Spectroscopic and mutagenesis studies suggest that nickel binds to NmtR in octahedral coordination, with the likely involvement of Asp91, His93, His104, and His107 along with residues near the amino-terminus (Cavet et al. 2002; Pennella et al. 2003; Reyes-Caballero et al. 2011). These residues are not conserved in KmtR and its higher affinity nickel binding site was suggested to involve His88, Glu101, His102, His110, and His111 (Campbell et al. 2007). The dimeric NmtR protein binds two nickel with $K_d \sim 10^{-10}$ M (Reyes-Caballero et al. 2011). The solution structure for the NmtR apoprotein, determined by NMR methods (Lee et al. 2012), revealed the winged-helix appearance that is typical for this family of proteins (Fig. 14.2c).

Related nickel sensor proteins have been characterized in two other microorganisms. An NmtR sensor exists in *Streptomyces coelicolor* where it regulates production of a P-type ATPase efflux transporter (Kim et al. 2015). *Streptomyces griseus* contains another example of the ArsR/SmtB family named SrnR. This protein forms a complex with SrnQ that regulates *sodF*, encoding an iron-containing superoxide dismutase, by binding to the inverted repeat sequence TTGCA-$N_7$-TGCAA. As originally proposed, neither protein binds to DNA in the absence of nickel whereas the nickel-bound hetero-octamer functions as a repressor (Fig. 14.1a) (Kim et al. 2003b). More recent efforts suggested that SrnR does bind DNA and activates transcription, whereas further binding of nickel-bound SrnQ leads to dissociation and reduced levels of transcription (Fig. 14.1d) (Beniamino et al. 2020). SrnR binds nickel with moderate affinity ($K_d$ ~ 0.65 μM) (Beniamino et al. 2020), but the primary nickel-binding regulatory site is associated with SrnQ (one nickel per protein subunit) (Kim et al. 2003b). The structure of SrnRQ and its nickel-binding site(s) are unknown.

#### 14.2.1.4 Nur

The *S. coelicolor* Nur (*n*ickel *u*ptake *r*egulator) protein, a member of the Fur family of transcriptional regulators, binds nickel to form a complex that represses transcription of some genes (Fig. 14.1a) while activating transcription of another gene (Fig. 14.1c). Specifically, nickel is a co-repressor of the *nikABCDE* and *nikMNOQ* operons for nickel uptake and of *sodF* encoding an iron-dependent superoxide dismutase, while the metal is a co-activator of *sodN* coding for a nickel-dependent superoxide dismutase (Ahn et al. 2006; An et al. 2009). The nickel-Nur complex binds to the "Nur box" palindromic sequence tTGCaa-N5-ttGCAA. The structure of the 16-kDa Nur protein (Fig. 14.2d) reveals a homodimeric winged-helix motif that wraps around DNA and binds four metals per dimer (An et al. 2009). Two sites near the subunit interface coordinate nickel in octahedral geometry with three side chain residues (His70, His72, and His126) along with three oxygen atoms from buffer components. Two other sites, initially suggested to not be responsive to nickel, coordinate the metals in square-planar geometry using His33, His86, His88, and His90 side chains. More recent studies using a combination of mutagenesis, metal titration, and fluorescence anisotropy methods suggest that nickel binding to this site is the critical regulatory process used for protein binding to the DNA, with the other site having a fine-tuning role (Manley et al. 2020). Isothermal titration calorimetry (ITC) studies confirm the dimeric protein binds four nickel ions in pairs with $K_d$ values of 10 nM and 280 nM (Musiani et al. 2015).

#### 14.2.1.5 CnrX

*Cupriavidus metallidurans* (formerly named *Ralstonia metallidurans*) CH34 contains a nickel sensor, CnrX, that operates by a very different process. This organism

tolerates high concentrations of several types of heavy metals by using a set of efflux pumps. In particular, this microorganism contains the *cnrYXH-cnrCBA* gene cluster (located on the pMOL28 plasmid) that is associated with, and named for, *c*obalt and *n*ickel *r*esistance (Grass et al. 2000; Tibazarwa et al. 2000). CnrCBA is the nickel exporter, CnrH is a sigma factor regulating both halves of the gene cluster, CnrY is a trans-membrane connector, and CnrX is a periplasmic nickel-sensing protein (Fig. 14.2e). The cytoplasmic face of CnrY binds CnrH while its periplasmic face binds CnrX. These three proteins work together in what is termed an extracellular function-type sigma factor; nickel coordination to CnrX ($K_d \sim$ pM) leads to a conformational change that propagates through CnrY causing the release of CnrH, which then binds to the appropriate DNA sequence to stimulate transcription by RNA polymerase. This mechanism is akin to, but more complicated than, the co-activator mechanism described earlier (Fig. 14.1c); in particular, the nickel sensor resides in the periplasm.

The X-ray crystal structure of dimeric CnrX is available for residues 31–148 of the apoprotein and the copper-bound forms (Pompidor et al. 2008). The copper is coordinated by His42, His46, Glu63, and His119, with Met123 (numbering based on the full-length protein) also being nearby. Follow-up studies reveal structures of the nickel- (Fig. 14.2e), cobalt-, and zinc-bound forms; the nickel and cobalt species exhibit octahedral coordination involving these same five residues with bidentate Glu63 accounting for the metal-specific conformational changes needed for signaling (Trepreau et al. 2011b). The structure of the nickel-bound species includes residues 39–148, and the amino terminal region is membrane embedded. A crystal structure of the complex between the cytosolic domain of CnrY (residues 2–30) and much of CnrH (residues 5–190 except for 92–122) is known (Maillard et al. 2014). The conformational changes associated with nickel binding to CnrX were explored in greater detail by metal titration analysis and high resolution (1.1 Å) structural studies of selected variant forms of the protein (Maillard et al. 2015). The spectroscopic properties of cobalt-bound CnrX are defined and two additional cobalt binding sites are demonstrated to exist at the amino terminus of the protein (Trepreau et al. 2011a). A structure also is available for the related NccX protein from strain 31A of the same species; significant structural differences are noted when comparing to the strain CH34-derived CnrX protein, but these variations are attributed to the redistribution of hydrophobic surfaces during solubilization of the protein by detergent (Ziani et al. 2014).

#### 14.2.1.6 NrsRS

A microorganism already mentioned, *Synechocystis* sp. PCC 6803, contains a second nickel sensor that operates by a very different mechanism from that detailed earlier (Sect. 14.2.1.2). According to the current model (Garcia-Dominguez et al. 2000; Lopez-Maury et al. 2002), NrsS has an amino-terminal domain localized in the periplasm, two transmembrane helices, and a carboxyl-terminal kinase domain. Nickel binding to the periplasmic region stimulates the kinase domain to transfer

phosphate to the cytoplasmic membrane-localized NrsR, which activates transcription by binding at up to four sites in the intergenic region of the divergent *nrsBACD* and *nrsRS* gene clusters. No structural studies have been described for the NrsRS system. The behavior of this two-component system is reminiscent of the co-activator mechanism detailed earlier (Fig. 14.1c). Note that the *nrsD* mentioned here is the same gene as that regulated more directly by InrS, which uses a promoter binding site that immediately precedes the gene.

#### 14.2.1.7 NimR

*Haemophilus influenzae* possesses a distinct nickel sensor belonging to the Mer family of transcriptional regulatory proteins, typically associated with regulatory responses to toxic metals such as mercury, cadmium, and lead. This protein, NimR, regulates the *nikKLMQO* operon encoding an ABC transporter for nickel uptake by a combination of two mechanisms shown in Fig. 14.1 (Kidd et al. 2011). Specifically, the NimR apoprotein binds to a site of dyad symmetry in the operator/promoter region of the nickel transport operon resulting in transcriptional activation (Fig. 14.1d); upon binding nickel, NimR ceases to activate and rather the complex functions as a co-repressor (Fig. 14.1b). The dimeric protein (15.6-kDa subunit) binds a single nickel at a site that has not been further characterized and the structure of the protein has not been reported.

#### 14.2.1.8 Other Nickel Sensors

Nickel-sensitive transcriptional regulatory proteins exist in many microorganisms beyond those mentioned above. These regulators often are related in sequence to the proteins already described, but novel types of sensor proteins also are known. Detailed structural studies and careful analyses of the corresponding nickel-binding sites generally are not available. When functionally characterized, these additional nickel-sensor proteins often have been found to control nickel-transport systems; however, other roles also are known such as regulating the production of nickel-containing enzymes. Such non-homeostatic regulatory functions of nickel sensors were noted earlier: the control of urease expression by NikR in *H. pylori* (van Vliet et al. 2002) and regulation of superoxide dismutases by Nur in *S. coelicolor* (Ahn et al. 2006) and SrnRQ in *S. griseus* (Beniamino et al. 2020; Kim et al. 2003b). Two additional examples of nickel sensors not involved in nickel transport are summarized below, followed by a brief discussion of a nickel-sensing RNA.

YqjI of *E. coli* is a nickel-binding regulatory protein that associates with inverted-repeat sequences in the region between the divergently transcribed *yqjH* and *yqjI* genes (Wang et al. 2011). The complex regulation pattern of this system requires that YqjI apoprotein bind to both promoter regions in a cooperative manner for full repression (Wang et al. 2014). Binding of nickel reduces the DNA-binding activity of the regulatory protein, allowing for *yqjH* expression (Wang et al. 2011). YqjH is a

flavin-containing enzyme that functions as an iron-siderophore reductase so it was renamed NfeF for *n*ickel-responsive *Fe* uptake *f*lavoprotein; consequently, YqjI was renamed NfeR for *n*ickel-response *Fe*-uptake *r*egulator (Blahut et al. 2018). In vivo transcriptional studies were used to assess mRNA levels of the wild-type protein and site-substituted variants, while purified YqjI/NfeR and several of its variants were analyzed by ITC, XAS, and other studies to better define the nickel-binding site. Although the metal exhibits 5-coordinate geometry with a sulfur ligand, none of the Cys-substituted variants affect nickel binding. Nevertheless, Cys42 and Cys43 are required for the in vivo response and these residues are suspected to form a vicinal disulfide (Blahut et al. 2018). Structural studies are needed to better define the NfeR nickel-binding site.

The *H. pylori* HP0868 gene product is a nickel-binding protein that affects the activity level of urease; thus, it was named Mua for *m*odulator of *u*rease *a*ctivity (Benoit and Maier 2011). Dimeric Mua binds two nickel ions, and high nickel concentrations lead to repression of urease activity by this protein. Mua does not bind to the urease promoter region, or other DNA promoter sequences, and the mechanism of regulation is unknown. The nickel-coordinating residues are not identified and the structure of this nickel sensor has not been elucidated.

Comparative sequence analysis of genomes in the order Clostridiales reveals a novel class of structured RNA often residing upstream of *czcD* genes that encode CDF proteins (Furukawa et al. 2015). The corresponding RNA from *Clostridium botulinum* binds nickel and cobalt with a $K_d$ of 12 and 6 μM, respectively, leading to structural changes. The metal-bound form of the NiCo riboswitch is thought to prevent formation of a terminator loop in the RNA, thus allowing the *cdf* gene to be transcribed. Subsequent in vitro and in vivo studies demonstrated the riboswitch also responds to ferrous ion (Xu and Cotruvo Jr. 2020). The crystal structure is available for the cobalt-bound RNA from *Erysipelotrichaceae bacterium* (Fig. 14.2f), revealing two cobalt (and presumably nickel) sites, two magnesium atoms, and seven bound potassium ions (Furukawa et al. 2015).

### *14.2.2 Nickel Import Systems*

Microorganisms possess nickel *uptake* systems to supply the requirements for nickel-containing enzymes and they use nickel *efflux* systems (Sect. 14.2.3) to limit the toxicity of this cation. Regulation of these transporters often is facilitated by using the nickel sensors described in Sect. 14.2.1. The following subsections describe mechanisms of nickel uptake that fall into two general classes: ABC transporters and permeases (or secondary transporters). The ABC transporter family is subdivided into those with a soluble substrate-binding protein or domain (Sect. 14.2.2.1) and those of the energy-coupling factor (ECF) subfamily (Sect. 14.2.2.2). The permease family (Sect. 14.2.2.3) includes the so-called NiCoT, UreH, and HupE/UreJ subfamilies (Chivers 2015; Eitinger and Mandrand-Berthelot 2000; Nies et al. 2017; Rodionov et al. 2006; Rodrigue et al. 2017). In addition to

describing each of these systems, this section summarizes the process used to facilitate import across the OM of Gram-negative cells (Sect. 14.2.2.4). The described examples are those with high specificity for nickel, although some other metals such as cobalt are often recognized. In addition to these nickel-targeted import processes, this metal also enters some cells via transporters that function in uptake of magnesium (Snavely et al. 1991), other metals (Degen et al. 1999), metal-citrate complexes (Willecke et al. 1973), or other systems that are not detailed.

#### 14.2.2.1 Nickel Uptake by ABC Transporters Possessing a Substrate-Binding Protein/Domain

The most intensively studied ABC transporter system for nickel uptake is the NikABCDE system of *E. coli* (Navarro et al. 1993). NikA is a periplasmic substrate (nutrient)-binding protein, NikB and NikC are integral membrane proteins, and NikD and NikE are ATPases that drive the uptake process. Nickel binds to NikA with a $K_d$ of less than 0.1 μM (de Pina et al. 1995), but this value is shifted to ~75 nM for the complex of metal bound to L-histidine (Chivers et al. 2012). Analysis of the structure of NikA provides a fascinating glimpse into the power and limitations of crystallography. The initial apoprotein and holoprotein structures revealed the same overall fold with two domains connected by a hinge used to enclose the substrate binding site; however, the bound pentahydrate nickel lacked any direct interaction with the protein (Heddle et al. 2003)—a coordination environment incompatible with earlier XAS analysis (Allan et al. 1998). A subsequent structure of NikA complexed with EDTA-bound iron implicated the binding of a metallophore, rather than the free metal ion (Cherrier et al. 2005). Another NikA structure was proposed to resolve the disparate findings; it used a variant protein and identified a second, distant nickel-binding site with His54 and His442 as coordinating ligands (Addy et al. 2007). The notion of NikA binding a metallophore was later supported by another structure in which NikA binds a complex of nickel and an endogenous ligand, tentatively identified as butane-1,2,4-tricarboxylate (Cherrier et al. 2008). Finally, after evidence had indicated NikA actually binds the Ni-(L-histidine)$_2$ complex (Chivers et al. 2012), the structure of this form of the protein was obtained and confirmed the metal coordination by His416 (Lebrette et al. 2013). In contrast to these extensive structural studies of NikA, no structure is reported for the other components of the Nik system. Because the NikBCDE components are likely to resemble other ABC-type metal transporters, Fig. 14.3a provides the structure of the transmembrane and ATPase components of a putative metal-chelate ABC transporter from *H. influenzae* (Pinkett et al. 2007) as a mimic of the nickel-specific proteins, along with that of the NikA-Ni-(L-His)$_2$ complex (Lebrette et al. 2013).

Many other microorganisms possess Nik-type ABC-transporters with a soluble periplasmic nickel-binding protein (or for Gram-positive bacteria, an attached extracellular domain), although in some cases different terminology is used for the components. Examples with experimental evidence for a nickel transport function include proteins encoded by *niuBDE* of *H. pylori* (Fischer et al. 2016), *nikABCDE* of

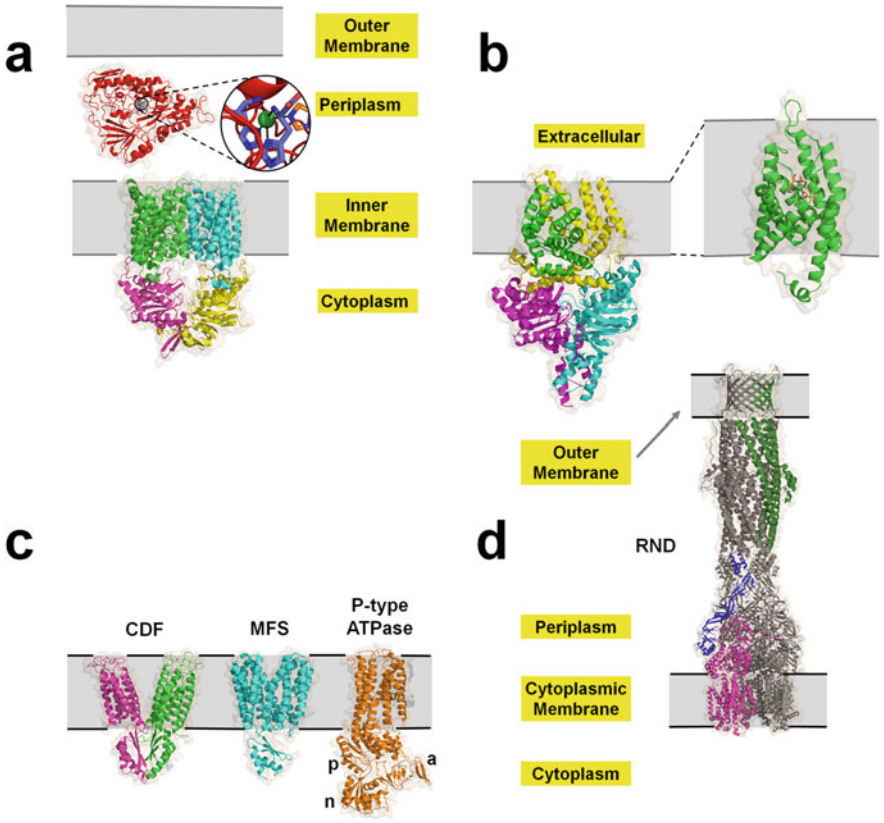


**Fig. 14.3** Structures of nickel transporters. (**a**) *Escherichia coli* NikA and a NikBCDE-like complex used for nickel import. The periplasmic NikA substrate-binding protein (red, PDB ID 4i8c) includes an inset illustrating the metal-binding site with His416 in orange sticks, two molecules of L-histidine in blue sticks, and nickel as a green sphere. The structure of NikBCDE is unknown, but likely resembles that depicted for the metal-chelate ABC transporter of *Haemophilus influenzae* (PDB ID 2nq2) with transmembrane (green/cyan) and ATPase (magenta/yellow) components. (**b**) *Thermoanaerobacter tengcongensis* NikM2 (green, PDB ID 4m58), the S component of a multi-component nickel ECF-type ABC importer, with the nickel-coordinating sidechains (Met1, His2, and His67) shown as orange sticks. The full importer structure is not established, but likely resembles the four-component folate transporter shown from *Lactobacillus brevis* (PDB ID 4huq; S in green, T in yellow, and A in magenta and cyan). (**c**) Structural mimics of CDF, MFS, and P-type ATPase nickel exporters are the homodimeric, zinc-specific, YiiP from *E. coli* (PDB ID 3h90, green and magenta), the monomeric, putative drug exporting, YajR from *E. coli* (PDB ID 3wdo, cyan), and the four-domain, single-component, copper-transporting, CopB from *Legionella pneumophila* (PDB ID 3rfu, orange). The latter includes a transmembrane region, actuator domain (a), phosphorylation domain (p), and nucleotide binding-domain (n). (**d**) A structural mimic of an RND export pump for nickel is CusABC that exports copper primarily from the periplasm of *E. coli* (PDB ID 3ne5 for CusAB and 3pik for CusC). The RND pump is gray, except for single subunits of CusA (red), CusB (blue), and CusC (dark green). All components are shown in cartoon mode with partially transparent surfaces

*Brucella suis* (Jubier-Maurin et al. 2001), *yntABCDE* of *Yersinia pseudotuberculosis* (Sebbane et al. 2002) and *Proteus mirabilis* (Brauer et al. 2020), *nikZYXWV* of *Campylobacter jejuni* (Howlett et al. 2012), and *cntABCDE* from *Staphylococcus aureus* (Remy et al. 2013). The latter Gram-positive microorganism lacks a periplasm so its NikA-like protein, CntA, is tethered to the membrane by an amino-terminal extension. Several NikA-related structures are known including CntA from *S. aureus* (Song et al. 2018), NikA from the same microorganism (Lebrette et al. 2015), CeuE from *H. pylori* (Shaik et al. 2014), NikA from *B. suis*, YntA from *Yersinia pestis*, NikZ from *C. jejuni* (Lebrette et al. 2014), and the analogous protein from *Sinorhizobium meliloti* (unpublished, PDB ID 4web). Although the overall structures of these nickel-binding proteins are related, the ligand binding sites are distinct. This finding is consistent with diversity in the substrate being transported (i.e., other than the Ni(L-His)$_2$ complex), as exemplified by CntA's interaction with the complex of nickel and staphylopine—a broad-spectrum nicotianamine-like metallophore (Ghssein et al. 2016; Song et al. 2018).

#### 14.2.2.2 Nickel Uptake by ECF-Type ABC Transporters

The second type of ABC transporter used for nickel uptake lacks a soluble periplasmic protein or extracellular domain for binding the metal ion or metallophore. Rather, CbiMNQO, NikMNQO, and related ECF-type importers possess a small (~20 kDa), integral-membrane protein for binding nickel, termed the S component, that interacts with another integral-membrane T component and two similar or identical cytosolic ATPases known as A components (Finkenwirth and Eitinger 2019; Rodionov et al. 2006; Slotboom 2014). Early examples of such systems are those reported in *Actinobacillus pleuropneumoniae* (Bossè et al. 2001) and *Streptococcus salivarius* 57.I (Chen and Burne 2003), where the nickel import genes are located adjacent to urease genes and shown to be important for nickel incorporation into this enzyme. Among other examples, nickel transport is demonstrated for the products of *nik(MN)QO* (where *nikM* and *nikN* are fused) of *Rhodopseudomonas capsulatus* (Rodionov et al. 2006), *nikLMNQO* of *H. influenza*e (Kidd et al. 2011), and *lar(MN)QO* (where *lar* indicates association with genes encoding the nickel-dependent lactate racemase) of *Lactobacillus plantarum* (Desguin et al. 2014). The structure of the S component for the nickel importer of *Thermoanaerobacter tengcongensis*, NikM, is shown in Fig. 14.3b (Yu et al. 2014). Nickel is 4-coordinated with the Met1 amine, His2 imidazole and amide, and His67 imidazole providing square-planar ligation. This figure also illustrates a four-component *Lactobacillus brevis* ECF-type transporter for folic acid as a mimic of the nickel ECF-type transporter.

#### 14.2.2.3 Nickel Uptake by Permeases/Secondary Transporters

Many microorganisms possess single-protein nickel uptake systems that operate either by facilitated diffusion or are driven by the proton motive force (Eitinger and Mandrand-Berthelot 2000; Eitinger et al. 2005; Rodionov et al. 2006; Rodrigue et al. 2017). The nickel/cobalt transporter (NiCoT) subgroup of these proteins is probably the best characterized. The archetype member of this family is HoxN from *Cupriavidus necator* (formerly named *Alcaligenes eutrophus* and *Ralstonia eutropha*). Early studies identified the gene encoding this protein to be in the hydrogenase gene cluster (Eberz et al. 1989) and showed it participates in nickel transport (Eitinger and Friedrich 1991). A topological model indicated eight trans-membrane domains (Eitinger and Friedrich 1994) and the probable nickel-binding residues have been identified by mutagenesis studies (Eitinger et al. 1997). Another NiCoT family member used to import nickel for [NiFe] hydrogenase activation is HupN of *Bradyrhizobium japonicum* (Fu et al. 1994). By contrast, NixA of *H. pylori* is a NiCoT family member that was first identified by its relationship to synthesis of active urease (Mobley et al. 1995a). As in the case of HoxN, membrane topology and extensive mutagenesis studies defined the potential nickel-binding motifs (Fulkerson Jr. et al. 1998; Fulkerson Jr. and Mobley 2000). A second subgroup of nickel permeases with only six trans-membrane domains is named for the first representative identified: UreH encoded within the urease gene cluster of the thermophile *Bacillus* sp. TB-90 (Maeda et al. 1994). The corresponding family member in *Y. pseudotuberculosis* facilitates high-affinity, nickel-specific transport (Sebbane et al. 2002). HupE and UreJ are included in the third subgroup of nickel permeases (Eitinger et al. 2005). The *R. leguminosarum* HupE facilitator protein, encoded by a gene co-localizing with hydrogenase genes, was investigated by mutagenesis methods that identified critical residues for nickel uptake (Albareda et al. 2015; Brito et al. 2010). UreJ of *Bordetella bronchiseptica* possesses 37% identity with the *R. leguminosarum* protein, but is encoded within the urease gene cluster (McMillan et al. 1998). *Synechococcus* sp. strain WH8102 also contains a *hupE* gene; however, the function of the encoded protein is not defined and nickel transport in this organism is associated with a different permease named SodT (Dupont et al. 2012). Of further interest, a eukaryotic example of a nickel permease, Nic1p, occurs in *Schizosaccharomyces pombe* (Eitinger et al. 2000). Despite their importance for nickel transport in a wide range of microorganisms, no structures have been reported for any uptake nickel permease.

#### 14.2.2.4 Nickel Uptake Through the OM

Although the OM of Gram-negative bacteria possesses porin proteins that allow passage across this barrier by small molecules (< ~600 Da), it is known that uptake of iron siderophores, heme, some sugars, and other compounds is promoted by making use of OM receptors that are energized by TonB, ExbB, and ExbD proteins,

with periplasmic substrate-binding components delivering the nutrient to inner membrane transporters (Braun and Hantke 2011). Evidence has accumulated that nickel is taken up in a similar way. For example, NikR and nickel regulate *H. pylori* genes (*hp1512*, *hp1339–1340*, and *hp1561*) thought to encode a receptor (FrpB4), energizer components (ExbB/ExbD), and a periplasmic protein (CeuE) (Contreras et al. 2003). Other groups confirmed the finding that FrpB4 is an outer membrane protein whose synthesis is regulated by NikR, and they identified the NikR-regulated FecA3 (encoded by *HP1400*) as a second likely OM receptor (Davis et al. 2006; Ernst et al. 2006). Mutagenesis studies demonstrated that *H. pylori* uses the TonB/ExbB/ExbD machinery to drive nickel uptake via FrpB4 (Schauer et al. 2007). *H. hepaticus* appears to have a similar system with NikR-regulated expression of a gene (*hh0418*) encoding an OM receptor (Benoit et al. 2013). Furthermore, *H. mustelae* possesses *nixA*, *fecDE*, *nikH*, and *ceuE* (encoding a permease, inner membrane ABC transporter, OM receptor, and periplasmic substrate-binding protein) involved in nickel transport, along with two *tonB* genes; TonB1 is needed for heme uptake and TonB2 is used for nickel uptake (Stoof et al. 2010a, b). Structural characterization of an outer membrane system for nickel uptake is lacking.

## *14.2.3 Nickel Export Systems*

This section describes five systems by which microorganisms export nickel from the cell: RcnA and related proteins (Sect. 14.2.3.1), cation diffusion facilitators (CDFs, Sect. 14.2.3.2), the major facilitator protein superfamily (MFS, Sect. 14.2.3.3), P-type ATPases (Sect. 14.2.3.4), and resistance nodulation cell division (RND)-type efflux systems (Sect. 14.2.3.5). As in the case of the importer systems, these exporter systems often are not specific to nickel; however, each system emphasized here promotes nickel efflux.

### 14.2.3.1 Nickel Export via RcnAB and Related Systems

The nickel efflux pump of *E. coli* is the inner membrane-bound protein RcnA as shown by the cellular decrease in nickel resistance when the corresponding gene is mutated (Rodrigue et al. 2005). An increase in cellular nickel concentration leads to dissociation of the RcnR regulatory protein from the DNA (Sect. 14.2.1.2), leading to enhanced *rcnA* transcription (Iwig et al. 2006). RcnA is distantly related to the NiCoT family (Sect. 14.2.2.3). RcnB, encoded by a gene located immediately downstream of *rcnA*, is a periplasmic, copper-binding protein that modulates the nickel export activity of RcnA by an unclear process (Blériot et al. 2011, 2015). Genes related to *rcnA*, sometimes paired with *rcnB*-like genes, have been identified in several other bacteria and typically have alternative names. A few examples for which an involvement in nickel resistance is demonstrated are *mrdH* in *Pseudomonas putida* KT2440 (Haritha et al. 2009), *nirC* of *Klebsiella oxytoca* (Park et al.

2008), and *nrcC* from three species: *Hafnia alvei* 5-5 (Park et al. 2004), *L. ferriphilum* (mentioned in Sect. 14.2.1.2 as being regulated by NcrB) (Tian et al. 2007), and *Serratia marscescens* (Marrero et al. 2007). No structure is available for any RcnA protein, but modeling studies suggest the presence of six trans-membrane regions (Rodrigue et al. 2017).

#### 14.2.3.2 Export of Nickel by Cation Diffusion Facilitators (CDF)

Nickel export via proton antiporters is carried out by CDF family members. FieF and DmeF of *C. metallidurans* export nickel, although they are more effective at transporting other metals (Munkelt et al. 2004). DmeF proteins from *R. leguminosarum* and *A. tumefaciens* are efficient nickel exporters (Dokpikul et al. 2016; Rubio-Sanz et al. 2013). The nickel-efflux CDF protein of *M. tuberculosis* is called Rv2025c and regulated by KmtR (Campbell et al. 2007), as described in Sect. 14.2.1.3. *Rhizobium etli* possesses a CDF transporter of nickel termed NepA (Cubillas et al. 2013). Although no structure is reported for a nickel-specific CDF, the architecture of the zinc-specific CDF transporter YiiP from *E. coli* is available by crystallography (Lu et al. 2009). This protein (Fig. 14.3c, left) provides a reasonable facsimile of what one might expect for a nickel-transporting CDF. The homodimer is Y-shaped with each subunit having six transmembrane regions and a C-terminal cytoplasmic region.

#### 14.2.3.3 Nickel Export Involving the Major Facilitator Protein Superfamily (MFS)

As expected for the term superfamily, MFS is a large group of membrane secondary transporters that act on a vast number of substances (Saier Jr. et al. 1999). The best example of a nickel-specific exporter is NreB from *Achromobacter xylosoxidans* 31A, which confers nickel resistance in the native host or when synthesized in *E. coli* (Grass et al. 2001). NreB has a histidine-rich C-terminal region, but this sequence is not essential to its function. A related example, NrsD, exists in *Synechocystis* sp. strain PCC 6803 (Garcia-Dominguez et al. 2000). This protein was mentioned earlier (Sect. 14.2.1.2) because it is regulated by the nickel-sensor InrS. Although structures are not available for NreB or NrsD, several MFS transporters have been structurally characterized including the putative drug exporter YajR from *E. coli* (Jiang et al. 2013). The MRS proteins are thought to use a rocker-switch mechanism requiring conformational changes involving their 12 transmembrane helices. YajR, shown in its outward-facing conformation, exemplifies the likely structure of the nickel exporters (Fig. 14.3c, middle).

#### 14.2.3.4 P-Type ATPases Used for Nickel Efflux

ATP hydrolysis is used to drive the export of a wide range of substances via single-component P-type ATPases (Palmgren and Nissen 2011). NmtA from *M. tuberculosis* or *S. coelicolor*, mentioned earlier as being regulated by NmtR (Sect. 14.2.1.3), is likely to be such a protein (Cavet et al. 2002; Kim et al. 2015). CtpD of *Mycobacterium smegmatis* exports nickel, though it has a greater preference for cobalt, and deletion of the corresponding gene leads to accumulation and sensitivity to both metals (Raimunda et al. 2012). Another member of this family of proteins is *S. meliloti* Nia, named for being a nickel-iron ATPase (Zielazinski et al. 2013). Nia synthesis is induced by the presence of either metal and deletion of the corresponding gene leads to the accumulation of both cations. An extra domain near the C-terminus resembles hemerythrin and binds a dinuclear iron center, suggesting an additional role for this protein may exist. While none of these proteins have been structurally characterized, they are likely to exhibit extensive similarity to the copper-transporting P-type ATPase CopB from *Legionella pneumophila* (Gourdon et al. 2011). This protein, illustrated as a mimic for a nickel P-type ATPase (Fig. 14.3c, right), possesses a transmembrane portion, and the actuator (a), phosphorylation (p), and nucleotide binding (n) domains.

#### 14.2.3.5 RND Pumps for Export from the Periplasm

RND pumps are complicated systems for expelling a compound from the periplasm, although they are also capable of less efficient export from the cytoplasm. These systems are used as multidrug transporters and for transporting various other compounds. They consist of three parts: (1) the trimeric inner membrane RND pump that is driven by the proton motive force, (2) the periplasmic adaptor proteins that form a multimeric ring which spans between the inner and outer membranes, and (3) the trimeric OM factor (Symmonds et al. 2015). Nickel export via an RND pump was first described for *C. metallidurans* CH34 (Liesegang et al. 1993). The *cnrCBA* genes encoding this system are regulated by the products of *cnrYXH* (Sect. 14.2.1.5), where CnrX is a periplasmic nickel sensor protein (Maillard et al. 2015). Additional RND exporters of nickel include those encoded by *cznABC* of *H. pylori* (Stähler et al. 2006), *nrsAB* of *Synechocystis* (regulated by NrsRS, Sect. 14.2.1.6) (Garcia-Dominguez et al. 2000), and *cnrA* of *Bradyrhizobium* strains associated with a legume that grows in a high-nickel environment (Chaintreuil et al. 2007). No structure is available for any of these nickel export proteins, but the copper exporter CusABC (Fig. 14.3d) from *E. coli* provides a reasonable illustration of what one might expect. The CusA component of this RND pump forms a homotrimer in the cytoplasmic membrane, with each subunit possessing 12 transmembrane helices (Long et al. 2010). Six molecules of the CusB adaptor attach to the CusA homotrimer, forming a tunnel through part of the periplasm (Su et al. 2011). The distal end of this tunnel attaches to the trimeric OM component CusC that was

structurally characterized as an independent protein (Kulathila et al. 2011). This homotrimer completes the tunnel through the periplasm and forms a β-barrel in the OM that is anchored by a triacylated N-terminus.

## 14.3 Other Aspects of Nickel Toxicity and Resistance

Microorganisms have long been investigated with regard to nickel toxicity and nickel resistance. In 1967, for example, R factors were shown to mediate nickel tolerance of *E. coli* and *Salmonella* strains (Smith 1967). Early reviews of nickel toxicity documented the sensitivities of various microorganisms to this metal when growing under different conditions (Babich and Stotzky 1983; Gadd and Griffiths 1978), but in general the basis for the sensitivity to this metal ion remained enigmatic. This section begins by describing studies that define the primary site of nickel toxicity in *E. coli* (Sect. 14.3.1), then it briefly surveys other established mechanisms of nickel stress (Sect. 14.3.2). Following a similar sequence, initial microbial screening methods identified nickel-tolerant strains of microorganisms and by the mid-1980s genetic studies [e.g. (Mergeay et al. 1985; Siddiqui and Schlegel 1987)] began to identify some of the resistance determinants. More recent studies have identified nickel efflux, described in Sect. 14.2.3, as the most widely used system for allowing microorganisms to tolerate high concentrations of this metal ion. Aspects of these exporters will not be repeated here; rather, alternative resistance mechanisms will be summarized (Sect. 14.3.3).

### *14.3.1 The Primary Site of Nickel Toxicity in* E. coli*: Fructose-1,6-Bisphosphate Aldolase*

Growth of *E. coli* on glucose or fructose minimal medium is inhibited by the addition of 8 μM nickel, but no growth inhibition was observed for this environmentally-relevant concentration of nickel when using succinate, lactate, or glycerol as carbon sources (Macomber et al. 2011). As expected, the inhibitory effect was exacerbated for *rcnA* mutant cells, which are inhibited by only 4 μM of this metal ion. These results are consistent with a direct effect of nickel on fructose-1,6-bisphosphate aldolase (FbaA)—a critical enzyme for the metabolism of glucose and fructose, but not required for degradation of the other nutrients. The loss of cellular FbaA activity following nickel stress and the restoration of growth in the *rcnA* mutant cells by overexpression of *fbaA* confirmed this enzyme as the target of nickel toxicity. Prior structural studies had demonstrated that FbaA, a class II aldolase, possesses zinc at its active site (coordinated by His110, His226, and His264) with another zinc (coordinated by Asp144, Glu174, and Glu181) bound at a nearby non-catalytic metal-binding site (Hall et al. 1999). Nickel-treated FbaA lost approximately one

of these zinc atoms while binding about one nickel atom. Significantly, the D144A and E174A FbaA variants, affecting the non-catalytic site, are resistant to nickel inhibition. These studies provide clear evidence that the primary site of nickel toxicity for glucose- or fructose-grown *E. coli* is the non-catalytic zinc site of FbaA (Macomber et al. 2011). Cells grown on succinate, lactate, or glycerol are inhibited by high concentrations of nickel, but the target of toxicity under these conditions remains unknown.

### *14.3.2 Other Sites of Nickel Toxicity in Microorganisms*

In contrast to the detailed mechanistic understanding of nickel toxicity for glucose- or fructose-grown *E. coli*, described above, few studies have investigated the basis of nickel's deleterious effects in other microorganisms (Macomber and Hausinger 2011). This section summarizes other potential sites of nickel toxicity in microbes (Fig. 14.4): oxidative stress effects, substitution of active site metal ions in important metalloenzymes (with redox-active or non-redox sites), and inhibitory binding to non-active sites of essential enzymes.

Proteomic studies of nickel-challenged *Burkholderia vietnamiensis* and *P. putida* UW4 showed increased production of proteins related to oxidative stress (Cheng et al. 2009; Van Nostrand et al. 2008), consistent with nickel increasing the cellular formation of reactive oxygen species (ROS). Furthermore, *E. coli* cells lacking both

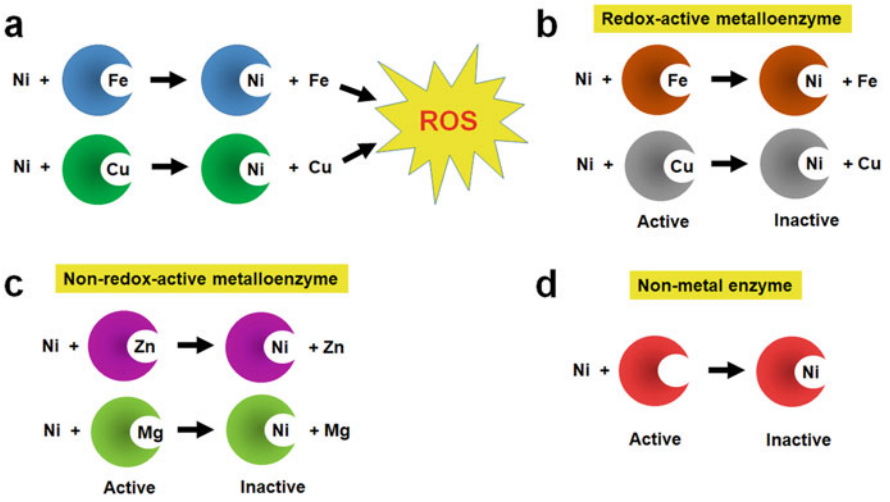


**Fig. 14.4** Mechanisms of nickel toxicity. (**a**) Substitution of nickel for a protein-bound redox-active metal ion with subsequent generation of ROS (reactive oxygen species). (**b**) Replacement of a redox-active metallocenter in an enzyme by nickel. (**c**) Substitution of a non-redox metal ion in an essential enzyme by nickel. (**d**) Other types of inactivation of an enzyme by nickel binding

its manganese- and iron-containing superoxide dismutases exhibited greater sensitivity towards nickel, consistent with formation of superoxide in nickel-stressed cells (Geslin et al. 2001). On the other hand, direct observations indicate that oxidative stress was not induced when treating cells with low concentrations of nickel that still inhibited growth (Kumar et al. 2017). Rather, these metal ions led to double-strand breaks in the DNA and blockage of the SOS repair pathways. These results are consistent with the known properties of free nickel ions that function poorly in generating reactive oxygen species compared to iron and copper (Valko et al. 2005). A plausible explanation for the connection between oxidative stress and nickel toxicosis is metal substitution, with the released iron and copper reacting with oxygen and leading to ROS with its consequent deleterious effects (Fig. 14.4a). Thus, nickel interaction with bacteria is unlike the situation with eukaryotes where the metal ion has been shown to directly cause oxidative stress with accompanying damage to DNA (Guo et al. 2019; Kasprzak and Salnikow 2007), alteration of the thiol/disulfide ratio (Randhawa et al. 2001), or enhanced lipid peroxidation (Niki et al. 2005; Paraszkiewicz et al. 2010).

Substitution of the relatively redox-stable nickel ion for a redox-active metal can inactivate a metalloenzyme, potentially leading to inhibition of cell metabolism (Fig. 14.4b). For example, nickel replaces the ferrous ion in taurine hydroxylase of *E. coli* by a slow-binding inhibition mechanism thus preventing its reactivity with oxygen (Kalliri et al. 2005); such inactivation of the enzyme would hinder growth of cells using taurine as the sole sulfur source. Similar inhibitory results are expected for other 2-oxoglutarate dependent oxygenases that play diverse roles in various bacteria (Herr and Hausinger 2018; Jia et al. 2017). Other examples of bacterial iron-containing enzymes inhibited by nickel include protocatechuate 3,4-dioxygenase and catechol 1,2-dioxygenase of *R. trifolii* (Chen et al. 1984, 1985), ATP:corrinoid adenosyltransferase of *Salmonella enterica* (Buan and Escalante-Semerena 2006), atrazine chlorohydrolase from a *Pseudomonas* species (Seffernick et al. 2002), and extracellular uricase from a strain of *Sphingobacterium thalpophilum* (Ravichandran et al. 2015). Similarly, nickel inhibits some copper and cobalt enzymes such as nitrous oxide reductase of *Rhodobacter sphaeroides* (Sato et al. 1998) and cobaltochelatase of *Pseudomonas denitrificans* (Debussche et al. 1992). Depending on nutrient availability, the decreases in these enzyme activities could interfere with cell growth.

Nickel also can be a toxicant by substituting for a non-redox metal ion, such as zinc, magnesium, or calcium, in an essential enzyme (Fig. 14.4c). In these situations, the change in metal specificity may lead to subtle changes in protein structure or affect the coordination geometry of the metal. A structurally-characterized example of the latter situation was reported for glyoxalase I, which in some species is a zinc-dependent enzyme and in others requires nickel (Honek 2015). Whereas the native forms of the enzymes exhibit octahedral coordination of the appropriate metal using four protein ligands and two waters (replaced by substrate), an altered coordination geometry is observed for enzymes with the inactive metal bound (He et al. 2000). Partial or nearly complete inhibition was reported for a range of different non-redox metal enzymes such as the magnesium-dependent DNA polymerase I (Klenow

fragment) of *E. coli* (Snow et al. 1993), zinc- or calcium-dependent aminopeptidases from different species of *Streptomyces* (Arima et al. 2004), and a zinc-containing tripeptidase from *Pediococcus pentosaceus* (Simitsopoulou et al. 1997).

Finally, it is important to note that nickel can be inhibitory to non-metalloenzymes or by binding to sites distant from a metallocenter (Fig. 14.4d). A few such examples include cytosine 5-methyltransferase and uracil 5-methyltransferase of *E. coli* (Hurwitz et al. 1964), *N*-carbamoyl D-amino acid amidohydrolase of an *Agrobacterium* species (Louwrier and Knowles 1996), and mercuric ion reductase of *Azotobacter chroococcum* (Ghosh et al. 1999). The detailed inhibition mechanism generally has not been investigated, but the propensity of nickel to bind to histidine and cysteine side chains offers a reasonable hypothesis for enzyme inactivation. For example, *N*-carbamoyl D-amino acid amidohydrolase from *Agrobacterium radiobacter* contains a cluster of three histidine residues required for activity (Wang et al. 2001) and mercuric reductases possess a pair of cysteine residues that function in catalysis (Barkay et al. 2003); binding of nickel to these side chains could readily lead to loss of enzyme activity.

Although deleterious effects of nickel ions are proposed to include the production of reactive oxygen species and the inhibition of various types of microbial enzymes, the critical site of nickel toxicity in any particular microorganism is almost never known. Clearly, the basis of nickel stress in microbes requires further investigation.

### *14.3.3 Non-Efflux Mechanisms of Nickel Tolerance*

Although nickel efflux is the most typical approach used by microorganisms for dealing with elevated concentrations of this metal ion, particular microbes handle nickel ion stress by avoidance, reduction, sequestration, compartmentalization, and several other mechanisms (Macomber and Hausinger 2011).

One straightforward technique to circumvent nickel stress is to simply avoid high concentrations of this toxic metal ion by responding to it as a chemotactic repellent, as demonstrated in *E. coli* (Englert et al. 2010). The mechanism of this response is not established, but it does not require nickel transport or the periplasmic NikA nickel-binding protein and it does utilize the Tar methyl-accepting chemotaxis protein.

When nickel ions cannot be avoided, some microbes minimize its toxicity by reducing the cation to the harmless elemental form. Precipitation of elemental nickel in the periplasm and on the cytoplasmic membrane was reported for *Pseudomonas aeruginosa* (Sar et al. 2001); the deposited metal was identified using energy-dispersive X-ray analysis. It is currently unclear whether this microorganism uses the reductive process as a means of nickel resistance. Reduction as a resistance mechanism was demonstrated for *Pseudomonas* sp. MBR that was grown aerobically with a wide range of electron donors (Zhan et al. 2012). Transmission electron microscopy identified nickel deposits in the periplasm and cytoplasmic membrane of this highly nickel-tolerant microorganism. Similarly, reduction of nickel ions to

elemental nickel in the cytoplasm was demonstrated using *Thiocapsa roseopersicina* and shown to be associated with nickel resistance (Zadvornyy et al. 2010). This microorganism produces dense nanoparticles of nickel metal in the cytoplasm when treated with nickel, but only in the presence of hydrogen gas. The purified *hyn*-encoded [NiFe] hydrogenase from these cells recapitulates the catalytic production of the reduced metal particles.

Another approach to overcome nickel stress is to reduce its concentration by sequestering it externally, in the periplasm, or within the cell. An external process is used by a nickel-resistant, sulfate-reducing strain of *Desulfotomaculum* that generates a soluble dark-brown nickel sulfide product (Fortin et al. 1994). External binding of nickel to anionic capsular polysaccharides is another way to potentially reduce the available concentration of this metal ion. The poly-γ-glutamate capsule of *Bacillus licheniformis* and the cell wall of *Bacillus subtilis* are known to bind nickel; however, no studies have examined whether such binding confers nickel resistance to the cells (Beveridge and Murray 1976; McLean et al. 1990). Periplasmic sequestration of nickel is an option suggested for an isolate of *P. putida* S4 (Tripathi and Srivastava 2006). When these cells were exposed to nickel they produced an 18-kDa protein that may tightly bind the metal; however, detailed characterization of nickel binding by the peptide was not reported. Similarly, nickel sequestration in the periplasm was proposed for *Cupriavidus pauculus* KPS 201 that had been isolated from a nickel-rich ultramafic ecosystem; however, in this case two larger proteins of 74- and 66-kDa were suggested to be involved in binding the metal (Pal and Paul 2010). Again, no analysis of the proteins' interactions with nickel was reported. Cellular sequestration of nickel ions by an 82-residue peptide (SCO4226) in *S. coelicolor* was proposed (Lu et al. 2014), though clear evidence for participation in nickel resistance has not appeared. The structure of the holoprotein reveals a homodimer with ferredoxin-like folds containing four weakly bound ($K_d$ of 10 μM) nickel per dimer at distinct surface sites. Other cytoplasmic proteins used to sequester nickel are Hpn-1 and Hpn-2 (Sect. 14.4.12), which are abundant proteins of *H. pylori* and related microorganisms. These proteins are characterized for their nickel-binding abilities and are known to confer nickel resistance to these cells (Ge et al. 2006a; Seshadri et al. 2007; Vinella et al. 2015).

An alternative version of the sequestration mechanism is compartmentalization. An illustration of this approach involves nickel-resistant strains of *Saccharomyces cerevisiae* that place the metal into a vacuole as a complex with the amino acid histidine (Joho et al. 1990, 1992; Nishimura et al. 1998; Pearce and Sherman 1999). Such import of nickel into a subcellular organelle is not available to bacteria.

A poorly characterized system is operant in *B. vietnamiensis* $PR1_{301}$ that exhibits greater resistance to nickel when grown at pH 5 than at pH 7 (Van Nostrand et al. 2008). Two-dimensional gel electrophoresis coupled with mass spectrometric methods identified several proteins that are produced at greater abundance using the nickel-resistant conditions; surprisingly, these proteins are associated with cell shape and membrane composition. Fatty acid methyl ester analysis revealed a change in membrane structure for cells capable of growth at higher nickel

concentrations. The precise mechanism of resistance in this microorganism remains to be defined.

A genome-wide functional screening approach identified seven genes associated with nickel resistance in *Acidiphilium* sp. MP, a microbe isolated from the metal-contaminated Rio Tinto river in Spain (San Martin-Uriz et al. 2014). Two genes (*hslVU*) encode an ATP-dependent protease that, when heterologously expressed, confer nickel resistance to *E. coli* by an unknown mechanism. The other genes encode enzymes involved in lipopolysaccharide or branched chain amino acid biosynthesis; in these cases, it is unclear whether these molecules are directly involved in nickel resistance.

A proteomic analysis comparing the effects of 2 mM nickel treatment on *P. putida* UW4 revealed significant increases in 82 proteins and significant decreases of 81 proteins (Cheng et al. 2009). The proteins amplified during nickel stress include those for general stress adaptation, oxidative stress, and heavy metal efflux.

A role for superoxide dismutase in nickel resistance was suggested from studies using *E. coli* (Geslin et al. 2001). The nickel resistance of individual *sodA* or *sodB* mutants, encoding the manganese- or iron-dependent superoxide dismutase enzymes, was comparable to the wild type cells; however, the double mutant which lacked both activities exhibited increased sensitivity to this metal. These results suggest that excess levels of cellular nickel can promote the generation of ROS with deleterious consequences, and that superoxide dismutase alleviates these issues.

In summary, a wide range of mechanisms beyond the use of nickel efflux systems are likely to play a role in allowing microorganisms to tolerate this metal ion. Unfortunately, the relevance of many of these systems to nickel stress is not convincingly demonstrated and much work on alternative resistance mechanisms remains to be done.

## 14.4 Nickel Utilization by Microorganisms

In the past decade, nickel-containing enzymes have been the subject of several general review articles (Alfano and Cavazza 2020; Boer et al. 2014; Cheng et al. 2016; Kaluarachchi et al. 2010; Maroney and Ciurli 2014) and a book (Zamble et al. 2017). Here, the biochemical reactions of these enzymes are described (Fig. 14.5), their structures are highlighted (Fig. 14.6), and in many cases the pathways for biosynthesis of their metallocenters are summarized. The order of presentation is approximately in order of the complexity of their active site metallocenters, with glyoxalase I (Glo1), acireductone dioxygenase (ARD), quercetin 2,4-dioxygenase (QueD), and superoxide dismutase (SOD) each containing mononuclear nickel centers, urease using a dinuclear nickel site, [NiFe] hydrogenases possessing a heterodinuclear center along with auxiliary [FeS] clusters, carbon monoxide dehydrogenase (CODH) possessing an inorganic [Ni-4Fe-4S] complex plus other [FeS] clusters, acetyl-coenzyme A (CoA) synthase/decarbonylase (ACS)

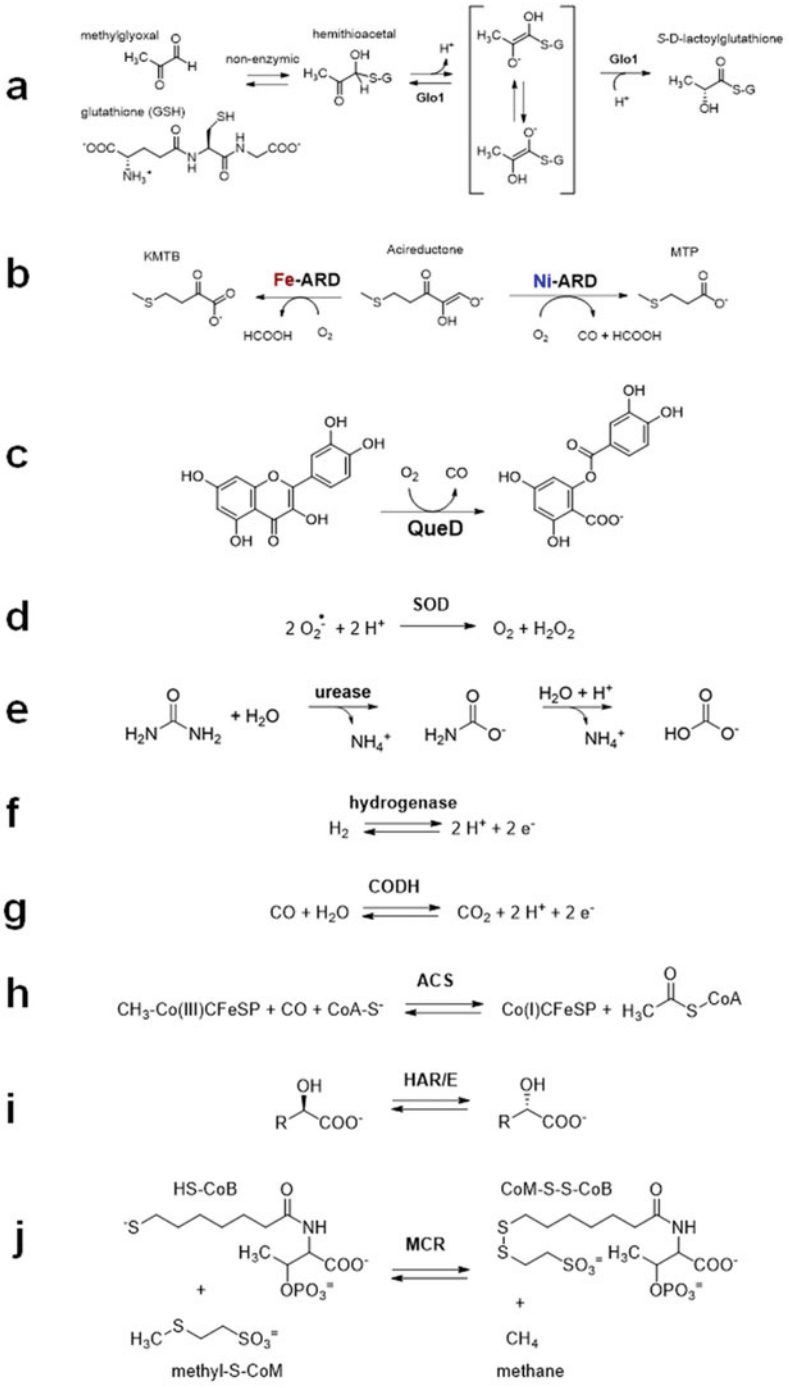


**Fig. 14.5** Reactions of nickel-dependent enzymes. (**a**) Glyoxalase (Glo1). (**b**) Two distinct acireductone dioxygenase (ARD) reactions depending on whether iron or nickel is bound. (**c**)

having both the CODH components and a [4Fe-4S]-Ni-Ni cluster, and finally 2-hydroxyacid racemases/epimerases (HAR/E) and methyl-*S*-coenzyme M reductase (MCR) possessing organometallic cofactors [the nickel-pincer nucleotide (NPN) and nickel-tetrapyrrole cofactor (F430), respectively] with nickel coordinated to an organic framework. In addition, other examples of possible nickel-containing enzymes are mentioned. Finally, cellular nickel storage is briefly addressed.

### *14.4.1 Glyoxalase I (Glo1)*

Methylglyoxal and other 2-ketoaldehydes are naturally produced compounds, but they are toxic due to their electrophilic reactivity with biological molecules leading to advanced glycation end-products. The glyoxalase enzyme system converts these molecules into D-hydroxyacids in a three-step sequence: the substrate initially reacts reversibly and non-enzymatically with glutathione (γ-glutamyl-L-cysteinylglycine, GSH) or other intracellular thiol, glyoxalase I (abbreviated Glo1 here, but sometimes referred to as GlxI) isomerizes the hemithioacetal intermediate to form the corresponding thioester, such a *S*-D-lactoylglutathione, via a *cis*-enediolate intermediate (Fig. 14.5a), and glyoxalase II (Glo2) catalyzes its hydrolysis to obtain the product and regenerate the thiol (Honek 2015). Of interest for this chapter, Glo1 is a nickel-containing enzyme in some microorganisms (Honek 2017).

Glo1 from humans, yeast, and some bacteria is a zinc-dependent enzyme (Honek 2015, 2017), thus it came as a surprise to find the zinc-bound *E. coli* protein is inactive while the nickel-bound enzyme exhibits maximal activity (Clugston et al. 1998). Structural studies of *E. coli* Glo1 revealed a homodimer with its two active sites positioned at the interface of the subunits (Fig. 14.6a), closely resembling the structure of the human enzyme (He et al. 2000). Each nickel of *E. coli* Glo1 coordinates His5 and Glu56 from one subunit, His74′ and Glu122′ from the other subunit, and two water molecules, mimicking the octahedral zinc site of the human enzyme. The lack of activity for zinc-bound *E. coli* Glo1 arises from a switch to trigonal bipyramidal geometry for the metal, as shown by the crystal structure and XAS analysis (Davidson et al. 2000, 2001; He et al. 2000). These findings are consistent with the need for substrate to coordinate the metal binding site in a bidentate manner for the reaction to occur. Several other bacterial Glo1 enzymes utilize nickel including those from the important pathogens *Y. pestis*, *P. aeruginosa*, and *Neisseria meningitis* (Sukdeo et al. 2004), the solvent-producing bacterium *Clostridium acetobutylicum* (Suttisansanee et al. 2011), and the soil-dwelling

**Fig. 14.5** (continued) Quercetin 2,4-dioxygenase (QueD). (**d**) Superoxide dismutase (SOD). (**e**) Urease. (**f**) Hydrogenase. (**g**) Carbon monoxide dehydrogenase (CODH). (**h**) Acetyl-CoA synthase/decarbonylase (ACS). (**i**) 2-Hydroxyacid racemase/epimerase (HAR/E). (**j**) Methyl coenzyme M reductase (MCR)

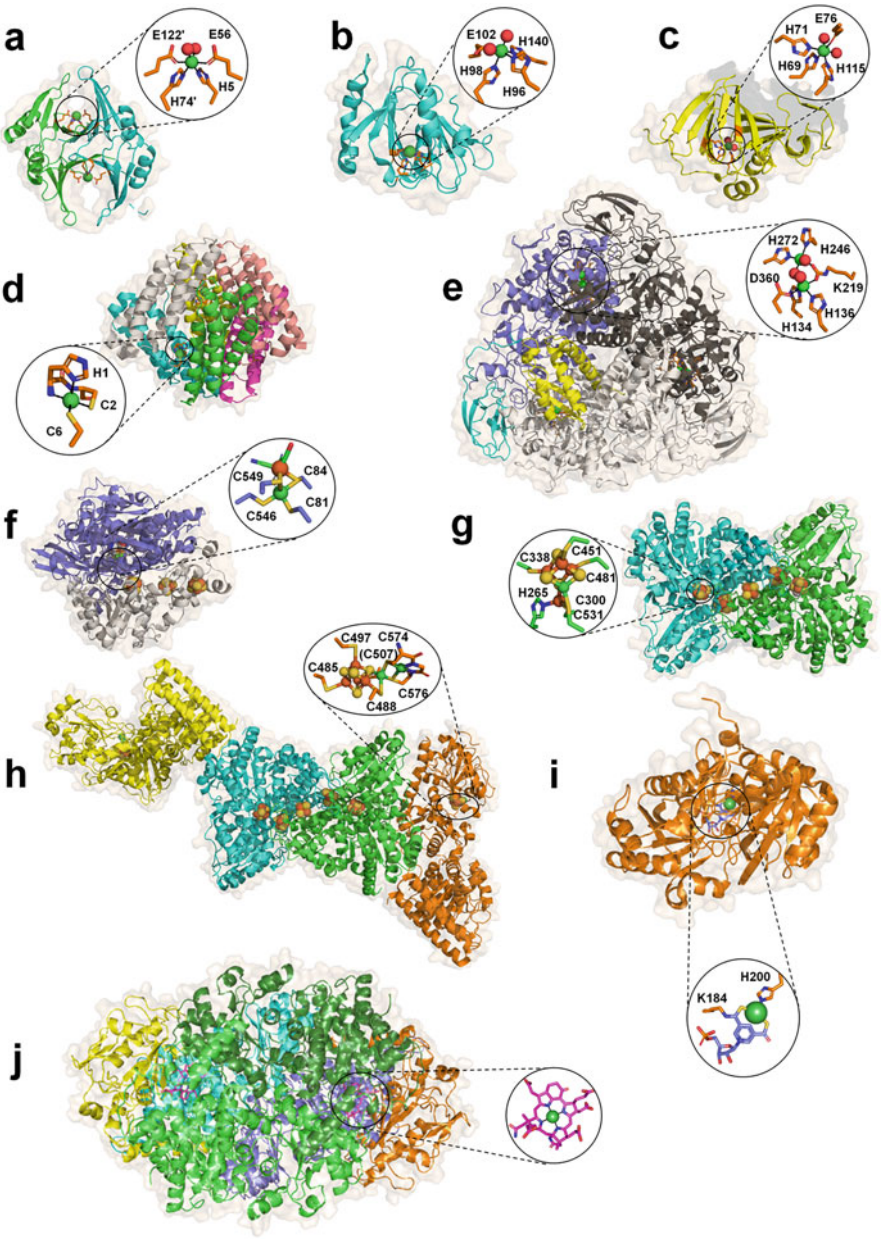


**Fig. 14.6** Structures of nickel-dependent enzymes and expanded views of their active sites. (**a**) *E. coli* glyoxalase homodimer (PDB ID 1f9z) showing a bridging nickel site bound to four side chains and two waters. (**b**) Acireductone dioxygenase of *K. oxytoca* monomer (PDB ID 1zrr) showing the nickel atom bound to four side chains and two waters. (**c**) Quercetin 2,4-dioxygenase from *Streptomyces* sp. strain FLA (PDB ID 5flh) with nickel bound to four side chains and two waters. (**d**) Homohexameric superoxide dismutase of *Streptomyces coelicolor* (PDB ID 1t6u) with nickel bound to the N-terminal amine, an amide, and three side chains. (**e**) Urease from *Klebsiella*

actinomycete *S. coelicolor* (Suttisansanee and Honek 2019). The structure of the *C. acetobutylicum* enzyme demonstrated the conformational flexibility of the enzyme, with domain swapping allowing for metal coordination by side chains that all derive from the same subunit (Suttisansanee et al. 2011). *S. coelicolor* Glo1 is of special interest because it uses mycothiol, 1-D-myo-inositol-2-(*N*-acetyl-L-cysteinyl)amido-2-deoxy-α-D-glucopyranoside, instead of glutathione in the reaction. An alternate thiol known as trypanothione, $N^1$,$N^8$-bis(L-γ-glutamyl-L-hemicysteinyl-L-glycyl)spermidine, is used by the enzymes from the eukaryotic protozoa *Leishmania major*, *Leishmania donovani*, and *Trypanosoma cruzi*, which also depend on nickel for activity (Ariza et al. 2006; Greig et al. 2006; Padmanabhan et al. 2005; Vickers et al. 2004). The mechanism by which nickel is specifically incorporated into Glo1 is unknown, and no auxiliary proteins have been shown to facilitate its biosynthesis.

### *14.4.2 Acireductone Dioxygenase (ARD)*

ARD catalyzes a key step in the methionine salvage cycle by converting 1,2-dihydroxy-3-keto-5-(thiomethyl)pent-1-ene (acireductone) to formate and 2-keto-4-methylthiobutyrate (KMTB) (Fig. 14.5b). KMTB is subsequently transaminated to form methionine, an amino acid and a precursor of *S*-adenosylmethionine (AdoMet). Among several cellular metabolic transformations that utilize AdoMet, polyamine biosynthesis produces methylthioadenosine (MTA). MTA is transformed by a series of reactions to regenerate acireductone, thus conserving the valuable sulfur atom in these metabolites. In 1993, a bacterial enzyme was purified that uses acireductone as substrate, but rather than producing KMTB it generates carbon monoxide, formate, and 3-methylthiopropionate (MTP) (Wray and

**Fig. 14.6** (continued) aerogenes (PDB ID 1fwj) with one copy of each of three types of subunits colored and the other two copies shown in light and dark gray (see text for a description of non-$(UreABC)_3$ aggregation states) along with its dinuclear nickel site, coordinating residues, and three waters. (**f**) Heterodimeric [NiFe] hydrogenase from *Desulfovibrio vulgaris* Miyazaki F (PDB ID 4u9h) with its [NiFe] cluster in the $H_2$-reduced state, four coordinating side chains, three diatomic iron ligands, and a bridging hydride atom. (**g**) *Rhodospirillum rubrum* carbon monoxide dehydrogenase homodimer (PDB ID 1jqk) containing an exposed [4Fe-4S] D-cluster bridging the subunits, a [4Fe-4S] B-cluster within each subunit, and the two [1Ni-4Fe-4S] C-clusters. (**h**) The $\alpha_2\beta_2$ acetyl-CoA synthase/decarbonylase from *Clostridium autoethanogenum* (PDB ID 6ytt) with a central CODH component shown as in (**g**) and the terminal ACS components containing the [4Fe-4S]-Ni-Ni A-cluster. (**i**) Monomeric lactate racemase from *Lactobacillus plantarum* (PDB ID 5huq) as an example of a 2-hydroxyacid racemase/epimerase with its covalently tethered nickel-pincer nucleotide cofactor. (**j**) The $(\alpha\beta\gamma)_2$ methyl coenzyme M reductase from *Methanothermobacter marburgensis* (PDB ID 1mro) with its coenzyme F430 cofactor. For each protein, the different subunits are shown in cartoon view in different colors and with semi-transparent surfaces. Key residues and diatomic ligands are shown as sticks. Spheres are shown for nickel (green), water molecules (red), iron (brown), and inorganic sulfur (yellow)

Abeles 1993). Six years later this enzyme from *K. oxytoca* was shown to be a metal-substituted ARD (Dai et al. 1999). Thus, ARD catalyzes two distinct reactions depending on the identity of the metal that is bound: it produces KMTB when possessing iron and generates MTP when coordinating nickel. The purpose of the off-cycle pathway is unknown, but the observed partial nickel occupancy of the protein from wild-type cells suggests this reaction is physiologically relevant (Deshpande et al. 2017).

The nickel in *K. oxytoca* ARD, as probed by XAS analysis, is octahedral with O/N ligands that include 3–4 His residues (Al-Mjeni et al. 2002). The solution structure of nickel-ARD from this microorganism was obtained by NMR spectroscopy using special methods to overcome issues related to the metal ion paramagnetism (Pochapsky et al. 2002, 2008). Nickel coordinates His96, His98, Glu102, and His140, along with two water molecules (Fig. 14.6b). A crystal structure for cadmium-bound ARD from *Bacillus anthracis* indicated an essentially identical structure. NMR, XAS, and mutagenesis studies of *K. oxytoca* ARD revealed that iron binds to the same site of the protein as nickel (Chai et al. 2008; Ju et al. 2006), but ferrous ion resulted in subtle structural changes in the C-terminal region, a loop, and two helices so the two isoforms can be chromatographically separated. An extensive series of biomimetic studies have investigated the distinct chemistries in models of the active site with bound nickel versus iron [reviewed in (Deshpande et al. 2017)]. In all active forms, substrate displaces two waters from the six-coordinate metal and binds with bidentate coordination. Importantly, this binding likely results in a 6-membered ring for nickel and a 5-membered ring for iron. Subsequent reactions with oxygen generate distinct intermediates that decompose differentially to the observed products. Nothing is known about how the cell controls the metal specificity of the enzyme; e.g., no accessory proteins are known to be required for metal delivery.

### *14.4.3 Quercetin 2,4-Dioxygenase (QueD)*

Many soil fungi and bacteria decompose flavonoid plant metabolites such as quercetin (3,5,7,3′,4′-pentahydroxyflavone) via oxidative metabolism that initiates by the action of quercetin 2,4-dioxygenase or quercetinase, releasing carbon monoxide and forming 2-protocatechuoylphloroglucinolcarboxylic acid (Fig. 14.5c) (QueD). The fungal enzyme uses copper as a cofactor, whereas bacterial forms of the protein are more promiscuous in their metal ion requirements (Fetzner 2012). For example, *Bacillus subtilis* quercetinase purifies with stoichiometric manganese, but is also active with cobalt and copper (Schaab et al. 2006). Of particular interest here is QueD from *Streptomyces* sp. FLA. This dioxygenase contains nickel when isolated from the wild-type microorganism and is most active using this metal ion (Nianios et al. 2015). *Streptomyces* QueD is dimeric, with each subunit exhibiting the typical 6-stranded β-barrel cupin fold (Fig. 14.6c) (Jeoung et al. 2017). Nickel binds to three histidine and one glutamic acid, with additional coordination by two water

molecules. The C3 hydroxyl group of the substrate displaces one of the waters and binds to the metal ion. The second water molecule is lost upon binding of oxygen which exhibits side-on coordination (Jeoung et al. 2017). No information is available regarding how the protein specifically binds nickel.

### *14.4.4 Superoxide Dismutase (SOD)*

The superoxide anion, $O_2^-$, is both a reactive oxygen species and a cellular signaling compound (Wang et al. 2018). To limit the internal levels of this compound, cells utilize one or more superoxide dismutases (Fig. 14.5d) or a superoxide reductase (an enzyme that reduces this molecule to $H_2O_2$ and is not discussed further) (Abreu and Cabelli 2010; Sheng et al. 2014). Biology has evolved three types of SODs with independent sequences, structures, and metallocenters; i.e., the copper/zinc SODs, the manganese- or iron-containing SODs, and the nickel-containing SODs. This section describes the discovery, properties, structure, and activation of the latter enzymes (Campeciño and Maroney 2017).

In 1996, the first examples of nickel-containing SODs were purified from *Streptomyces seoulensis* IMSNU-1 and *S. coelicolor* ATCC 10147 (Kim et al. 1996; Youn et al. 1996a). These enzymes possess near stoichiometric amounts of nickel (0.74 equivalents per 13.4-kDa subunit) and, unlike Glo1 or ARD, exhibit distinct spectral properties associated with their metallocenters. For example, the ultraviolet-visible (UV-vis) spectrum of nickel SOD possesses an absorption maximum near 380 nm, a broad peak near 530 nm, and the typical protein-derived electronic transitions. More remarkable, the nickel-containing SOD exhibits an electron paramagnetic resonance (EPR) spectrum with *g* values of 2.304, 2.248, and 2.012, where the latter component is split into a triplet (Youn et al. 1996a). This spectrum was attributed to a low spin ($S = ½$) $Ni^{3+}$ with an axial N-ligand leading to hyperfine splitting of the high-field feature. *S. griseus* possesses both a nickel-containing SOD, with properties essentially identical to that just described (0.89 Ni/13.0-kDa subunit, analogous UV-vis and EPR spectra), and an iron-containing SOD (Youn et al. 1996b). *S. coelicolor* also possesses both types of SOD, and their synthesis was found to be regulated by nickel (Kim et al. 1996). Analysis of a variety of *Streptomyces* isolates from clinical and soil samples demonstrates the universality of nickel-dependent SODs in this genus, with many strains also having iron-dependent activity (Leclere et al. 1999). Furthermore, a phylogenetic analysis demonstrates that *sodN*, the gene encoding these enzymes, is distributed widely in actinomycetes and cyanobacteria, along with being present in some gammaproteobacteria, bacteriodetes, planctomycetes, deltaproteobacteria, and even two marine eukaryotes (Dupont et al. 2008). Curiously, a *Mycobacterium* sp. has two copies of *sodN*, though it is unknown if either is functional.

Analysis of *S. coelicolor sodN* indicates ninefold enhanced transcription in the presence of nickel and shows that it encodes a 14-residue-extended precursor protein lacking activity (Kim et al. 1998b). Expression of *sodN* in *E. coli* provides only the

longer version of the protein with no activity, whereas expression of a truncated gene yields small levels of SOD activity (Kim et al. 1998b). Transcription of the gene encoding the iron-containing SOD, *sodF*, also is regulated at the transcriptional level by nickel, but in this case the transcript levels are reduced by the presence of this metal (Chung et al. 1999; Kim et al. 1998a). The repression of *sodF* in *S. griseus* is accomplished by a complex of SrnR, a nickel sensor, and SrnQ (Sect. 14.2.1.3) (Kim et al. 2003b). In addition, the nickel-bound sensor Nur acts as a repressor of *sodF* and an activator of *sodN* in *S. coelicolor* (Sect. 14.2.1.4) (Ahn et al. 2006; An et al. 2009).

Initial structural studies of the nickel-containing SOD focused on XAS of the *S. seoulensis* enzyme, revealing a five-coordinate metal site with about three sulfur donors, one nitrogen donor, and a nitrogen or oxygen donor (Choudhury et al. 1999). Reduction of nickel by dithionite results in loss of a nitrogen or oxygen donor, suggesting ligand dissociation. EPR spectra for the recombinant protein purified from *E. coli* with truncated *S. coelicolor sodN* has the same appearance as the wild-type enzyme, whereas the H1Q variant protein spectrum is altered; this result is consistent with His1 serving as a nickel ligand (Bryngelson et al. 2004). Studies comparing the XAS and magnetic circular dichroism spectra of the wild-type protein with variants involving Cys2 and Cys6 confirmed these residues also coordinate the metal (Johnson et al. 2010; Ryan et al. 2010). A detailed understanding of the nickel SOD metallocenter and the overall protein architecture is derived from crystal structures for the *S. seoulensis* (Wuerges et al. 2004) and *S. coelicolor* (Barondeau et al. 2004) enzymes (Fig. 14.6d). The proteins from both sources reveal nearly identical hexamers of 4-helix bundle monomers, as expected for the almost identical sequences. Nickel binds to what has been termed a "nickel-hook motif", which requires protein truncation. Planar coordination of the metal is provided via the N-terminal amine, the backbone amide of the second residue, and the side chains of Cys2 and Cys6. This coordination environment is thought to lower the reduction potential of the metal by over 1 V, allowing it to be capable of catalyzing the dismutation reaction. The oxidized form of the protein also includes His1 as an axial ligand, but this ligand dissociates upon reduction (Barondeau et al. 2004; Wuerges et al. 2004). Several other nearby residues help to stabilize these interactions, including Pro5 that is present in *cis* configuration, but the region is unfolded in the absence of the metal.

Genomic sequence analyses were used to identify a gene adjacent to *sodN* in *Prochlorococcus marinus* MIT9313 that was hypothesized, then shown, to encode a protease specific for the N-terminus of SOD, as needed for enzyme activation (Eitinger 2004). The product of *sodX* is an SOD-specific peptidase that allows for generation of active SOD activity in *E. coli* cells co-expressing the *P. marinus sodN*. Bioinformatics studies have shown that most, but not all, *sodN* genes are adjacent to *sodX* (Dupont et al. 2008). Another protein, CbiXhp, had been proposed to function during activation of nickel-containing SOD in *S. seoulensis* (Kim et al. 2003a). This protein, named on the basis of its sequence similarity to cobaltochelatase (CbiX) of *Bacillus megaterium*, was purified by its ability to bind to nickel-nitrilotriacetic acid resin using a histidine-rich sequence at its C-terminus. Co-expression of the

*S. seoulensis* genes encoding CbiXhp and SodN in *Streptococcus lividans* leads to greater levels of SOD activity than for expression of only *sodN*. It is possible this protein functions in nickel storage or as a nickel metallochaperone; however, no further analysis of *S. seoulensis* CbiXhp has been reported and homologs to this gene are not associated with *sodN* of other microorganisms. Thus, it is likely the enhanced SOD activity noted in those studies was fortuitous.

### *14.4.5 Urease*

Urease and its substrate urea hold a special place in the history of science. The Dutch botanist Herman Boerhaave first isolated urea from urine in ~1727, although the French chemist Hilaire Marin Rouelle is often credited with the discovery of this substance in 1773 (Kurzer and Sanderson 1956). The name urea was coined by Antoine Francis comte de Fourcroy and Louis Vauquelin, who studied the compound in 1799 (Fourcroy and Vauguelin 1799). Urea is the first organic molecule ever synthesized from inorganic materials, an accomplishment of the German chemist Friedrich Wöhler in 1828 (Wöhler 1828). Others had shown that urea in urine transforms into carbonate and ammonia, but Louis Pasteur reported in 1860 that a living organism is responsible for this alkaline fermentation (Pasteur 1860). Shortly thereafter Philippe van Tieghem isolated a bacterium, later called *Micrococcus ureae*, that catalyzes this decomposition reaction (van Tieghem 1984), and in 1890 Pierre Miguel described several additional "ureolytic" microorganisms and termed the transforming agent "urease" (Miquel 1890). The next few decades included intense discussions of what physical components confer enzyme activities. Key to answering this question was the discovery by Takeuchi in 1909 that soybean, among other plants, possesses large amounts of urease activity (Takeuchi 1909). Working with seeds of the jack bean plant in 1929, James B. Sumner purified urease by crystallization, the first enzyme ever crystallized, hence demonstrating that enzymes are proteins (Sumner 1926). Nearly 50 years later, Bert Zerner and colleagues showed that jack bean urease contains nickel (Dixon et al. 1975), therefore becoming the first identified nickel-dependent enzyme. Bacterial ureases also contain nickel, as first demonstrated for the enzyme from *Arthrobacter oxydans* (Schneider and Kaltwasser 1984). The following paragraphs describe the reaction, distribution, structures, and biosynthesis of microbial ureases.

#### 14.4.5.1 Urease Functional Significance

Urea is an important metabolite in the global nitrogen cycle and its hydrolysis by urease (Fig. 14.5e) has far-reaching consequences. The substrate urea is produced industrially at a vast scale (>200 million metric tons per year) for use as a nitrogen-based fertilizer. When such fertilizers are released into the environment, urea hydrolysis by plant and microbial ureases produces ammonium ions for use by

crops and raises the pH due to consumption of protons. Rapid metabolism of fertilizer urea may damage agricultural crops due to ammonia toxicity or alkalinity, and these conditions volatilize the ammonia causing loss of this valuable nitrogen source (Mobley and Hausinger 1989). Several biological sources of urea exist, with the most prominent being the arginase-catalyzed hydrolysis of arginine. Arginase is found in many microorganisms and plays an essential role in mammals, where it functions to detoxify ammonia via the urea cycle that produces the urea found in urine. Urea metabolism by microorganisms can have detrimental medical consequences (Burne and Chen 2000; McLean et al. 1988; Mobley and Hausinger 1989; Mobley et al. 1995b). Ureolytic pathogens of the urinary tract are responsible for a substantial fraction (10–15%) of urinary stones due to high pH-induced precipitation of struvite and apatite salts (Flannigan et al. 2014; Griffith et al. 1976). The same process accounts for encrustation of catheters (Norsworthy and Pearson 2017). Infections of the urinary tract also can lead to pyelonephritis, the acute inflammation of the kidney and its pelvis (Nielubowicz and Mobley 2010). Peptic ulcers, gastritis, and even stomach cancers are associated with colonization of the stomach lining by *H. pylori*, a pathogen containing very high levels of urease (Atherton 2006; Covacci et al. 1999; Kusters et al. 2006; Wroblewski et al. 2010). Enzymatic metabolism of urea diffusing into the stomach from the bloodstream consumes protons immediately around the microorganism, thus acting as a buffer against the low pH environment (Sachs et al. 2002). Also of interest, high concentrations of ammonia produced by microbial metabolism of urea is implicated in cases of ammonia encephalopathy, hepatic encephalopathy, and hepatic coma (Mobley and Hausinger 1989; Mobley et al. 1995b; Rai et al. 2015).

Microbial urease activity is widespread in the environment, with the enzyme distributed in selected bacteria, archaea, yeasts, filamentous fungi, and algae (Mobley and Hausinger 1989). Its regulation varies with the source (Collins and D'Orazio 1993). For example, many microorganisms increase urease production during times of nitrogen starvation so as to utilize urea as a nitrogen source. Some strains that infect the urinary tract induce urease synthesis in the presence of elevated concentrations of urea. Furthermore, still other species exhibit generally constant levels of the enzyme. Urease typically is localized in the cytoplasm; however, this protein is quite stable and maintains its activity when released into the environment upon cell death, leading to the incorrect notion that urease is secreted by microbes (Marcus and Scott 2001).

#### 14.4.5.2 Urease Structure

The structure of urease exhibits one of four architectures, depending on the source. Most bacterial forms of the enzyme contain three types of subunits (UreA, UreB, and UreC), each present in three copies, i.e. $(UreABC)_3$, with the entire structure containing three dinuclear nickel active sites as first elucidated for urease from *Klebsiella aerogenes* (Fig. 14.6e) (Jabri et al. 1995; Pearson et al. 1997). The extensively studied enzyme from *Sporosarcina* (formerly *Bacillus*) *pasteurii* has

an analogous structure (Benini et al. 1999). *Yersinia enterocolitica* urease also has three similar types of subunits, but structures obtained by crystallography (unpublished) and cryo-electron microscopy (Righetto et al. 2020) have shown these subunits assemble into a $[(UreABC)_3]_4$ supermolecular spherical structure containing 12 active sites. Similarly, crystallography and cryo-electron microscopy studies indicate a dodecamer spherical structure is present in *H. pylori* and other *Helicobacter* species (Cunha et al. 2021; Ha et al. 2001); however, in these cases only two types of subunits are present with the smaller subunit (UreA) corresponding to a fusion of UreA plus UreB of most bacteria, and the larger subunit (UreB) corresponding to UreC in other genera. This $[(UreAB)_3]_4$ situation also occurs for a dinuclear iron-containing urease from *Helicobacter mustelae* (Carter et al. 2011). In eukaryotes, a single type of subunit contains sequences homologous to each of the bacterial subunits. Three copies of this fused subunit assemble into a trimer, and two trimers stack together back-to-back forming a hexamer with six active dinuclear nickel active sites. Although no microbial example of such a structure has been reported, the architecture of fungal ureases probably resembles that of the jack bean enzyme (Balasubramanian and Ponnuraj 2010). The active sites of all ureases are identical, with their two nickel metal ions bridged by a carbamylated lysine residue, two histidine residues binding one of those nickel ions, and two histidine residues plus an aspartic acid residue coordinated to the second nickel ion. Each metal ion has a terminally-bound water and a third water bridges the two nickel ions, thus providing 5-coordinate and 6-coordinate geometries for the dinuclear site. The reaction mechanism of the enzyme metallocenter was recently reviewed (Mazzei et al. 2020).

#### 14.4.5.3 Urease Maturation

The bacterial genes encoding the urease subunits typically are clustered with genes encoding accessory proteins that are required for urease activation (Mobley et al. 1995b). For example, *ureDABCEFG* of *K. aerogenes* encodes the three-subunit urease and four proteins (UreD, UreE, UreF, and UreG) needed to obtain a mature enzyme (Lee et al. 1992; Mulrooney and Hausinger 1990). Similarly, *ureABIEFGH* of *H. pylori* codes for the two-subunit enzyme, a proton-gated urea channel (UreI) (Weeks et al. 2000), and the same four maturation components (note: *Helicobacter* UreH is homologous to UreD of other bacteria) (Cussac et al. 1992; Labigne et al. 1991). In other microorganisms, the order of these genes may vary and additional genes may interrupt or flank the cluster such as those encoding ABC-type nickel transporters (Sect. 14.2.2.2) in *A. pleuropneumoniae* (Bossè et al. 2001) and *S. salivarius* 57.1 (Chen and Burne 2003) or encoding nickel permeases (Sect. 14.2.2.3) such as UreH and UreJ in *Bacillus* TB-90 (Maeda et al. 1994) and *B. bronchiseptica* (McMillan et al. 1998), respectively. In addition, the products of non-contiguous genes may facilitate urease activation in some species by assisting in nickel uptake, such as NixA in *H. pylori* (Wolfram and Bauerfeind 2002) (Sect. 14.2.2.3), or nickel delivery, such as HypA and HypB in the same organism (Olson

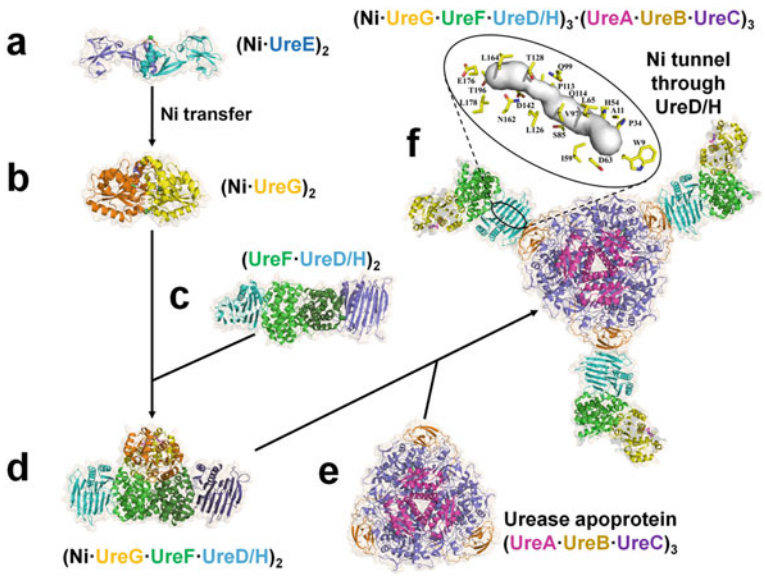


**Fig. 14.7** Urease maturation pathway. (**a**) UreE is a homodimeric nickel metallochaperone, as shown for the protein from *Sporosarcina pasteurii* (PDB ID 4l3k). (**b**) UreE forms complexes with and transfers nickel to its cognate UreG, as depicted for the homodimeric UreG from *Klebsiella pneumoniae* with bound nickel and GMPNP (PDB ID 5xkt). (**c**) UreG binds to a complex of UreF and UreD/H, as illustrated for the $(UreF{\cdot}UreD)_2$ complex of *Helicobacter pylori* (PDB ID 3sf5). (**d**) The resulting complex of three accessory proteins is illustrated by the GDP-bound $(UreG{\cdot}UreF{\cdot}UreD)_2$ from *H. pylori* (PDB ID 4hi0). (**e**) The accessory proteins bind to urease apoprotein, shown for $(UreA{\cdot}UreB{\cdot}UreC)_3$ of *Klebsiella aerogenes* (PDB ID 1kra). (**f**) A model of the resulting complex has (UreG·UreF·UreD/H) bound via the UreD/H component to UreB of the urease apoprotein. GTP hydrolysis at UreG is coupled to release of nickel from that component, with the metal traversing a molecular tunnel through UreF and UreD (see inset) to be delivered to the nascent active site in UreC. Proteins are depicted in distinct colors using cartoon mode with semi-transparent surfaces, nickel atoms are shown as green spheres, and selected side chains along with nucleotides are indicated by sticks

et al. 2001). The biosynthesis of active urease almost universally requires the participation of UreD/H (two designations for the same protein), UreE, UreF, and UreG (Farrugia et al. 2013b; Nim and Wong 2019). One dramatic exception to this statement is urease of *B. subtilis* which possesses three types of subunits closely related to those of other bacterial ureases yet lacks genes related to the four urease maturation genes (Kim et al. 2005).

The urease maturation pathway (Fig. 14.7) begins with the metallochaperone or metal-delivery protein UreE. This protein from *Klebsiella aerogenes* possesses a carboxyl terminal His-rich sequence (10 of the last 15 residues) that binds multiple nickel ions (5–6 nickel per dimer, $K_d \sim 10$ μM) (Grossoehme et al. 2007; Lee et al. 1993). By inserting a stop codon into the corresponding gene, one obtains a truncated protein that lacks the His-rich region yet it still functions in urease

activation and binds ~2 nickel ions per dimer (Colpas et al. 1998, 1999; Colpas and Hausinger 2000). The His-rich region is not a universal component of UreE as demonstrated by the *H. pylori* protein (Musiani et al. 2004). Crystal structures of UreE (Fig. 14.7a) are known for the proteins from *K. aerogenes* (Song et al. 2001), *S. pasteurii* (Remaut et al. 2001; Zambelli et al. 2013), and *H. pylori* (Banaszak et al. 2012; Shi et al. 2010). In all cases, the protein exists as a homodimer with each subunit possessing a metal-binding domain and a separate domain that is disposable for urease maturation (Mulrooney et al. 2005). The essential nickel-binding site is located at the interface of the UreE subunits (Colpas et al. 1999; Colpas and Hausinger 2000) where it is bound by complementary histidine residues and additional ligands in a disordered region near the carboxyl terminus (Banaszak et al. 2012; Zambelli et al. 2013). Secondary metal-binding sites may "feed" the metal into the essential UreE interfacial site for subsequent transfer to urease (Colpas et al. 1999; Grossoehme et al. 2007; Lee et al. 1993). In *H. pylori*, HypA·UreE is known from chemical cross-linking of the proteins (Benoit et al. 2007). This complex presumably reflects the previously mentioned *H. pylori*-specific enhancement of urease activity by HypA (Olson et al. 2001). Evidence indicates that nickel is transferred from HypA to UreE via a HypA·$(UreE)_2$ complex (Hu et al. 2018; Yang et al. 2014), with HypA and UreG competing for the UreE binding site (Benoit et al. 2012).

The second critical component in urease maturation is UreG. This protein, a nickel-binding GTPase, has been purified and characterized from a wide range of organisms, including the bacteria *K. aerogenes* (Boer et al. 2010; Martin-Diaconescu et al. 2017; Moncrief and Hausinger 1997), *Klebsiella pneumoniae* (Yuen et al. 2017), *S. pasteurii* (D'Urzo et al. 2014; Zambelli et al. 2005), *H. pylori* (Fong et al. 2013; Yang et al. 2015; Zambelli et al. 2009), *M. tuberculosis* (Zambelli et al. 2007b), and the archaea *Methanocaldococcus jannaschii* and *Metallosphaera sedula* (Miraula et al. 2015). Whereas some UreG proteins are monomeric in dilute solution (Boer et al. 2010; Moncrief and Hausinger 1997), others are dimers (Zambelli et al. 2005, 2007b), and still others exhibit a monomer-to-dimer equilibrium with the latter species stabilized by addition of zinc (D'Urzo et al. 2014; Miraula et al. 2015; Zambelli et al. 2009). All UreG species bind zinc or nickel, but the number of equivalents bound and the measured affinities differ for each protein [reviewed in Martin-Diaconescu et al. (2017)]. The structure of an N-terminally truncated UreG from *K. pneumoniae* in the presence of nickel and the GTP analogue GMPPNP reveals a dimer, with the critical nickel ion coordinated symmetrically by the conserved Cys-X-His motifs at the interface of the subunits (Fig. 14.7b) (Yuen et al. 2017). Additional nickel ions associate with each of the two GMPPNP molecules, corresponding to the more typical Mg·GTP interaction. Despite the ability of isolated *K. pneumoniae* UreG to crystallize into a distinct structure (Yuen et al. 2017) and the reported structure of a protein complex including *H. pylori* UreG (Fong et al. 2013), extensive evidence suggests that the *S. pasteurii* and archaeal proteins are intrinsically disordered (Miraula et al. 2015; Palombo et al. 2017; Zambelli et al. 2005, 2012). The significance of this finding is unclear.

Several studies have demonstrated an interaction between UreG and UreE, consistent with the two proteins transiently sharing coordination of the nickel. For example, nickel stimulates the interaction between the *K. aerogenes* proteins, forming a UreG·Ni·$(UreE)_2$ complex (Boer et al. 2010). In contrast, a $(UreG)_2$·Ni·$(UreE)_2$ complex was identified for the *S. pasteurii* proteins (Merloni et al. 2014). Using the *H. pylori* components, $(UreG)_2$·Zn·$(UreE)_2$ (Bellucci et al. 2009) along with UreG·Ni·$(UreE)_2$ and $(UreG)_2$·Ni·$(UreE)_2$ were observed, with the latter found to predominate when Mg·GTP was present (Yang et al. 2015). No structure is available for any complex of UreE and UreG, but a model was proposed for the *H. pylori* species (Bellucci et al. 2009). A consensus hypothesis has emerged that nickel-loaded UreE transfers nickel to UreG by direct interaction of these protein components.

In the next step, UreG interacts with UreF and UreD/H to form a complex that has been characterized for components from *H. pylori* and *K. aerogenes*. Most notably, the crystal structure of *H. pylori* $(UreG·UreF·UreD)_2$ is available with GDP bound to UreG (Fig. 14.7d) (Fong et al. 2013), as well as structures of the precursors $(UreF·UreD)_2$ (Fig. 14.7c) (Fong et al. 2011) and $(UreF)_2$ (Lam et al. 2010). In addition, chemical cross-linking and ion mobility-mass spectrometric analysis of *K. aerogenes* proteins identified $(UreG·UreF·UreD\text{-}MBP)_2$, where UreD-MBP is a fusion of UreD with the maltose-binding protein (MBP, used to enhance solubility) (Carter and Hausinger 2010). This *K. aerogenes* complex binds to the cognate urease apoprotein, $(UreA·UreB·UreC)_3$ (Fig. 14.7e), to form $(UreG·UreF·UreD\text{-}MBP)_3$·$(UreA·UreB·UreC)_3$ (Fig. 14.7f) (Eschweiler et al. 2018; Farrugia et al. 2013a). The *K. aerogenes* apoprotein is identical in structure to the holoprotein, except for the absence of nickel and the lack of carbamylation at the active site lysine (Jabri and Karplus 1996). The connection between the accessory protein heterotrimer and urease occurs via UreD and UreB as shown by production and characterization of a $(UreD)_3$·$(UreA·UreB·UreC)_3$ complex (Park et al. 1994). Similarly, co-expression of *ureF*, *ureD*, and *ureABC* allows for production of $(UreF·UreD)_3$·$(UreA·UreB·UreC)_3$ (Moncrief and Hausinger 1996). Significantly, incubation of $(UreF·UreD)_3$·$(UreA·UreB·UreC)_3$ with UreG, UreE, and nickel resulted in GTP-dependent generation of near fully active urease (Soriano and Hausinger 1999; Soriano et al. 2000). No structure is reported for any accessory protein bound to the urease apoprotein.

A current model for activation of bacterial urease (Fig. 14.7e) is derived by merging studies of the *K. aerogenes* and *H. pylori* urease systems. From ion mobility-mass spectrometry studies (Eschweiler et al. 2018; Farrugia et al. 2013a), it appears that the dimeric $(UreG·UreF·UreD)_2$ complex dissociates to monomeric UreG·UreF·UreD units when forming the $(UreG·UreF·UreD)_3$·$(UreA·UreB·UreC)_3$ apoprotein complex. Chemical cross-linking studies indicate specific interactions between UreD and UreB, requiring the urease subunit to undergo a hinge-like motion that provides better access to the nascent active site, and small angle X-ray scattering studies are consistent with the overall structure of this species (Chang et al. 2004; Quiroz-Valenzuela et al. 2008). Computational studies using the *H. pylori* $(UreH·UreF·UreG)_2$ crystal structure (Fong et al. 2013) and a homology model for

*K. aerogenes* UreG·UreF·UreD (Farrugia et al. 2015) indicated the likely existence of a molecular channel for nickel transfer through UreF and UreH/D. Support for such a tunnel was obtained for the *K. aerogenes* components; UreD variants predicted to occlude the tunnel abolished the ability to activate the urease apoprotein (Farrugia et al. 2015). Although the role of GTP hydrolysis during activation remains unclear, a reasonable hypothesis is that nucleotide hydrolysis is coupled to the release of nickel into the tunnel. Diffusion of the metal ion through the molecular channel provides access to the nascent active site that otherwise is buried within UreC. Coordination of nickel to the active site residues leads to conformational changes resulting in release of the accessory proteins.

## *14.4.6 [NiFe] Hydrogenase*

Hydrogenases catalyze the reversible oxidation of dihydrogen gas to form two protons and two electrons (Fig. 14.5f) (Adams et al. 1981; Peters et al. 2015; Vignais et al. 2001; Vignais and Billoud 2007). In some microorganisms, the electrons derived from hydrogen are used to reduce oxygen, sulfate, carbon dioxide, nitrate, or other electron acceptors, and this coupling serves as a means to provide energy to the cell. In particular microbes, the reverse reaction is used to eliminate excess cellular reducing potential derived by fermentation or photosynthesis. Thus, hydrogenases play central roles in the energy metabolism of many microorganisms. Three main enzyme classes are differentiated on the basis of their metallocenters: [NiFe] hydrogenases, [FeFe] hydrogenases, and iron-only hydrogenases. Only the [NiFe] hydrogenases are relevant to this chapter.

### 14.4.6.1 Types and Structures of [NiFe] Hydrogenases

All of the [NiFe] hydrogenases possess at least two types of subunits: a large subunit (~60 kDa) containing nickel plus iron at a dinuclear [NiFe] active site cluster and a small subunit (~30 kDa) typically containing three iron-sulfur clusters that shuttle electrons between the [NiFe] active site and an external electron carrier. The names of the genes encoding the subunits are quite variable in different microorganisms with further nomenclature complications arising in microorganisms possessing multiple [NiFe] hydrogenases. Four distinct functional groupings and 22 subgroups of these enzymes have been identified on the basis of sequence analyses (Greening et al. 2016; Peters et al. 2015; Vignais and Billoud 2007).

Group 1 [NiFe] hydrogenases are periplasmic or membrane-associated and utilize $H_2$ for energy generation. Many periplasmic, heterodimeric enzymes have been characterized; e.g., the first [NiFe] hydrogenase to be structurally elucidated was the heterodimeric enzyme from *Desulfovibrio gigas* (Volbeda et al. 1995). The large subunit contains the deeply buried [NiFe] center (this site will be described separately, below), and the small subunit contains a linear arrangement of [4Fe-4S],

[3Fe-4S], and [4Fe-4S] clusters for electron transfer with a partner electron carrier located in the membrane. Similar heterodimeric structures are characterized for [NiFe] hydrogenases from other sulfate-reducing bacteria including *Desulfovibrio desulfuricans*, *Desulfovibrio vulgaris* Miyazaki F (Fig. 14.6f), *Desulfomicrobium norwegicum* (formerly *D. baculatum*), *D. vulgaris* Hildenborough, and *Desulfovibrio fructosovorans* (Garcin et al. 1999; Higuchi et al. 1997; Marques et al. 2010; Matias et al. 2001; Volbeda et al. 2005). Duplication of this architecture is seen in several non-sulfate-reducing bacteria such as *Hydrogenovibrio marinus*, the photosynthetic purple-sulfur bacterium *Allochromatium vinosum*, and an enzyme with very high affinity for $H_2$ from the actinobacterium *C. necator* (Ogata et al. 2010; Schäfer et al. 2016; Shomura et al. 2011). Additional enzymes that operate using low concentrations of $H_2$ are found in soil bacteria such as *Streptomyces* (Constant et al. 2010, 2011) and may have similar structures.

Additional subunits beyond the dimeric enzyme are present in many other group 1 cases. For example, *E. coli* uses a membrane-bound cytochrome *b* to shuttle electrons from hydrogenase-1 into the quinone pool, which then transfers electrons to an external electron acceptor. This enzyme is encoded by *hyaAB* and the cytochrome *b* is encoded by *hyaC*, all found in the *hyaABCDEF* operon (Sargent 2016). The structure of *E. coli* hydrogenase-1 contains two copies of each hydrogenase subunit (Volbeda et al. 2012) and this $(HyaAB)_2$ unit forms a complex with a single copy of HyaC (Volbeda et al. 2013). The C-termini of each small subunit have helical extensions that interact with a four-helix bundle of the membrane-bound cytochrome *b*. The three [FeS] clusters in each small subunit [including one with an extra cysteine residue replacing an inorganic sulfide (Volbeda et al. 2012)] aligns with the heme of HyaC to facilitate electron transfer. A second group 1 [NiFe] hydrogenase in *E. coli*, hydrogenase-2, has two standard subunits encoded by *hybO* and *hybC* plus an [FeS]-containing protein in the periplasm and a membrane-associated protein, encoded by *hybA* and *hybB* respectively, all associated with the *hybOABCDEFG* operon (Sargent 2016). The structure of $(HybCO)_2$ is known and closely resembles that of $(HyaAB)_2$, but only a predicted structure is available for the $(HybCOAB)_2$ complex (Beaton et al. 2018).

Group 2 [NiFe] hydrogenases are cytoplasmic proteins that catalyze $H_2$ uptake. Four subgroupings are found, but only two are briefly mentioned here. First, the cyanobacterial enzymes (with subunits often designated HupSL) recapture the $H_2$ that is produced as a requisite side reaction of nitrogenase during its reduction of $N_2$ (Tamagnini et al. 2007). Second, $H_2$-sensing enzymes (commonly designated HupUV or HoxBC) participate in the transcriptional regulation of other hydrogenases. *C. necator* provides a paradigm for this type of [NiFe] hydrogenase system; its group 2 cytoplasmic $H_2$-sensor HoxBC is used to regulate production of the NAD-dependent, membrane-bound, HoxFUYH group 3 enzyme (see below) (Lenz and Friedrich 1998). No group 2 [NiFe] hydrogenase is structurally characterized at this time.

The group 3 [NiFe] hydrogenases typically function as bidirectional cytoplasmic enzymes that possess more than the two standard subunits. These additional components bind and transfer electrons to cytoplasmic electron carriers such as $NAD^+$,

$NADP^+$, or 8-hydroxy-5-deazaflavin (coenzyme $F_{420}$, a cofactor found primarily found in methanogenic archaea). The structure of the $F_{420}$-reducing [NiFe] hydrogenase from *Methanothermobacter marburgensis* is known from cryo-electron microscopy studies (Vitt et al. 2014). The large and small hydrogenase subunits, FrhA and FrhG, are relatively standard (except the first [4Fe-4S] is coordinated by Asp and three Cys instead of the usual four Cys). Also present is the $F_{420}$-binding component, FrhB, that contains another [4Fe-4S] (aligned with the three clusters in FrhG) and FAD that interacts with the coenzyme $F_{420}$. These three components form a spherical $(FrhABG)_{12}$ complex; i.e., a dodecamer of the heterotrimer. Such a large assemblage is not found in all group 3 members. For example, a cytoplasmic, $NAD^+$-reducing [NiFe] hydrogenase from *Hydrogenophilus thermoluteolus* Th-1 is a heterotetramer (Shomura et al. 2017). This protein complex includes the large subunit HoxH (with an extra glutamate ligand of nickel compared to the typical situation, see below), the small subunit HoxU (with a non-typical and non-linear [4Fe-4S], [4Fe-4S], [2Fe-2S] arrangement), HoxY (containing a [4Fe-4S] between the [NiFe] site and first [4Fe-4S] of the small subunit), and HoxF (possessing a [4Fe-4S] in line with two clusters in the small subunit and an FMN at the $NAD^+$-binding site). Of further interest, some enzymes in this group act in electron bifurcation reactions, such as a methanogen MvhAGD enzyme that uses $H_2$ ($E'_o = -414$ mV) to simultaneously carry out an energetically downhill reaction (the reduction of a heterodisulfide, $E'_o = -140$ mV) and an energetically uphill reaction (the reduction of a ferredoxin, $E'_o = -500$ mV) (Thauer et al. 2010).

Group 4 [NiFe] hydrogenases are complex membrane-bound enzymes, typically containing at least six types of subunits, that evolve hydrogen from cells using low potential reductants, such as carbon monoxide or formate, and often use ferredoxin as an electron carrier. The classic example of this type of enzyme is *E. coli* hydrogenase-3, encoded by *hycBCDEFGHI* where *hycEG* corresponds to the standard subunit-encoding genes. This enzyme functions as a formate hydrogenlyase to metabolize formate to $H_2$ and $CO_2$ (Sargent 2016). Closely resembling the operon sequence for hydrogenase-3 is *hyfABCGHIJ* of *E. coli*, encoding hydrogenase-4 that may also function in formate metabolism; however, hydrogenase-4 activity has not been established. Also noteworthy are group 4 enzymes that function as energy-converting hydrogenases (ECHs) that couple electron transfer to ion translocation. One example of this type of enzyme is EchABCDEF of *Methanosarcina barkeri* that utilizes the proton motive force to facilitate the thermodynamically unfavorable reduction of ferredoxin by $H_2$ (Meuer et al. 1999). Sequence analyses indicate the small subunits of these enzymes contain a single [4Fe-4S] cluster (Greening et al. 2016) although other components may provide further electron transfer sites. No structures of group 4 enzymes are available.

The active sites of all four groups of [NiFe] hydrogenases possess a [NiFe] dinuclear cluster. The structure of the heterodimeric, periplasmic enzyme from *D. gigas* first revealed this site as nickel with another metal (tentatively assigned to iron) that binds three non-protein ligands depicted at the time as water molecules (Volbeda et al. 1995). Four cysteine residues bind the nickel and two of these ligands bridge to the second metal. Follow-up studies with this protein confirmed the

identity of iron and suggested the three non-protein ligands are diatomic molecules (Volbeda et al. 1996). The nature of the iron-coordinating ligands was established from studies in which *Chromatium vinosum* [NiFe] hydrogenase was purified from cells grown on medium containing $^{13}C$ and $^{15}N$, then subjected to infrared spectroscopy (Happe et al. 1997; Pierik et al. 1999). Intense features in the 2150 to 1850 $cm^{-1}$ region demonstrate the presence of one carbon monoxide and two cyanide ligands. Subsequent studies (Ash et al. 2019; Fontecilla-Camps et al. 2007; Lubitz et al. 2014; Ogata et al. 2016; Shafaat et al. 2013; Volbeda and Fontecilla-Camps 2017), clarified the structures and properties of the [NiFe] site in enzymes from different species and in different states. Of particular interest is the active site structure of the $H_2$-reduced protein from *D. vulgaris* Miyazaki F at the remarkable resolution of 0.89 Å (Fig. 14.6f) revealing a hydride bridging the two metal ions (Ogata et al. 2015). In contrast to the typical four cysteines binding the dinuclear site, the *D. norwegicum* and *D. vulgaris* Hildenborough enzymes have a selenocysteine substituting for the C-terminal cysteine residue (Garcin et al. 1999; Marques et al. 2010). Another interesting structural variation is a [NiFe] hydrogenase from *C. necator* that binds four cyanide ligands (Van der Linden et al. 2004). The biosynthesis of the extraordinary [NiFe] site is an amazingly complicated process as described in the following paragraphs.

#### 14.4.6.2 [NiFe] Hydrogenase Maturation

Our understanding of [NiFe] hydrogenase maturation is highly dependent on genetic and biochemical studies performed in *E. coli* where investigators have shown the *hypABCDE* operon is needed for activation of hydrogenases-1, -2, and -3 (Jacobi et al. 1992; Lutz et al. 1991). The HybA-HypE proteins encoded by this operon, the non-subunit gene products encoded by the *hya*, *hyb*, and *hyc* operons, and other *E. coli* proteins all work in concert to generate active forms of the organism's three enzymes. A detailed description of these extensive studies for *E. coli*, and analogous biochemical and genetic work carried out with other microorganisms, is beyond the scope of this chapter, so the reader is referred to review articles describing the multiple insights generated by the laboratories of August Böck (Böck et al. 2006), Deborah Zamble (Lacasse and Zamble 2016; Leach and Zamble 2007), Gary Sawers (Forzi and Sawers 2007; Sawers and Pinske 2017), and others (Cheng et al. 2016; Peters et al. 2015; Sargent 2016; Senger et al. 2017). Here, I focus on a structural description of the elaborate [NiFe] hydrogenase activation process (Fig. 14.8), where much of this remarkable set of work was carried out using *Thermococcus kodakarensis* KOD1 components in the laboratory of Kunio Miki (Miki et al. 2020).

The cyanide ligands of the metallocenter are generated by a multi-step reaction sequence involving HypE and HypF. Structures are known for dimeric HypE from *T. kodakarensis* (Watanabe et al. 2007) as well as monomeric HypF proteins from this organism (Tominaga et al. 2012), *Caldanaerobacter subterraneus* (Shomura and Higuchi 2012), and (in truncated form) *E. coli* (Petkun et al. 2011). In addition, the structure is known for the transient heterotetramer $(HypE{\cdot}HypF)_2$ from

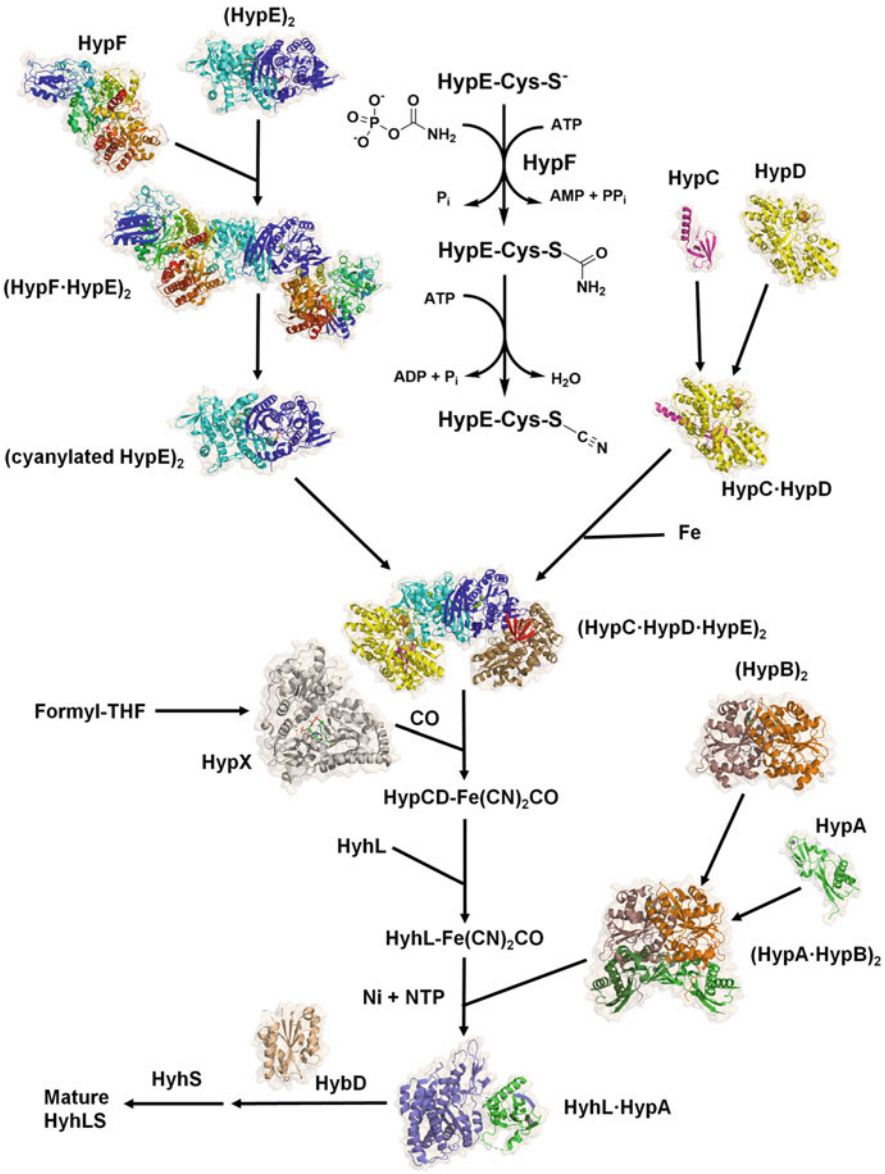


**Fig. 14.8** Hydrogenase maturation pathway. All structures are from *Thermococcus kodakarensis* except where indicated. (Upper left) The HypE homodimer (PDB ID 3wjr, cyan and dark blue) binds to monomeric HypF (PDB ID 4g9i, red to blue rainbow color to illustrate its four domains) forming the heterotetramer (HypF-HypE)$_2$ (PDB ID 3vti, from *Caldanaerobacter subterraneus* subspecies *tengcongensis* MB4). (Upper middle) HypF hydrolyzes carbamoylphosphate, adenylylates the resulting carbamate, and converts the carboxyl terminal cysteine of HypE to the carbamoylated residue (PDB ID 3wjp). HypE dehydrates this modification to generate a thiocyanylated cysteine (PDB ID 3wjq). (Upper right) Monomeric HypC (PDB ID 2z1c, maroon) and monomeric HypD (PDB ID 2z1d, yellow) generate a heterodimer (PDB ID 3vyr). Two

*C. subterraneus* (Shomura and Higuchi 2012). The four-domain HypF hydrolyzes carbamoylphosphate to form carbamate that reacts with ATP to generate carbamoyladenylate, which is used to generate a thiocarboxamide at the C-terminal cysteine residue of HypE (Reissmann et al. 2003). HypE then catalyzes an ATP-dependent dehydration reaction to yield the thiocyanate derivative of this cysteine. In addition to the non-modified HypE species, structures of the thiocarboxamide and thiocyanate forms are reported (Tominaga et al. 2013).

HypC and HypD function as the scaffold for the iron atom of the [NiFe] site. Structures are known for the individual proteins and for HypC·HypD from *T. kodakarensis* (Watanabe et al. 2007, 2012). HypC has a β-barrel domain containing the essential Cys2 residue and an α-helix extension at its C-terminus. HypD is a larger protein containing a [4Fe-4S] bound by four cysteine residues, four other redox-active cysteine residues located immediately adjacent to the cluster, and the essential Cys38 residue. The HypC·HypD heterodimer is hypothesized to bind iron (from a still unidentified source) using HypC Cys2 and HypD Cys38. Two molecules of HypC·HypD bind to the HypE homodimer, and the $(HypC{\cdot}HypD{\cdot}HypE)_2$ structure is known. The cyanide adduct of the HypE C-terminal cysteine is transferred onto the HypC·HypD-bound iron atom, presumably making use of reductive chemistry involving the [4Fe-4S] and the cysteine tetrad electron transfer components of HypD. This process is repeated twice to provide two cyanide ligands on the iron. The CO ligand is derived from formyl-tetrahydrofolate (THF) using formyl-THF decarbonylase, or HypX (Schulz et al. 2020), which was structurally defined for the protein from *Aquifex aeolicus* (Muraki et al. 2019). Studies with the *C. necator* enzyme show the formyl group is first transferred onto a tightly bound CoA molecule, with decarbonylation leading to release of CO and reformation of CoA (Schulz et al. 2020). The HypC·HypD-bound iron-$(CN)_2CO$ complex is subsequently transferred into the hydrogenase large subunit HyhL by a process that remains obscure.

**Fig. 14.8** (continued) molecules of this heterodimer bind iron and form a complex with the cyanylated HypE dimer, yielding the dimer of HypC·HypD·HypE (PDB ID 3vys). (Middle left) Monomeric HypX (PDB ID 6j0p, white, from *Aquifex aeolicus*) is a formyl-THF decarbonylase. Carbon monoxide derived from this reaction and two cyanide from cyanylated HypE become ligands to iron bound to HypC·HypD. The iron and its diatomic ligands are transferred into the hydrogenase large subunit, HyhL. (Bottom right) Dimeric HypB (PDB ID 3vx3, orange and brown) binds two molecules of monomeric HypA (PDB ID 3a43, green) to form a complex (PDB ID 5aun) with multiple nickel-binding sites. Nucleotide hydrolysis (ATP or GTP depending on the species) by this complex is coupled to nickel insertion into HyhL (slate blue) via HyhL·HypA (PDB ID 5yy0). (Bottom left) The HybD endoprotease (PDB ID 5ija, wheat) cleaves near the carboxyl terminus of HyhL causing the [NiFe] cluster to become buried in the protein and allowing for complex formation with the small subunit HyhS. Proteins are shown in cartoon depictions with semi-transparent surfaces. Metal and inorganic sulfur atoms are shown as spheres (nickel in green, zinc in grey, iron as brown, and sulfide as yellow). Selected side chains and nucleotides are illustrated in stick mode

Nickel is provided to HyhL by the metallochaperones HypA and HypB that are universally required for [NiFe] hydrogenase activation (Böck et al. 2006; Lacasse and Zamble 2016; Miki et al. 2020). Extensive efforts have characterized the nickel-binding properties and other features of these proteins from various organisms, and the structures of dimeric HypB and monomeric HypA from *T. kodakarensis* are known (Sasaki et al. 2013; Watanabe et al. 2009) as is that of their complex in the presence of ATPγS (Watanabe et al. 2015). In this microorganism, HypB does not bind nickel so it cannot deliver the metal to HypA as described for the *E. coli* proteins. Rather, the binding of HypB to HypA increases the affinity for nickel at the HypA site from a $K_d$ of 4.1 μM for the free protein to 7.3 nM for HypA·HypB. Nucleotide hydrolysis (typically using GTP, but the *T. kodakarensis* HypB protein uses ATP) is coupled to nickel insertion into HyhL via HyhL·HypA, for which the structure is established (Kwon et al. 2018). In *E. coli*, HypA is used only to activate hydrogenase-3 whereas a second version named HybF activates hydrogenase-1 and hydrogenase-2 (Blokesch et al. 2004). In *B. japonicum*, HypB binds ~9 nickel ions per monomer (predominantly using a His-rich region at the amino terminus) and was suggested to be, but not established as, a nickel storage protein named nickelin (akin to the term ferritin used for iron storage proteins) (Olson and Maier 2000). HypB of this microorganism is critical for activation of its [NiFe] hydrogenase, and its GTPase activity promotes nickel insertion into the protein (Fu et al. 1995). In *E. coli*, SlyD participates in nickel delivery to [NiFe] hydrogenases and perhaps also in nickel storage (Kaluarachchi et al. 2011; Zhang et al. 2005). This protein is one of several host factors required for lysis by a bacteriophage (hence, giving rise to the *s*ensitive to *ly*sis *D* or *slyD* name) (Maratea et al. 1985) and it is a common contaminant of poly-histidine-tagged proteins purified by immobilized metal affinity chromatograph (Wülfing et al. 1994). SlyD contains a histidine-rich region near its carboxyl terminus and a domain with peptidyl-prolyl *cis-trans* isomerase activity. Deletion of the corresponding gene results in large reductions of cellular nickel content and hydrogenase activity (Leach et al. 2007; Pinske et al. 2015; Zhang et al. 2005). Of additional interest, SlyD of *H. pylori* interacts with the NiuD permease (Denic et al. 2021), hinting at a possible handoff of metal from a nickel uptake protein to a nickel delivery protein.

Upon nickel binding, a conformational change occurs in HyhL to bury the metallocenter and expose the histidine cleavage site to the endopeptidase HybD with a known structure (Kwon et al. 2016). Structures are also known for *E. coli* HybD and HycI, analogous proteases used for maturation of hydrogenase-2 and hydrogenase-3 (Fritsche et al. 1999; Yang et al. 2006). After HyhL cleavage and release of HypA, the small subunit of hydrogenase, HyhS, binds to form the mature, active [NiFe] hydrogenase.

### *14.4.7 Carbon Monoxide Dehydrogenase (CODH)*

A critical reaction for many microorganisms is the reversible interconversion between carbon monoxide (CO) and carbon dioxide (Fig. 14.5g). In aerobic

organisms, this reaction is carried out by using a copper-molybdopterin-[FeS] cluster-containing enzyme (King and Weber 2007). In contrast, anaerobes use an oxygen-labile nickel-dependent carbon monoxide dehydrogenase (CODH) of interest here (Can et al. 2014; Kung and Drennan 2017). CODHs are widely distributed in microorganisms, with one report indicating that over 6% of bacterial and archaeal genomes possess such genes that were resolved into six distinct clades (Techtmann et al. 2012). A more recent bioinformatics study identified 1942 non-redundant CODH genes in 1375 genomes covering 36 phyla and divided them into seven clades with 24 structural groups (Inoue et al. 2019). This section summarizes the properties of CODHs from carboxydotrophs that utilize the low potential electrons derived from CO ($E^{\circ\prime}$ −524 mV) for energy metabolism, such as that resulting in hydrogen production, or for autotrophic growth. Described separately (Sect. 14.4.8) are CODHs present in larger protein assemblages containing acetyl-CoA synthase/decarbonylase (ACS) activities that are used for $CO_2$ fixation and for aceticlastic growth of methanogens.

Particularly well-characterized sources of homodimeric CODHs are *C. hydrogenoformans* and *Rhodospirillum rubrum*, microbes in which CO oxidation is coupled to the production of hydrogen gas, along with *D. vulgaris*, which does not utilize CO as an energy source (Hadj-Saïd et al. 2015; Voordouw 2002). Notably, the *C. hydrogenoformans* genome encodes five CODHs (Wu et al. 2005), and each of the corresponding enzymes has been characterized [e.g., (Domnik et al. 2017)]. The *R. rubrum* enzyme was the first CODH purified and shown to possess a metallocenter containing nickel, iron, and inorganic sulfide (Bonam and Ludden 1987). The nickel-free forms of the *R. rubrum* and *D. vulgaris* proteins were obtained by growing cells in medium lacking this metal ion or by growing in the absence of the CooC accessory protein (see below), allowing for studies involving nickel-dependent activation (Bonam et al. 1988; Ensign et al. 1990; Hadj-Saïd et al. 2015). An extensive array of spectroscopic and mechanistic studies have been summarized for the *R. rubrum* CODH (Can et al. 2014; Kung and Drennan 2017) and will not be repeated here. Rather, I focus below on the structures of these proteins.

#### 14.4.7.1 CODH Structure

The crystal structures of homodimeric CODHs from *C. hydrogenoformans* and *R. rubrum* were first reported in 2001 (Dobbek et al. 2001; Drennan et al. 2001) and shown to possess a [4Fe-4S] D-cluster that bridges the subunits, two additional [4Fe4S] B-clusters, and the deeply buried unique nickel-iron-sulfur C-clusters (Fig. 14.6g). The initial reports identified the *R. rubrum* CODH C-cluster as a [1Ni-3Fe-4S] cubane connected by one sulfide to a mononuclear Fe site, whereas the *C. hydrogenoformans* enzyme had an additional sulfide between the nickel and the non-core Fe (Dobbek et al. 2001; Drennan et al. 2001). Subsequent studies indicated the additional sulfide is not present in the catalytically active state of the enzyme (Kung and Drennan 2017). An essentially identical crystal structure was

obtained for a nickel-depleted form of one CODH from *Thermococcus* sp. AM4 (two such enzymes are present in that microorganism) (Benvenuti et al. 2020). The CODH structure from *D. vulgaris* is of special interest. This enzyme exhibits redox-dependent changes in its C cluster such that the Ni and mononuclear Fe alter their positions (Wittenborn et al. 2018). In addition, this protein tolerates short-term exposure to small concentrations of oxygen because the exposed D-cluster has a more stable [2Fe-2S] cluster rather than a [4Fe-4S] cluster (Wittenborn et al. 2020). External electron transfer proteins deliver reducing equivalents to or remove electrons from the D-cluster that connects, via the B-clusters, to the active site C-clusters, which interconverts CO and $CO_2$.

#### 14.4.7.2 CODH Maturation

CODH of *R. rubrum* is encoded by *cooS* that is immediately followed by *cooC*, *cooT*, and *cooJ*. Deletion analysis demonstrated that *cooC* is required for biosynthesis of the [1Ni-4Fe-4S] metallocenter in CODH unless high concentrations of nickel are provided in the medium, whereas deletions in the adjacent *cooT* and *cooJ* genes have less marked effects (Kerby et al. 1997). In *C. hydrogenoformans*, *cooS-1* is located near *cooC1*, *cooS-2* is adjacent to *cooF*, and two other *cooC* copies along with a *cooT* are found elsewhere in the genome (Merrouch et al. 2018). Both *cooS* copies in *Thermococcus* are located near *cooC* genes, a third *cooC* has no clear function, and no *cooT* or *cooJ* is reported in this genome (Benvenuti et al. 2020). In *D. vulgaris*, *cooS* is immediately adjacent to *cooC*, but no *cooT* or *cooJ* has been described (Hadj-Saïd et al. 2015). A bioinformatics analysis of microorganisms possessing CODH reveals the genes encoding CooT and CooJ often are missing and that some microbes also lack CooC; thus, these proteins are not strictly needed for CODH enzyme activation in all microbes (Merrouch et al. 2018). The following paragraphs briefly highlight these proteins.

CooC is an ATPase or GTPase with sequence similarities to the HypB and UreG proteins involved in activation of hydrogenases and ureases (Jeon et al. 2001). The structurally-characterized CooC from *C. hydrogenoformans* is a nickel-binding protein with the metal bound to four cysteine residues located at the interface of the subunits (Fig. 14.9a) (Jeoung et al. 2009, 2010). Deletion of *cooC* in *D. vulgaris* leads to the synthesis of a nickel-free CODH whose structure was determined (Wittenborn et al. 2019).

CooT from *R. rubrum* and *C. hydrogenoformans* are nickel-binding proteins with known structures (Alfano et al. 2018; Timm et al. 2017). NMR, XAS, and modeling analyses of nickel-bound *R. rubrum* CooT suggested the presence of a unique square-planar nickel site at the subunit interface, with coordination by the side chains and amide groups of two Cys2 residues (note: the amino terminal Met1 residue was removed) (Fig. 14.9b, left) (Alfano et al. 2019c). *C. hydrogenoformans* CooT has a similar overall structure (Fig. 14.9b, right) despite being only 19% identical in sequence to that from *R. rubrum*; however, the presumed nickel site is modified and thought to involve coordination by the Cys2 and His55 side chains in

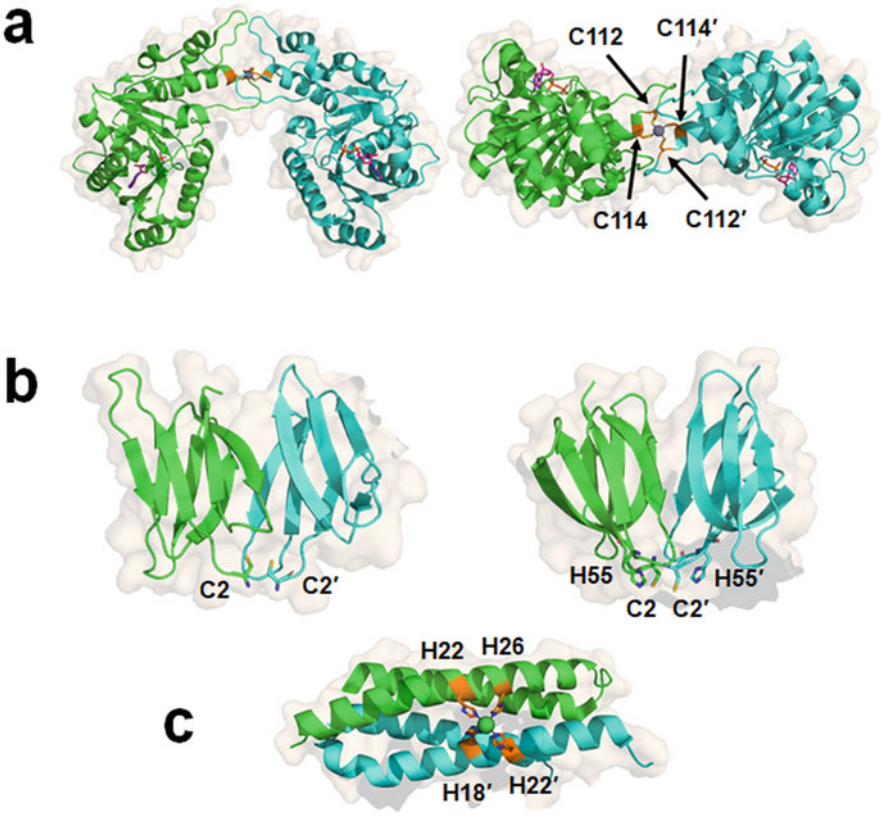


**Fig. 14.9** Structures of CODH maturation proteins. (**a**) Two views of CooC1 from *Carboxydothermus hydrogenoformans* (PDB ID 3kji) with bound ADP and zinc at the presumed nickel site. (**b**) CooT apoproteins from (left) *R. rubrum* and (right) *C. hydrogenoformans* (PDB ID 5n76 and 6fan) with their distinct nickel-binding sites. (**c**) Truncated CooJ from *R. rubrum* (PDB ID 6hk5) missing residues Asp69-Pro115 (the carboxyl terminal His-rich region) and highlighting the remaining nickel-binding site. Glu29″, not shown, from an adjacent dimer in the crystal coordinates as a bidentate ligand to the metal and completes its octahedral coordination sphere. The homodimeric proteins are shown in cartoon mode (green and cyan) with semi-transparent surfaces. Metals are shown as spheres and selected residues are depicted as sticks

each subunit (Alfano et al. 2018). Sequence comparisons show the two distinct nickel-binding motifs exist in other bacterial and archaeal CooT sequences (Alfano et al. 2019c).

CooJ from *R. rubrum* may assist in CODH maturation and is a potential nickel storage protein due to its His-rich carboxyl terminus (16 histidine residues in the last 34 amino acids) (Watt and Ludden 1998). The protein binds five nickel per dimer (four with a $K_d \sim 1.6$ μM and one with a $K_d$ of 380 nM) (Alfano et al. 2019a). The structure of CooJ (truncated at the carboxyl region to remove the His-rich region) reveals nickel coordination by His22 and His26 from one subunit along with His18

and His22 of the second subunit, plus bidentate binding by Glu29 from another dimer (PDB ID 6hk5, Fig. 14.9c). The interaction with a neighboring dimer is consistent with the known ability of the protein to form higher-order oligomers in the presence of nickel (Alfano et al. 2019b). Direct evidence that the unique nickel-binding site is critical to CooJ function is lacking.

### *14.4.8 Acetyl-CoA Synthase/Decarbonylase (ACS)*

In many microorganisms, CODH is a component of a larger protein complex known as acetyl-CoA synthase/decarbonylase (ACS) that includes a second nickel-containing metallocenter referred to as the A-cluster (Can et al. 2014; Kung and Drennan 2017). Versions of this enzyme are found in autotrophic anaerobes that use the Wood-Ljungdahl pathway for $CO_2$ fixation, such as many acetogens, methanogens, and sulfate-reducing bacteria, and in aceticlastic methanogens that grow anaerobically on acetate using a version of the enzyme that operates in the reverse direction. In the Wood-Ljungdahl pathway, one $CO_2$ undergoes three sequential two-electron reductions to generate a methyl group that is bound to tetrahydrofolate. The methyl group is then donated to a corrinoid-iron-sulfur protein (CFeSP), forming a methyl-Co bond. Meanwhile, the CODH component of ACS reduces one $CO_2$ to CO. In a remarkable reaction, the A cluster of ACS condenses the CFeSP-bound methyl group, the CO, and CoA to generate acetyl-CoA (Fig. 14.5h), used to synthesize all cellular carbon compounds. By contrast, the A-cluster of ACS in aceticlastic methanogens splits acetyl-CoA into CoA, CO, and a methyl group that becomes bound to a CFeSP. Subsequently, the methyl group is transferred to tetrahydromethanopterin, then to 2-thioethanesulfonate (CoM), the product of which is reduced by methyl-*S*-coenzyme M reductase (MCR) to generate methane (see Sect. 14.4.10). The electrons required for this last reduction step are derived from the oxidation of CO to form $CO_2$ by the CODH component of the protein.

#### 14.4.8.1 Structure of ACS

Structures are available for the native ACS from *Moorella thermoacetica* (formerly *Clostridium thermoaceticum*) (Darnault et al. 2003; Doukov et al. 2002) and *Clostridium autoethanogenum* (Lemaire and Wagner 2020). In addition, both the CODH component of ACS from *M. barkeri* (Gong et al. 2008) and the CODH-free ACS component from *C. hydrogenoformans* (Svetlitchnyi et al. 2004) have been structurally defined. The native $\alpha_2\beta_2$ proteins from *M. thermoacetica* and *C. autoethanogenum* (Fig. 14.6h) contain the central core, equivalent to the homodimeric CODH enzyme, with two active site [1Ni-4Fe-4S] C-clusters, two [4Fe-4S] B-clusters for internal electron transfer, and the single [4Fe-4S] D-cluster for electron exchange with an external electron carrier. Flanking the CODH

component are subunits that contain the A-cluster as well as acetyl-CoA and CFeSP-binding sites. The highly dynamic nature of this subunit is shown by its two distinct conformations in crystallized *M. thermoacetica* and *C. autoethanogenum* enzymes and by the multiple structural arrangements found in *C. thermoacetica* ACS when examined by negative-stain electron microscopy (Cohen et al. 2020). The A-cluster is a novel [4Fe-4S]-Ni-Ni metallocenter that has a standard cubane cluster with one cysteine ligand bridging to a proximal nickel site ($Ni_p$). Two additional cysteines connect $Ni_p$ and a distal nickel atom ($Ni_d$). The planar, 4-coordinate geometry of $Ni_d$ is completed by two backbone amides. The tri-cysteine bound $Ni_p$ is highly labile, with early structures depicting an enzyme lacking this metal, containing copper (Doukov et al. 2002), or with zinc (Darnault et al. 2003) at this position. The monomeric, CODH-free form of ACS from *C. hydrogenoformans* possesses the same [4Fe-4S]-Ni-Ni site (Svetlitchnyi et al. 2004). The structure of native ACS from *M. thermoacetica* revealed the existence of a 140 Å long molecular tunnel connecting the two C clusters in the CODH component and extending to $Ni_p$ in each of the two A clusters. Direct evidence for this tunnel was obtained by showing that exogenous CO does not compete with CO produced at the C cluster for incorporation into acetyl-CoA at the A cluster and by demonstrating that addition of a CO-binding protein like myoglobin or hemoglobin has no effect on acetyl-CoA synthesis from $CO_2$, methyl-CFeSP, and CoA (Maynard and Lindahl 1999; Seravalli and Ragsdale 2000). Notably, crystals treated with pressurized xenon gas confirms the presence of a channel by showing these electron dense atoms within the protein (Darnault et al. 2003; Doukov et al. 2008).

The methanogen versions of ACS that operate in the direction of acetyl-CoA decomposition are best characterized for the proteins from *M. barkeri* and *Methanosarcina thermophila* (Grahame 1991; Terlesky et al. 1986). These corrinoid, nickel, iron, and sulfide-containing proteins each possess five types of subunits that aggregate into 2.4-MDa complexes with eight copies of each peptide. The structure of the intact complex is not known, but that for the $\alpha_2\varepsilon_2$ component exhibiting CODH activity is determined (Gong et al. 2008). The $\alpha_2$ portion of this complex closely resembles the CODH structures described above, but it contains five metalloclusters; i.e., the typical [4Fe-4S] D-cluster bridging the subunits, two [4Fe-4S] B-clusters, and two [1Ni-4Fe-4S] C-clusters, along with two [4Fe-4S] E-clusters and two [4Fe-4S] F-clusters. The functions of the E- and F-clusters and that of the ε subunits, not present in the previously described CODH and ACS structures, remain unknown.

#### 14.4.8.2 ACS Maturation

The remarkable complexity of the ACS metallocenters might lead one to suspect that multiple accessory proteins are required for their biosynthesis; however, that is not the case. Surprisingly, heterologous expression in *E. coli* of *acsA* and *acsB* (encoding the CODH component and the A cluster-containing protein) from *M. thermoacetica* provides a form of ACS that is indistinguishable from the native

enzyme missing $Ni_p$; subsequent incubation with nickel yields active enzyme (Loke et al. 2000). Somewhat similarly, heterologous expression in *E. coli* of the gene encoding only the β subunit (i.e. the site of the A cluster) of *M. thermophila* ACS yields a nickel-free inactive protein that developes ACS activity after incubation with nickel (Gencic and Grahame 2003). These results suggest no accessory genes are needed for ACS maturation, but other studies provide evidence counter to this conclusion. Located in the same *M. thermoacetica* gene cluster as *acsAB* are *cooC1* and *acsF*, homologues of *R. rubrum cooC* encoding a protein with a nickel insertion auxiliary role. *M. thermoacetica* CooC has not been studied, whereas AcsF was found to exhibit ATPase activity, but no involvement in ACS activation was identified (Loke and Lindahl 2003). By contrast, *cooC2* in the ACS gene cluster of *C. hydrogenoformans* encodes an AcsF that clearly functions as an ACS maturation factor (Gregg et al. 2016). Two molecules of AcsF bind to inactive, monomeric ACS that lacks CODH (Svetlitchnyi et al. 2004), and the complex coordinates two atoms of nickel. Subsequent ATP hydrolysis is coupled to A cluster activation (Gregg et al. 2016). The authors concluded that AcsF installs the two nickel atoms of the A cluster.

### *14.4.9 2-Hydroxyacid Racemase/Epimerase (HARE) Containing NPN*

The ability of microorganisms to interconvert D- and L-lactic acid was first described for *Clostridium acetobutylicum* and *Clostridium beijerinckii* (formerly *C. butylicum*) in 1936 (Tatum et al. 1936). This activity provides a means for some lactic acid bacteria to obtain D-lactate for incorporation into their cell walls (Chapot-Chartier and Kulakauskas 2014), for other microbes to obtain L-lactate for synthesis of odd-numbered fatty acids (Weimer and Moen 2013), and for lactate degraders to utilize both enantiomers. Extensive studies of lactate racemase were carried out in the 1960s (Desguin et al. 2017), but only since 2015 has a detailed understanding of this enzyme and identification of other nickel-pincer nucleotide (NPN)-containing racemases/epimerases (Fig. 14.5i) been accomplished.

#### 14.4.9.1 Structure of Lactate Racemase and Discovery of the NPN Cofactor

The gene encoding lactate racemase (*larA*) was first identified in *L. plantarum* and shown to be located in the *larABCDE* gene cluster, adjacent to and transcribed opposite *larRMNQO* (Desguin et al. 2014). These operons are regulated by LarR, a lactic acid-dependent transcription factor (Desguin et al. 2015a). LarD is a lactate permease that allows for cellular entry/egress of both enantiomers (Bienert et al. 2013). The sequences of LarMN, LarQ, and LarO resemble those of ABC-type

nickel transporters (Sect. 14.2.2.2), leading to studies demonstrating that lactate racemase is a nickel-dependent enzyme requiring LarB, LarC, and LarE for activation (Desguin et al. 2014). The structure of LarA (Fig. 14.6i) reveals the presence of a covalently tethered cofactor, pyridinium-3-thioamide-5-thiocarboxylic acid mononucleotide (Desguin et al. 2015b). Because this cofactor is a *n*ickel-containing *p*incer *n*ucleotide complex (Nevarez et al. 2020), it is abbreviated NPN. Notably, the nickel in this coenzyme exhibits square-planar geometry with coordination by the pyridinium C4 carbon, the two sulfur atoms of NPN, and a histidine side chain. This cofactor participates in catalysis by a proton-coupled hydride transfer mechanism as shown by kinetic isotope studies demonstrating cleavage/reformation of the substrate C2-H bond, trapping of the pyruvate intermediate by two different methods, substrate-dependent perturbation of the NPN spectrum consistent with its reduction, and structural studies (Rankin et al. 2018). The presence of the novel NPN cofactor in LarA provides an explanation for why LarB, LarC, and LarE are required for racemase activity; they synthesize the coenzyme.

#### 14.4.9.2 NPN Cofactor Biosynthesis

Biosynthesis of the NPN cofactor (Fig. 14.10) initiates by LarB catalyzing dual activities with its substrate, nicotinic acid adenine dinucleotide (NaAD): carboxylation at C5 of the pyridinium ring and hydrolysis of the phosphoanhydride to produce pyridinium 3,5-dicarboxylic acid mononucleotide (P2CMN) while releasing AMP (Desguin et al. 2016). The structurally-characterized LarE then catalyzes a three-step sequence involving P2CMN carboxylate activation by adenylylation (using ATP and releasing pyrophosphate), formation of a covalent bond between the mononucleotide and a cysteine side chain (while releasing AMP), and sacrificial loss of the cysteine sulfur atom (leaving the protein with dehydroalanine at this position) to generate the thioacid product. These steps are repeated for the second substrate carboxyl group using another LarE subunit, thus generating pyridinium 3,5-dithiocarboxylic acid mononucleotide (P2TMN) (Desguin et al. 2016; Fellner et al. 2017). LarC inserts nickel into this precursor via a stoichiometric cyclometallase reaction in a manganese- and CTP-dependent process (releasing CMP and pyrophosphate) (Desguin et al. 2018). LarC binds multiple atoms of nickel (Desguin et al. 2014), presumably using a histidine-rich sequence in its amino terminal domain, and may function as a metallochaperone. Efforts to crystallize LarC led to protein cleavage—perhaps involving trace amounts of protease acting on a highly susceptible sequence—to release the carboxyl-terminal domain (starting at residue 272) from the rest of the 420 residue full-length protein. The crystal structure was obtained for a hexamer of the smaller fragment, which lacks the nickel-binding region and the P2CMN-binding site; however, this domain binds $Mn_2$·CTP in a new nucleotide-binding configuration (Desguin et al. 2018).

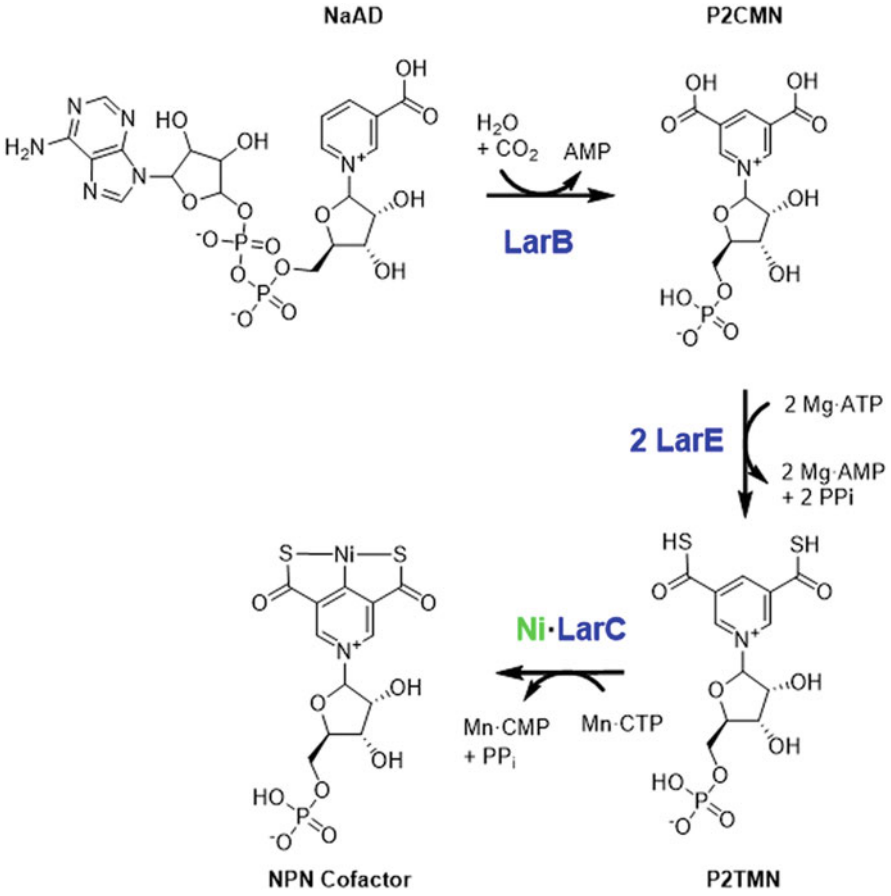


**Fig. 14.10** Biosynthesis of the nickel-pincer nucleotide (NPN) cofactor. LarB carboxylates C5 of the pyridinium ring and hydrolyzes the phosphoanhydride of nicotinic acid adenine dinucleotide (NaAD) releasing AMP and pyridinium 3,5-dicarboxylic acid mononucleotide (P2CMN). The carboxylic acids of P2CMN are converted to thioacids in pyridinium 3,5-dithiocarboxylic acid mononucleotide (P2TMN) by duplicate sacrificial sulfur transfer reactions from Cys side chains of two copies of LarE, generating dehydroalanine residues. LarC installs nickel into P2TMN to generate NPN in a reaction that requires CTP hydrolysis to CMP and pyrophosphate

### 14.4.9.3 Other NPN-Binding Proteins

Approximately 10% of bacterial and archaeal genomes possess homologs to *larA*, *larB*, *larE*, and *larC* (Desguin et al. 2014), indicating a widespread ability to synthesize NPN for incorporation into lactate racemase-type enzymes. Significantly, many species possess more than one paralog of *larA*—up to eight copies in *Clostridium asparagiforme* and *Thermosinus carboxydivorans*—consistent with activities other than lactate racemase (Hausinger et al. 2018). Furthermore, *gntE*, a

*larA* homolog from *Thermotoga maritima*, is proposed to encode an epimerase that interconverts D-mannonate and D-gluconate (Rodionova et al. 2012). Biochemical studies with purified proteins confirm this suspicion and identify other 2-hydroxyacid racemases including those for malate, phenyllactate, 2-hydroxyglutarate, and less specific short-chain aliphatic 2-hydroxyacids (Desguin et al. 2020). Of additional interest, many cyanobacteria and some other microorganisms possess homologs of *larB*, *larE*, and *larC*, but lack any homologs of *larA*, suggesting these microorganisms may synthesize NPN for incorporation into proteins with a distinct architecture and possibly a unique function.

## *14.4.10 Methyl-S-Coenzyme M Reductase (MCR)*

This chapter uses the name methyl-*S*-coenzyme M reductase (MCR) when referring to the enzyme of methanogenic archaea that forms methane as well as to the protein responsible for anaerobic oxidation of methane and short-chain alkanes in syntrophic methano(alkano)trophs. Excellent recent overviews of MCR including its proposed enzyme mechanism are available (Ragsdale et al. 2017; Thauer 2019).

### 14.4.10.1 Nickel-Containing MCR of Methanogenic and Methanotrophic Archaea

Methanogenic archaea reduce $CO_2$ to methane by a pathway that includes the intermediate methyl-*S*-coenzyme M (methyl-S-CoM) (Taylor and Wolfe 1974). In addition, selected methanogen strains are capable of metabolizing CO, formate, methanol, methylamine, and acetic acid by pathways that also form this key chemical species (Thauer 1998). In all cases, methane release involves the action of MCR that reacts methyl-*S*-CoM with 7-mercaptoheptanoylthreonine phosphate (coenzyme B, HS-CoB) (Noll et al. 1986) to form the mixed disulfide CoM-S-S-CoB (Fig. 14.5j) (Bobik et al. 1987; Ellermann et al. 1988). The $\alpha_2\beta_2\gamma_2$ enzyme associated with MCR activity (Fig. 14.6j) was first isolated from *Methanothermobacter thermoautotrophicus* (formerly *Methanobacterium thermoautotrophicum* ΔH) and shown to contain nickel based on the incorporation of radioactive $^{63}$Ni (Ellefson and Wolfe 1981; Ellefson et al. 1982). Numerous subsequent biochemical and spectroscopic studies of MCR have used the enzyme from this species and from *Methanothermobacter marburgensis* (formerly *Methanobacterium thermoautotrophicum* strain Marburg). Some methanogens possess multiple forms of MCR that are regulated differently (Rospert et al. 1990) and have distinct catalytic properties (Bonacker et al. 1993). The nickel of MCR is associated with a yellow organometallic cofactor named coenzyme F430 that occurs as protein-associated and free forms, with subtle differences in their spectra (Hausinger et al. 1984). An extensive series of studies ((Pfaltz et al. 1985) and earlier citations) identified the structure of coenzyme F430 as a highly reduced and

modified nickel-containing tetrapyrrole (see inset to Fig. 14.6j). Notably, derivatives of this cofactor exist in other methanogens and in anaerobic methanotrophs, as described below (Allen et al. 2014).

Microbial mats associated with anaerobic methane seeps in the Black Sea possess an abundant microorganism that contains an MCR-like protein with a nickel-containing cofactor resembling F430 (Krüger et al. 2003). This cofactor structure is the same as the methanogen-derived F430 except for the added presence of a methylthio group on the methylene carbon adjacent to the keto group in the carbocyclic ring (Mayr et al. 2008). The enzyme containing the modified cofactor is proposed to catalyze a reverse methanogenesis reaction (Shima and Thauer 2005), resulting in the anaerobic oxidation of methane. Indeed, *M. marburgensis* MCR also catalyzes this reverse reaction when subjected to appropriate experimental conditions (Scheller et al. 2010). Remarkably, MCR homologs in members of the *Candidatus* Syntrophoarchaeum, *Candidatus* Methanoliparia, *Candidatus* Ethanoperedens, and other genera of archaea are capable of specifically catalyzing the anaerobic oxidation of short chain alkanes, including butane and ethane (Chen et al. 2019; Hahn et al. 2020; Laso-Pérez et al. 2016, 2019; Wang et al. 2019, 2020).

#### 14.4.10.2 Structure of Methyl-*S*-Coenzyme M Reductase

The first reported MCR structure was that from *M. marburgensis* (Fig. 14.6j) (Ermler et al. 1997). Additional MCR structures have been elucidated from other methanogens [e.g. (Grabarse et al. 2000)] and from the Black Sea mat methanotroph (Shima et al. 2012). The structures are quite similar; e.g., each is an $\alpha_2\beta_2\gamma_2$ enzyme with HS-CoB-binding channels that lead to the buried coenzyme F430. Of additional interest, multiple amino acid residues in these proteins are enzymatically derivatized, with at least some of the modifications affecting the activity of the enzyme (Lyu et al. 2020; Nayak et al. 2017, 2020; Selmer et al. 2000). Depending on the microbial source, highly specific changes include methylations (of histidine, arginine, glutamine, and cysteine), thioamidation (of glycine), desaturation (of aspartic acid), and hydroxylation (of tryptophan or methionine) [reviewed in (Chen et al. 2020)].

#### 14.4.10.3 Biosynthesis of Coenzyme F430

The biosynthetic pathway for coenzyme F430 has long been known to begin with L-glutamic acid, with initial steps progressing through glutamyl-tRNA, glutamate 1-semialdehyde, 5-aminolevulinic acid, porphobilinogen, uroporphyrinogen III, and dihydrosirohydrochlorin [reviewed in Thauer and Bonacker (1994)]. In addition, early studies reported the purification and mass spectrometric identification of the intermediate 15,17$^3$-seco-F430-17$^3$-acid (Pfaltz et al. 1987). A critical breakthrough in further understanding the pathway derived from genomic analyses that revealed a cluster of five genes in methanogens and anaerobic methanotrophs with potentially relevant functions. The genes within the *cfbAEDCB* cluster of

*Methanosarcina acetivorans* C2A or the alternately named *cfbABCDE* cluster of *M. barkeri* were demonstrated to encode enzymes catalyzing the reactions shown in Fig. 14.11 (Moore et al. 2017). Thus (using the nomenclature of the first report), CfbA incorporates nickel into sirohydrochlorin, CfbB converts two acetate side chains to acetamides, CfbC and CfbD together reduce the diamide-containing tetrapyrrole by six electrons and convert one amide to a lactam ring, and CfbE converts a propionate side chain into a cyclohexanone ring. In methanotrophs and some methanogens additional modifications occur by still unclear processes (Allen et al. 2014). It is uncertain how the resulting coenzyme species are incorporated into the corresponding MCR proteins.

### *14.4.11 Other Nickel Enzymes*

It is likely that other nickel-containing enzymes exist, and experimental evidence already points to some probable representatives. For example, *Bacillus subtilis* AraM is a glycerol-1-phosphate dehydrogenase that depends on nickel for greatest activity and co-purifies with nickel from cells grown on LB medium supplemented with 1 mM of this metal ion (Guldan et al. 2008). Two chromatographically-resolved proteins from cell-free extracts of *Pyrococcus furiosus* contain nickel, but no enzymatic activity has been demonstrated (Cvetkovic et al. 2010). PF0056, a possible sugar-binding protein, binds 0.47 Ni/subunit and is predicted to possess a cupin fold that coordinates the metal using three histidine and one glutamate residues (much like the quercetinase structure, Sect. 14.4.3). PF0086 is annotated as an alanyl-tRNA editing hydrolase and is predicted to bind its metal (0.86 Ni/subunit) using three histidine and one cysteine residue. None of these proteins has been extensively characterized and their structures have not been determined.

One must use caution when claiming an enzyme is nickel dependent. A nice illustration of this point is provided by peptide deformylase, the enzyme responsible for removal of the *N*-formyl group from the amino terminal methionine residue of newly synthesized proteins. Early studies had suggested the *E. coli* protein contains an active site zinc ion; however, substantial increases in enzyme activity occur when this enzyme is isolated from cells grown in the presence of nickel (Ragusa et al. 1998). The stable nickel-containing protein was extensively characterized, including determination of its structure (Becker et al. 1998). Nevertheless, compelling evidence was later generated that the native enzyme contains ferrous ion, which undergoes rapid inactivation by oxygen due to conversion to the non-functional ferric species (Rajagopalan and Pei 1998).

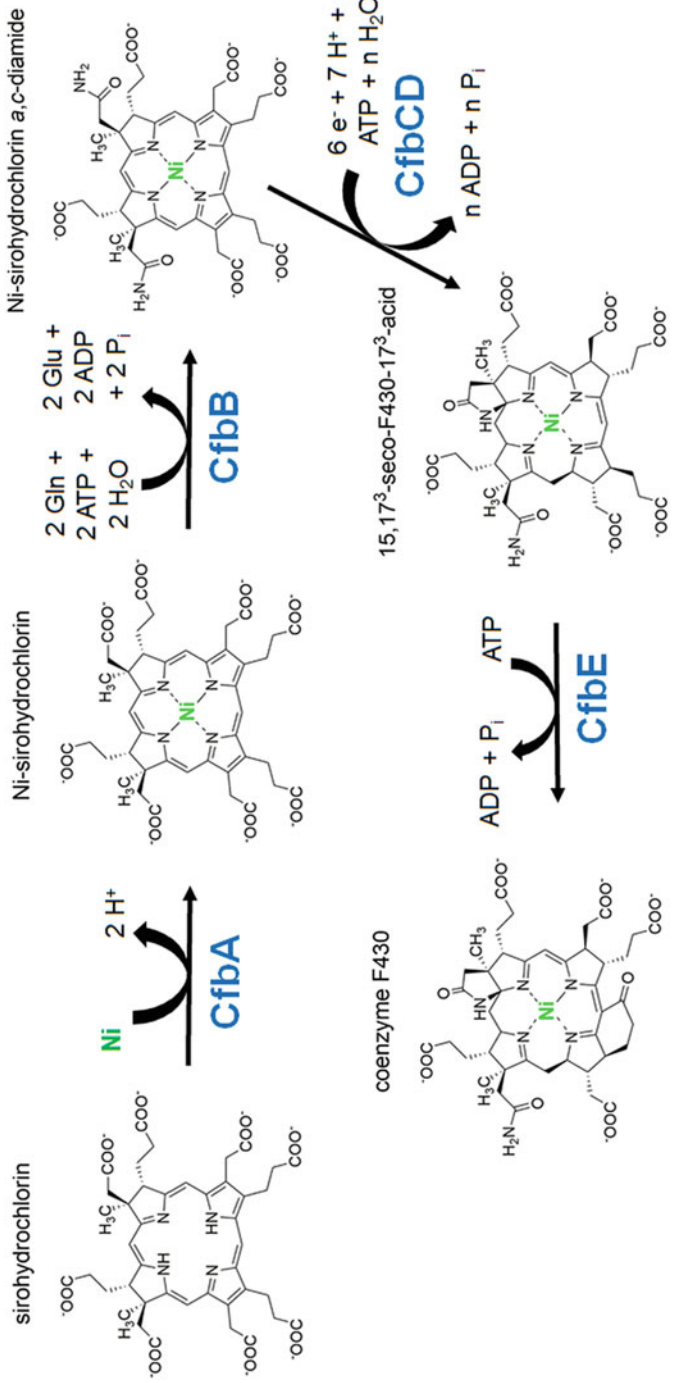


**Fig. 14.11** Biosynthesis of coenzyme F430. CfbA inserts nickel into sirohydrochlorin with the loss of two protons. CfbB converts two carboxylic acid side chains into amides via ATP-dependent activation and nitrogen transfer from glutamine. CfbC and CfbD catalyze a six-electron reduction of the nickel-sirohydrochlorin *a*,*c*-diamide and generate a lactam from one side chain. CfbE forms the carbocyclic ring of the coenzyme in an ATP-dependent reaction

### *14.4.12 Nickel Storage Proteins*

Several proteins (HypB, UreE, LarC, SlyD, CooJ, etc.) bind nickel for eventual incorporation into metalloenzymes, and these proteins could also reasonably store the metal within the cell. Unfortunately, experimental support for a nickel storage function is lacking in most cases. The exception might be *B. japonicum* HypB (Sect. 14.4.6.2), named nickelin on the basis of studies that were consistent with such a role (Olson and Maier 2000).

The most extensively-studied and most convincing examples of nickel storage proteins are Hpn (alternatively called Hpn-1) and Hpn-like (Hpnl or Hpn-2) proteins of *Helicobacter* species. First discovered in *H. pylori*, Hpn is a 60-amino acid long protein (7077 Da) that contains 28 His residues (47%) and tightly binds zinc or nickel (Gilbert et al. 1995). Hpn accounts for up to 2% of the *H. pylori* cellular protein, a feature that is compatible with a role in cellular nickel storage. Analogous proteins are present in *H. mustelae*, *H. felis*, and several other gastric species of this genus (Vinella et al. 2015). Biochemical and spectroscopic studies of the purified protein have demonstrated that *H. pylori* Hpn is multimeric (with the 20-mer being most prevalent), able to coordinate ~5 nickel ions per monomer ($K \sim 7.1$ μM), and also capable of binding zinc and copper (~5 Zn/monomer, 19.3 μM; ~8.5 Cu/monomer, ~2.2 μM) (Ge et al. 2006a, b). Deletion of the gene encoding Hpn leads to increased toxicity from nickel ions, consistent with a protective role against nickel stress; furthermore, gene deletion reduces the nickel content of cells whereas gene overexpression results in increased cellular nickel content, indicative of a nickel storage function (Ge et al. 2006a; Vinella et al. 2015). A large subset of Hpn-containing *Helicobacter* strains also produce Hpn-2 (Vinella et al. 2015). This 72-amino acid long protein is rich in His (nearly 25%), but has an even greater percentage of Gln residues (42%) (Seshadri et al. 2007). Gene deletion studies suggested that it too functions in metal detoxification (in this case against nickel, cobalt, and cadmium) and a role in nickel storage was suggested. The purified Hpn-2 protein is oligomeric, like Hpn, and binds ~2 nickel ions per monomer ($K \sim 3.8$ μM) (Zeng et al. 2008). The two nickel-binding sites are distinct, with the region involving His29 to His32 being critical for one binding site, whereas substitutions of other His residues do not affect nickel binding (Zeng et al. 2011). About one atom of copper, cobalt, or zinc also binds per Hpn-2 monomer, consistent with distinct environments for the two nickel sites. Chemical cross-linking studies show that Hpn and Hpn-2 interact with more than 100 proteins in *Helicobacter* cells, including UreA/UreB urease subunits, UreG GTPase, and HypB [NiFe] hydrogenase accessory protein (Saylor and Maier 2018). Overall, these studies reveal that Hpn-type proteins bind nickel, reduce toxicity to this metal, and facilitate activation of nickel enzymes, but a nickel storage role remains less compelling.

## 14.5 Conclusions and Perspectives

Microorganisms have developed a vast array of proteins that function to sense nickel concentrations, import the metal ion when cellular needs are deficient, and export the cation when internal levels are too high. The basis for cellular toxicity by nickel is partially understood, as are the mechanisms used by cells to defend against this harmful metal ion. A number of nickel-containing enzymes have been identified, with several of these enzymes dependent on accessory proteins for their biosynthesis. Nickel storage proteins exist in at least one bacterial genus. Further studies are likely to identify additional nickel-dependent enzymes and are certain to expand our understanding and provide more examples of proteins involved in sensing, transporting, and utilizing.

**Note Added in Proof** During the interval since this chapter was submitted, several relevant publications have appeared; selected examples are mentioned here. With regard to nickel-sensing transcription factors, additional structural and functional insights have been reported for SrnR (Mazzei et al. 2021). Nickel importers and exporters in *H. pylori* were reviewed (Camporesi et al. 2021). The maturation components responsible for activation of nickel-dependent hydrogenase and urease in *H. pylori* were summarized (Tsang and Wong 2022). Dynamics studies were carried out to better characterize a "bucket brigade" mode of nickel movement within the UreF and UreD/H proteins during urease activation (Masetti et al. 2021). Related to CODH activation, 150 homologues of CooJ were identified and three were characterized for nickel binding and other properties (Darrouzet et al. 2021). The structure and mechanism were revealed for LarB, catalyzing the first step of NPN cofactor biosynthesis (Rankin et al. 2021). Newly reported features of LarC, catalyzing the CTP-dependent nickel insertion during NPN cofactor biosynthesis, include formation of a novel reaction intermediate (Turmo et al. 2022). The structure was revealed for an MCR that functions in anaerobic ethane oxidation and contains a modified F430 cofactor (Hahn et al. 2021).

**Acknowledgements** Experimental investigations of microbial nickel metabolism in the Hausinger lab are supported by the National Institutes of Health (GM128959) and the National Science Foundation (CHE-1807073). I thank the many colleagues of my laboratory who have contributed to this work over the years.

## References

Abreu IA, Cabelli DE (2010) Superoxide dismutases--a review of the metal-associated mechanistic variations. Biochim Biophys Acta 1804:263–274

Adams MWW, Mortenson LE, Chen J-S (1981) Hydrogenase. Biochim Biophys Acta 594:105–176

Addy C, Ohara M, Kawai F, Kidera A, Ikeguchi M, Fuchigami S, Osawa M, Shimada I, Park S-Y, Tame JRH, Heddle JG (2007) Nickel binding to NikA: an additional binding site reconciles spectroscopy, calorimetry and crystallography. Acta Crystallogr D63:221–229

Ahn B-E, Cha J, Lee E-J, Han A-R, Thompson CJ, Roe J-H (2006) Nur, a nickel-responsive regulator of the Fur family, regulates superoxide dismutases and nickel transport in *Streptomyces coelicolor*. Mol Microbiol 59:1848–1858

Albareda M, Rodrigue A, Brito B, Ruiz-Argüeso T, Imperial J, Mandrand-Berthelot M-A, Palacios J (2015) *Rhizobium leguminosarum* HupE is a highly-specific diffusion facilitator for nickel uptake. Metallomics 7:691–701

Alfano M, Cavazza C (2020) Structure, function, and biosynthesis of nickel-dependent enzymes. Protein Sci 29:1071–1089

Alfano M, Pérard J, Miras R, Catty P, Cavazza C (2018) Biophysical and structural characterization of the putative nickel chaperone CooT from *Carboxydothermus hydrogenoformans*. J Biol Inorg Chem 23:809–817

Alfano M, Pérard J, Carpentier P, Basset C, Zambelli B, Timm J, Crouzy S, Ciurli S, Cavazza C (2019a) The carbon monoxide dehydrogenase accessory protein CooJ is a histidine-rich multidomain dimer containing an unexpected Ni(II)-binding site. J Biol Chem 294:7601–7614

Alfano M, Pérard J, Cavazza C (2019b) Nickel-induced oligomerization of the histidine-rich metallochaperone CooJ from *Rhodospirillus rubrum*. Inorganics 7:84

Alfano M, Veronesi G, Musiani F, Zambelli B, Signor L, Proux O, Rovezzi M, Ciurli S, Cavazza C (2019c) A solvent-exposed cysteine forms a peculiar $Ni^{II}$-binding site in the metallochaperone CooT from *Rhodospirillum rubrum*. Chem Eur J 25:15351–15360

Allan CB, Wu L-F, Gu Z, Choudhury SB, Al-Mjeni F, Sharma ML, Mandrand-Berthelot M-A, Maroney MJ (1998) An X-ray absorption spectroscopic structural investigation of the nickel site in *Escherichia coli* NikA protein. Inorg Chem 37:5952–5955

Allen KD, Wegener G, White RH (2014) Discovery of multiple modified $F_{430}$ coenzymes in methanogens and anaerobic methanotrophic archaea suggests possible new roles for $F_{430}$ in nature. Appl Environ Microbiol 80:6403–6412

Al-Mjeni F, Ju T, Pochapsky TC, Maroney MJ (2002) XAS investigation of the structure and function of Ni in acireductone dioxygenase. Biochemistry 41:6761–6769

An YJ, Ahn B-E, Han A-R, Kim H-M, Chung KM, Shin J-H, Cho Y-B, Roe J-H, Cha S-S (2009) Structural basis for the specialization of Nur, a nickel-specific Fur homolog, in metal sensing and DNA recognition. Nucleic Acids Res 37:3442–3451

Arima J, Iwabuchi M, Hatanaka T (2004) Gene cloning and overproduction of an aminopeptidase from *Streptomyces septatus* TH-2, and comparison with a calcium-activated enzyme from *Streptomyces griseus*. Biochem Biophys Res Commun 317:531–538

Ariza A, Vickers TJ, Greig N, Armour KA, Dixon MJ, Eggleston IM, Fairlamb AH, Bond CS (2006) Specificity of the trypanothione-dependent *Leishmania major* glyoxalase I: structure and biochemical comparison with the human enzyme. Mol Microbiol 59:1239–1248

Ash PA, Kendall-Price SET, Vincent KA (2019) Unifying activity, structure, and spectroscopy of [NiFe] hydrogenases: combining techniques to clarify mechanistic understanding. Acc Chem Res 52:3120–3131

Atherton JC (2006) The pathogenesis of *Helicobacter pylori*-induced gastro-duodenal diseases. Annu Rev Pathol 1:63–96

Babich H, Stotzky G (1983) Toxicity of nickel to microbes: environmental aspects. Adv Appl Microbiol 29:195–265

Balasubramanian A, Ponnuraj K (2010) Crystal structure of the first plant urease from jack bean: 83 years of journey from its first crystal to molecular structure. J Mol Biol 400:274–283

Banaszak K, Martin-Diaconescu V, Bellucci M, Zambelli B, Rypniewski W, Maroney MJ, Ciurli S (2012) Crystallographic and x-ray absorption spectroscopic characterization of *Helicobacter pylori* UreE bound to $Ni^{2+}$ and $Zn^{2+}$ reveal a role for the disordered C-terminal arm in metal trafficking. Biochem J 441:1017–1026

Barkay T, Miller SM, Summers AO (2003) Bacterial mercury resistance from atoms to ecosystems. FEMS Microbiol Rev 27:355–384

Barondeau DP, Kassman CJ, Bruns CK, Tainer JA, Getzoff ED (2004) Nickel superoxide dismutase structure and mechanism. Biochemistry 43:8038–8047

Bartha R, Ordal EJ (1965) Nickel-dependent chemolithotrophic growth of two *Hydrogenomonas* strains. J Bacteriol 89:1015–1019

Beaton SE, Evans RM, Finney AJ, Lamont CM, Armstrong FA, Sargent F, Carr SB (2018) The structure of hydrogenase-2 from *Escherichia coli*: implications for H2-driven proton pumping. Biochem J 475:1353–1370

Becker A, Schlichtling I, Kabsch W, Schultz S, Wagner AFV (1998) Structure of peptide deformylase and identification of the substrate binding site. J Biol Chem 273:11413–11416

Bellucci M, Zambelli B, Musiani F, Turano P, Ciurli S (2009) *Helicobacter pylori* UreE, a urease accessory protein: specific $Ni^{2+}$- and $Zn^{2+}$-binding properties and interaction with its cognate UreG. Biochem J 422:91–100

Benanti EL, Chivers PT (2010) *Geobacter uraniireducens* NikR displays a DNA binding mode distinct from other members of the NikR family. J Bacteriol 192:4327–4336

Beniamino Y, Pesce G, Zannoni A, Roncarati D, Zambelli B (2020) SrnR from *Streptomyces griseus* is a nickel-binding transcriptional activator. J Biol Inorg Chem 25:187–198

Benini S, Rypniewski WR, Wilson KS, Miletti S, Ciurli S, Mangani S (1999) A new proposal for urease mechanism based on the crystal structures of the native and inhibited enzyme from *Bacillus pasteurii*: why urea hydrolysis costs two nickels. Structure 7:205–216

Benini S, Cianci M, Ciurli S (2011) Holo-$Ni^{2+}$ *Helicobacter pylori* NikR contains four square-planar nickel-binding sites at physiological pH. Dalton Trans 40:7831–7833

Benoit SL, Maier RJ (2011) Mua (HP0868) is a nickel-binding protein that modulates urease activity in *Helicobacter pylori*. mBio 2:1–9

Benoit SL, Mehta N, Weinberg MV, Maier C, Maier RJ (2007) Interaction between the *Helicobacter pylori* accessory proteins HypA and UreE is needed for urease maturation. Microbiology 153:1474–1482

Benoit SL, McMurry JL, Hill SA, Maier RJ (2012) *Helicobacter pylori* hydrogenase accessory protein HypA and urease accessory protein UreG compete with each other for UreE recognition. Biochim Biophys Acta 1820:1519–1525

Benoit SL, Seshadri S, Lamichhane-Khadka R, Maier RJ (2013) *Helicobacter hepaticus* NikR controls urease and hydrogenase activities via the NikABDE and HH0418 putative nickel import proteins. Microbiology 159:136–146

Benvenuti M, Meneghello M, Guendon C, Jacq-Bailly A, Jeoung J-H, Dobbek H, Léger C, Fourmond V, Dementin S (2020) The two CO-dehydrogenases of *Thermococcus* sp. AM4. Biochim Biophys Acta 1861:148188

Beveridge TJ, Murray RGE (1976) Uptake and retention of metals by cell walls of *Bacillus subtilis*. J Bacteriol 127:1502–1518

Bienert GP, Desguin B, Chaumont F, Hols P (2013) Channel-mediated lactic acid transport: a novel function for aquaglyceroporins in bacteria. Biochem J 454:559–570

Blahut M, Dzul S, Wang S, Kandegedara A, Grossoehme NE, Stemmler TL, Outten FW (2018) Conserved cysteine residues are necessary for nickel-induced allosteric regulation of the metalloregulatory protein YqjI (NfeR) in *E. coli*. J Inorg Biochem 194:123–133

Blériot C, Effantin G, Lagarde F, Mandrand-Berthelot M-A, Rodrique A (2011) RcnB is a periplasmic protein essential for maintaining intracellular Ni and Co concentrations in *Escherichia coli*. J Bacteriol 193:3785–3793

Blériot C, Gault M, Gueguen E, Arnoux P, Mandrand-Berthelot M-A, Rodrigue A (2015) Cu binding by the *Escherichia coli* metal-efflux accessory protein RcnB. Metallomics 6:1400–1409

Blokesch M, Rohrmoser M, Rode S, Böck A (2004) HybF, a zinc-containing protein involved in NiFe hydrogenase biosynthesis. J Bacteriol 186:2603–2611

Bloom SB, Zamble DB (2004) Metal-selective DNA-binding response of *Escherichia coli* NikR. Biochemistry 43:10029–10038

Bobik TA, Olson KD, Noll KN, Wolfe RS (1987) Evidence that the heterodisulfide of coenzyme M and 7-mercaptoheptanoylthreonine phosphate is a product of the methylreductase reaction in *Methanobacterium*. Biochem Biophys Res Commun 149:455–460

Böck A, King PW, Blokesch M, Posewitz MC (2006) Maturation of hydrogenases. Adv Microb Physiol 51:1–71

Boer JL, Quiroz-Valenzuela S, Anderson KL, Hausinger RP (2010) Mutagenesis of *Klebsiella aerogenes* UreG to probe nickel binding and interactions with other urease-related proteins. Biochemistry 49:5859–5869

Boer JL, Mulrooney SB, Hausinger RP (2014) Nickel-dependent metalloenzymes. Arch Biochem Biophys 544C:142–152

Bonacker LG, Baudner S, Mörschel E, Böcher R, Thauer RK (1993) Properties of the two isoenzymes of methyl-coenzyme M reductase in *Methanobacterium thermoautotrophicum*. Eur J Biochem 217:587–595

Bonam D, Ludden PW (1987) Purification and characterization of carbon monoxide dehydrogenase, a nickel, zinc, iron-sulfur protein, from *Rhodospirillum rubrum*. J Biol Chem 262:2980–2987

Bonam D, McKenna MC, Stephens PJ, Ludden PW (1988) Nickel-deficient carbon monoxide dehydrogenase from *Rhodospirillum rubrum*: *in vivo* and *in vitro* activation by exogenous nickel. Proc Natl Acad Sci U S A 85:31–35

Bossè JT, Gilmour HD, MacInnes JI (2001) Novel genes affecting urease activity in *Actinobacillus pleuropneumoniae*. J Bacteriol 183:1242–1247

Brauer AL, Learman BS, Armbruster CE (2020) Ynt is the primary nickel import system used by *Proteus mirabilis* and specifically contributes to fitness by supplying nickel for urease activity. Mol Microbiol 114:185–199

Braun V, Hantke K (2011) Recent insights into iron import by bacteria. Curr Opin Chem Biol 15: 328–334

Brito B, Prieto R-I, Cabrera E, Mandrand-Berthelot M-A, Imperial J, Ruiz-Argüeso T, Palacios J-M (2010) *Rhizobium leguminosarum hupE* encodes a nickel transporter required for hydrogenase activity. J Bacteriol 192:925–935

Bryngelson PA, Arobo SE, Pinkham JL, Cabelli DE, Maroney MJ (2004) Expression, reconstitution, and mutation of recombinant *Streptomyces coelicolor* NiSOD. J Am Chem Soc 126:460–461

Buan NR, Escalante-Semerena JC (2006) Purification and initial biochemical characterization of ATP: cob(I)alamin adenosyltransferase (EutT) enzyme of *salmonella enterica*. J Biol Chem 281:16971–16977

Budnick JA, Prado-Sanchez E, Caswell CC (2018) Defining the regulatory mechanism of NikR, a nickel-responsive transcription regulator, in *Brucella abortus*. Microbiology 164:1320–1325

Burne RA, Chen Y-YM (2000) Bacterial ureases in infectious diseases. Microbes Infect 2:533–542

Bury-Moné S, Thiberg J-M, Contreras M, Maitournam A, Labigne A, De Reuse H (2004) Responsiveness to acidity via metal ion regulators mediates virulence in the gastric pathogen *Helicobacter pylori*. Mol Microbiol 53:623–638

Busenlehner LS, Pennella MA, Giedroc DP (2003) The SmtB/ArsR family of metalloregulatory transcriptional repressors: structural insights into prokaryotic metal resistance. FEMS Microbiol Rev 27:131–143

Campbell DR, Chapman KE, Waldron KJ, Tottey S, Kendall S, Cavallaro G, Andreini C, Hinds J, Stoker NG, Robinson NJ, Cavet JS (2007) Mycobacterial cells have dual nickel-cobalt sensors. Sequence relationships and metal sites of metal-responsive repressors are not congruent. J Biol Chem 282:32298–32310

Campeciño JO, Maroney MJ (2017) Reinventing the wheel: the NiSOD story. In: Zamble D, Rowinska-Zyrek M, Kozlowski H (eds) The biological chemistry of nickel. The Royal Society for Chemistry, Cambridge

Camporesi G, Minzoni A, Morasso L, Ciurli S, Musiani F (2021) Nickel import and export in the human pathogen *Helicobacter pylori*, perspectives from molecular modelling. Metallomics 13 (12):mfab066. https://doi.org/10.1093/mtomcs/mfab066

Can M, Armstrong FA, Ragsdale SW (2014) Structure, function, and mechanism of the nickel metalloenzymes, CO dehydrogenase, and acetyl-CoA synthase. Chem Rev 114:4149–4174

Carr CE, Foster AW, Maroney MJ (2017a) An XAS investigation of the nickel site structure in the transcriptional regulator InrS. J Inorg Biochem 177:352–358
Carr CE, Musiani F, Huang H-T, Chivers PT, Ciurli S, Maroney MJ (2017b) Glutamate ligation in the Ni(II)- and Co(II)-responsive *Escherichia coli* transcriptional regulator, RcnR. Inorg Chem 56:6459–6476
Carter EL, Hausinger RP (2010) Characterization of *Klebsiella aerogenes* urease accessory protein UreD in fusion with the maltose binding protein. J Bacteriol 192:2294–2304
Carter EL, Tronrud DE, Taber SR, Karplus PA, Hausinger RP (2011) Iron-containing urease in a pathogenic bacterium. Proc Natl Acad Sci U S A 108:13095–13099
Cavet JS, Meng W, Pennella MA, Appelhoff RJ, Giedroc DP, Robinson NJ (2002) A nickel-cobalt sensing ArsR-SmtB family repressor: contributions of cytosol and effector binding sites to metal selectivity. J Biol Chem 277:38441–38448
Chai SC, Ju T, Dang M, Goldsmith RB, Maroney MJ, Pochapsky TC (2008) Characterization of metal binding in the active sites of acireductone dioxygenase isoforms from *Klebsiella* ATCC 8724. Biochemistry 47:2428–2438
Chaintreuil C, Rigault F, Moulin L, Jaffré T, Fardoux J, Giraud E, Dreyfus B, Bailly X (2007) Nickel resistance determinants in *Bradyrhizobium* strains from nodules of the endemic New Caledonia legume *Serianthes calycina*. Appl Environ Microbiol 73:8018–8022
Chang Z, Kuchar J, Hausinger RP (2004) Chemical crosslinking and mass spectrometric identification of sites of interaction for UreD, UreF, and urease. J Biol Chem 279:15305–15313
Chapot-Chartier M-P, Kulakauskas S (2014) Cell wall structure and function in lactic acid bacteria. Microb Cell Factories 13(Suppl 1):59
Chen Y-YM, Burne RA (2003) Identification and characterization of the nickel uptake system for urease biosynthesis in *Streptococcus salivarius* 57.I. J Bacteriol 185:6773–6779
Chen YP, Dilworth MJ, Glenn AR (1984) Aromatic metabolism in *Rhizobium trifolii* - protocatechuate 3,4-dioxygenase. Arch Microbiol 138:187–190
Chen YP, Glenn AR, Dilworth MJ (1985) Aromatic metabolism in *Rhizobium trifolii* - catechol 1,2-dioxygenase. Arch Microbiol 141:225–228
Chen S-C, Musat N, Lechtenfeld OJ, Paschke H, Schmidt M, Said N, Popp D, Calabrese F, Stryhanyuk H, Jaekel U, Zhu Y-G, Joye SB, Richnow H-H, Widdel F, Musat F (2019) Anaerobic oxidation of ethane by archaea from a marine hydrocarbon seep. Nature 568:108–111
Chen H, Gan Q, Fan C (2020) Methyl-coenzyme M reductase and its post-translational modifications. Front Microbiol 11:578356
Cheng Z, Wei YYC, Sung WWL, Glick BR, McConkey BJ (2009) Proteomic analysis of the response of the plant growth-promoting bacterium *Pseudomonas putida* UW4 to nickel stress. Proteome Sci 7:18
Cheng T, Li H, Xia W, Jin L, Sun H (2016) Exploration into the nickel 'microcosmos' in prokaryotes. Coord Chem Rev 311:24–37
Cherrier MV, Martin L, Cavazza C, Jacquamet L, Lemaire D, Gaillard J, Fontecilla-Camps JC (2005) Crystallographic and spectroscopic evidence for high affinity binding of FeEDTA $(H_2O)^-$ to the periplasmic nickel transporter NikA. J Am Chem Soc 127:10075–10082
Cherrier MV, Cavazza C, Bochot C, Lemaire D, Fontecilla-Camps JC (2008) Structural characterization of a putative endogenous metal chelator in the periplasmic nickel transporter NikA. Biochemistry 47:9937–9943
Chivers PT (2015) Nickel recognition by bacterial importer proteins. Metallomics 7:590–595
Chivers PT (2017) Nickel regulation. In: Zamble DB, Rowinska-Zyrek M, Kozlowski H (eds) The biological chemistry of nickel. Royal Society of Chemistry, Cambridge
Chivers PT, Sauer RT (2000) Regulation of high affinity nickel uptake in bacteria. $Ni^{2+}$-dependent interaction of NikR with wild-type and mutant operator sites. J Biol Chem 275:19735–19741
Chivers PT, Sauer RT (2002) NikR repressor: high-affinity nickel binding to the C-terminal domain regulates binding to operator DNA. Chem Biol 9:1141–1148

Chivers PT, Tahirov TH (2005) Structure of *Pyrococcus horikoshi* NikR: nickel sensing and implications for the regulation of DNA recognition. J Mol Biol 348:597–607

Chivers PT, Benanti EL, Heil-Chapdelaine V, Iwig JS, Rowe JL (2012) Identification of Ni-(L-His)$_2$ as the substrate for NikABCDE-dependent nickel uptake in *Escherichia coli*. Metallomics 4:1043–1050

Choudhury SB, Lee J-W, Davidson G, Yim Y-I, Bose K, Sharma ML, Kang S-O, Cabelli DE, Maroney MJ (1999) Examination of the nickel site structure and reaction mechanism in *Streptomyces seoulensis* superoxide dismutase. Biochemistry 38:3744–3752

Chung H-Y, Choi J-H, Kim E-J, Cho Y-H, Roe J-H (1999) Negative regulation of the gene for Fe-containing superoxide dismutase by an Ni-responsive factor in *Streptomyces coelicolor*. J Bacteriol 181:7381–7384

Clugston SL, Barnard JFJ, Kinach R, Miedema D, Ruman R, Daub E, Honek JF (1998) Overproduction and characterization of a dimeric non-zinc glyoxylase I from *Escherichia coli*: evidence for optimal activation by nickel ions. Biochemistry 37:8754–8763

Cohen SE, Brignole EJ, Wittenborn EC, Can M, Thompson S, Ragsdale SW, Drennan CL (2020) Negative-stain electron microscopy reveals dramatic structural rearrangements in Ni-Fe-S-dependent carbon monoxide dehydrogenase/acetyl-CoA synthase. Structure 28:1–7

Collins CM, D'Orazio SEF (1993) Bacterial ureases: structure, regulation of expression and role in pathogenesis. Mol Microbiol 9:907–913

Colpas GJ, Hausinger RP (2000) *In vivo* and *in vitro* kinetics of metal transfer by the *Klebsiella aerogenes* urease nickel metallochaperone, UreE. J Biol Chem 275:10731–10737

Colpas GJ, Brayman TG, McCracken J, Pressler MA, Babcock GT, Ming L-J, Colangelo CM, Scott RA, Hausinger RP (1998) Spectroscopic characterization of metal binding by *Klebsiella aerogenes* UreE urease accessory protein. J Biol Inorg Chem 3:150–160

Colpas GJ, Brayman TG, Ming L-J, Hausinger RP (1999) Identification of metal-binding residues in the *Klebsiella aerogenes* urease nickel metallochaperone, UreE. Biochemistry 38:4078–4088

Constant P, Chowdhury SP, Pratscher J, Conrad R (2010) *Streptomycetes* contributing to atmospheric molecular hydrogen soil uptake are widespread and encode a putative high-affinity [NiFe]-hydrogenase. Environ Microbiol 12:821–829

Constant P, Chowdhury SP, Hesse L, Pratscher J, Conrad R (2011) Genome data mining and soil survey for the novel group 5 [NiFe]-hydrogenase to explore the diversity and ecological importance of presumptive high-affinity $H_2$-oxidizing bacteria. Appl Environ Microbiol 77:6027–6035

Contreras M, Thiberge J-M, Mandrand-Berthelot M-A, Labigne A (2003) Characterization of the roles of NikR, a nickel-responsive pleiotropic autoregulator of *Helicobacter pylori*. Mol Microbiol 49:947–963

Covacci A, Telford JL, Del Giudice G, Parsonet J, Rappuoli R (1999) *Helicobacter pylori* virulence and genetic geography. Science 284:1328–1333

Cubillas C, Vinuesa P, Tabche ML, Garcia-de los Santos A (2013) Phylogenomic analysis of cation diffusion facilitator proteins uncovers $Ni^{2+}$/$Co^{2+}$ transporters. Metallomics 5:1634–1643

Cunha ES, Chen X, Sanz-Gaitero M, Mills DJ, Luecke H (2021) Cryo-EM structure of *helicobacter pylori* urease with an inhibitor in the active site at 2.0 Å resolution. Nat Commun 12:230

Cussac V, Ferrero RL, Labigne A (1992) Expression of *Helicobacter pylori* urease genes in *Escherichia coli* grown under nitrogen-limiting conditions. J Bacteriol 174:2466–2473

Cvetkovic A, Menon AL, Thorgersen MP, Scott JW, Poole FL II, Jenney FE Jr, Lancaster WA, Praissman JA, Shanmukh S, Vaccaro BJ, Trauger SA, Kalisiak E, Apon JV, Siuzdak G, Yannone SM, Tainer JA, Adams MWW (2010) Microbial metalloproteomes are largely uncharacterized. Nature 466:779–782

Dai Y, Wensink PC, Abeles RH (1999) One protein, two enzymes. J Biol Chem 274:1193–1195

Darnault C, Volbeda A, Kim EJ, Legrand P, Vernède X, Lindahl PA, Fontecilla-Camps JC (2003) NiZn[$Fe_4S_4$] and NiNi[$Fe_4S_4$] clusters in closed and open a subunits of acetyl-CoA synthase/carbon monoxide dehydrogenase. Nat Struct Mol Biol 10:271–279

Darrouzet E, Rinaldi C, Zambelli B, Ciurli S, Cavazza C (2021) Revisiting the CooJ family, a potential chaperone for nickel delivery to [NiFe]-carbon monoxide dehydrogenase. J Inorg Biochem 225:111588. https://doi.org/10.1016/j.jinorgbio.2021.111588

Davidson G, Clugston SL, Honek JF, Maroney MJ (2000) XAS investigation of the nickel active site structure in *Escherichia coli* glyoxalase I. Inorg Chem 39:2962–2963

Davidson G, Clugston SL, Honek JF, Maroney MJ (2001) An XAS investigation of product and inhibitor complexes of Ni-containing GlxI from *Escherichia coli*: mechanistic implications. Biochemistry 40:4569–4582

Davis GS, Flannery EL, Mobley HLT (2006) *Helicobacter pylori* HP1512 is a nickel-responsive NikR-regulated outer membrane protein. Infect Immun 74:6811–6820

de Pina K, Navarro C, McWalter L, Boxer DH, Price NC, Kelly SM, Mandrand-Berthelot M-A, Wu L-F (1995) Purification and characterization of the periplasmic nickel-binding protein NikA of *Escherichia coli* K12. Eur J Biochem 227:857–865

de Pina K, Desjardin V, Mandrand-Berthelot M-A, Giordano G, Wu L-F (1999) Isolation and characterization of the *nikR* gene encoding a nickel-responsive regulator in *Escherichia coli*. J Bacteriol 181:670–674

Debussche L, Couder M, Thibaut D, Cameron B, Crouzet J, Blanche F (1992) Assay, purification, and characterization of cobaltochelatase, a unique complex catalyzing cobalt insertion in hydrogenobyrinic acid a,c-diamide during coenzyme B12 biosynthesis in *Pseudomonas denitrificans*. J Bacteriol 174:7445–7451

Degen O, Kobayashi M, Shimizu S, Eitinger T (1999) Selective transport of divalent cations by transition metal permeases: the *Alcaligenes eutrophus* HoxN and the *Rhodococcus rhodochrous* NhlF. Arch Microbiol 171:139–145

Delany I, Ieva R, Soragni A, Hilleringmann M, Rappuoli R, Scarlato V (2005) In vitro analysis of protein-operator interactions of the NikR and Fur metal-responsive regulators of coregulated genes in *Helicobacter pylori*. J Bacteriol 187:7703–7715

Denic M, Turlin E, Michel V, Fischer F, Khorasani-Motlagh M, Zamble D, Vinella D, de Reuse H (2021) A novel mode of control of nickel uptake by a multifunctional metallochaperone. PLoS Pathog 17:e1009193

Desguin B, Goffin P, Viaene E, Kleerebezem M, Martin-Diaconescu V, Maroney MJ, Declercq J-P, Soumillion P, Hols P (2014) Lactate racemase is a nickel-dependent enzyme activated by a widespread maturation system. Nat Commun 5:3615

Desguin B, Goffin P, Bakouche N, Diman A, Viaene E, Dandoy D, Fontaine L, Hallet B, Hols P (2015a) Enantioselective regulation of lactate racemization by LarR in *Lactobacillus plantarum*. J Bacteriol 197:219–330

Desguin B, Zhang T, Soumillion P, Hols P, Hu J, Hausinger RP (2015b) A tethered niacin-derived pincer complex with a nickel-carbon bond in lactate racemase. Science 349:66–69

Desguin B, Soumillion P, Hols P, Hausinger RP (2016) Nickel-pincer cofactor biosynthesis involves LarB-catalyzed pyridinium carboxylation and LarE-dependent sacrificial sulfur insertion. Proc Natl Acad Sci U S A 113:5598–5603

Desguin B, Soumillion P, Hols P, Hu J, Hausinger RP (2017) Lactate racemase and its niacin-derived, covalently-tethered, nickel cofactor. In: Zamble DB, Rowinska-Zyrek M, Kozlowski H (eds) The biological chemistry of nickel. Royal Society of Chemistry, Cambridge

Desguin B, Fellner M, Riant O, Hu J, Hausinger RP, Hols P, Soumillion P (2018) Biosynthesis of the nickel-pincer nucleotide cofactor of lactate racemase requires a CTP-dependent cyclometallase. J Biol Chem 293:12303–12317

Desguin B, Urdiain-Arraiza J, Da Costa M, Fellner M, Hu J, Hausinger RP, Desmet T, Hols P, Soumillion P (2020) Uncovering a superfamily of nickel-dependent hydroxyacid racemases and epimerases. Sci Rep 10:18123

Deshpande A, Pochapsky TC, Ringe D (2017) The metal drives the chemistry: dual functions of acireductone dioxygenase. Chem Rev 117:10474–10501

Dian C, Schauer K, Kapp U, McSweeney SM, Labigne A, Terradot L (2006) Structural basis of the nickel response in *Helicobacter pylori*: crystal structures of HpNikR in apo and nickel-bound states. J Mol Biol 361:715–730

Diederix REM, Fauquant C, Rodrigue A, Mandrand-Berthelot M-A, Michaud-Soret I (2008) Sub-micromolar affinity of *Escherichia coli* NikR for Ni(II). Chem Commun 1813–1815

Dixon NE, Gazzola C, Blakeley RL, Zerner B (1975) Jack bean urease (EC 3.5.1.5). A metalloenzyme. A simple biological role for nickel? J Am Chem Soc 97:4131–4133

Dobbek H, Svetlitchnyi V, Gremer L, Huber R, Meyer O (2001) Crystal structure of a carbon monoxide dehydrogenase reveals a [Ni-4Fe-5S] cluster. Science 293:1281–1285

Dokpikul T, Chaoprasid P, Saninjuk K, Sirirakphaisarn S, Johnrod J, Nookabkaew S, Sukchawilit R, Mongkolsuk S (2016) Regulation of the cobalt/nickel efflux operon *dmeRF* in *Agrobacterium tumefaciens* and a link between the iron-sensing regulator RirA and cobalt/nickel resistance. Appl Environ Microbiol 82:4732–4742

Domnik L, Merrouch M, Goetzl S, Jeoung J-H, Léger C, Dementin S, Fourmond V, Dobbek H (2017) CODH-IV: a high-efficiency CO-scavenging CO dehydrogenase with resistance to $O_2$. Angew Chem Int Ed 56:15466–15469

Dosanjh NS, West AL, Michel SL (2009) *Helicobacter pylori* NikR's interaction with DNA: a two-tiered mode of recognition. Biochemistry 48:527–536

Doukov TI, Iverson TM, Seravalli J, Ragsdale SW, Drennan CL (2002) A Ni-Fe-Cu center in a bifunctional carbon monoxide dehydrogenase/acetyl-CoA synthase. Science 298:567–272

Doukov TI, Blasiak LC, Seravalli J, Ragsdale SW, Drennan CL (2008) Xenon in and at the end of the tunnel of bifunctional carbon monoxide dehydrogenase/acetyl-CoA synthase. Biochemistry 47:3474–3483

Drennan CL, Heo J, Sintchak MD, Schreiter E, Ludden PW (2001) Life on carbon monoxide: X-ray structure of *Rhodospirillum rubrum* Ni-Fe-S carbon monoxide dehydrogenase. Proc Natl Acad Sci U S A 98:11973–11978

Dupont CL, Neupane K, Shearer J, Palenik B (2008) Diversity, function and evolution of genes coding for putative Ni-containing superoxide dismutases. Environ Microbiol 10:1831–1843

Dupont CL, Johnson DA, Phillippy K, Paulsen IT, Brahamsha B, Palenik B (2012) Genetic identification of a high-affinity Ni transporter and the transcriptional response to Ni deprivation in *Synechococcus* sp. strain WH8102. Appl Environ Microbiol 78:7822–7832

D'Urzo A, Santambrogio C, Grandori R, Ciurli S, Zambelli B (2014) The conformational response to Zn(II) and Ni(II) binding of *Sporosarcina pasteurii* UreG, an intrinsically disordered GTPase. J Biol Inorg Chem 19:1341–1354

Eberz G, Eitinger T, Friedrich B (1989) Genetic determinants of a nickel-specific transport system are part of the plasmid-encoded hydrogenase gene cluster in *Alcaligenes eutrophus*. J Bacteriol 171:1340–1345

Eitinger T (2004) In vivo production of active nickel superoxide dismutase from *Prochlorococcus marinus* MIT9313 is dependent on its cognate peptidase. J Bacteriol 186:7812–7825

Eitinger T, Friedrich B (1991) Cloning, nucleotide sequence, and heterologous expression of the high-affinity nickel transport gene from *Alcaligenes eutrophus*. J Biol Chem 266:3222–3227

Eitinger T, Friedrich B (1994) A topological model for the high-affinity nickel transporter of *Alcaligenes eutrophus*. Mol Microbiol 12:1025–1032

Eitinger T, Mandrand-Berthelot M-A (2000) Nickel transport systems in microorganisms. Arch Microbiol 173:1–9

Eitinger T, Wolfram L, Degen O, Anthon C (1997) A $Ni^{2+}$ binding motif is the basis of high affinity transport of the *Alcaligenes eutrophus* nickel permease. J Biol Chem 272:17139–17144

Eitinger T, Degen O, Böhnke U, Müller M (2000) Nic1p, a relative of bacterial transition metal permeases in *Schizosaccharomyces pombe*, provides nickel ion for urease biosynthesis. J Biol Chem 275:18029–18033

Eitinger T, Suhr J, Moore L, Smith JAC (2005) Secondary transporters for nickel and cobalt ions: theme and variations. Biometals 18:399–405

Ellefson WL, Wolfe RS (1981) Component C of the methylreductase system of *Methanobacterium*. J Biol Chem 256:4259–4262

Ellefson WL, Whitman WB, Wolfe RS (1982) Nickel-containing factor $F_{430}$: chromophore of the methylreductase of *Methanobacterium*. Proc Natl Acad Sci U S A 79:3707–3710

Ellermann J, Hedderich R, Böcher R, Thauer RK (1988) The final step in methane formation. Investigations with the highly purified methyl-CoM reductase (component C) from *Methanobacterium thermoautotrophicum* (strain Marburg). Eur J Biochem 172:669–677

Englert DL, Adase CA, Jayaraman A, Manson MD (2010) Repellent taxis in response to nickel ion requires neither $Ni^{2+}$ transport nor the periplasmic NikA binding protein. J Bacteriol 192:2633–2637

Ensign SA, Campbell MJ, Ludden PW (1990) Activation of the nickel-deficient carbon monoxide dehydrogenase from *Rhodospirillum rubrum*: kinetic characterization and reductant requirement. Biochemistry 29:2162–2168

Ermler U, Grabarse W, Shima S, Goubeaud M, Thauer RK (1997) Crystal structure of methyl-coenzyme M reductase: the key enzyme of biological methane formation. Science 278:1457–1462

Ernst FD, Kuipers EJ, Heijens A, Sarwari R, Stoof J, Penn CW, Kusters JG, van Vliet AH (2005) The nickel-responsive regulator NikR controls activation and repression of gene transcription in *Helicobacter pylori*. Infect Immun 73:7252–7258

Ernst FD, Stoof J, Horrevoets WM, Kuipers EJ, Kusters JG, Van Vliet AHM (2006) NikR mediates nickel-responsive transcriptional repression of the *Helicobacter pylori* outer membrane proteins FecA3 (HP1400) and FrpB4 (HP1512). Infect Immun 74:6821–6828

Eschweiler JD, Farrugia MA, Hausinger RP, Ruotolo BT (2018) A structural model of the urease activation complex derived from ion mobility-mass spectrometry and integrative modeling. Structure 26:599–606

Farrugia MA, Han L, Zhong Y, Boer JL, Ruotolo BT, Hausinger RP (2013a) Analysis of a soluble $(UreD:UreF:UreG)_2$ accessory protein complex and its interactions with *Klebsiella aerogenes* urease by mass spectroscopy. J Am Soc Mass Spectrom 24:1328–1337

Farrugia MA, Macomber L, Hausinger RP (2013b) Biosynthesis of the urease metallocenter. J Biol Chem 288:13178–13185

Farrugia MA, Wang B, Feig M, Hausinger RP (2015) Mutational and computational evidence that a nickel-transfer tunnel in UreD is used for activation of *Klebsiella aerogenes* urease. Biochemistry 54:6392–6401

Fellner M, Desguin B, Hausinger RP, Hu J (2017) Structural insights into the catalytic mechanism of a sacrificial sulfur insertase of the N-type ATP pyrophosphatase family, LarE. Proc Natl Acad Sci U S A 114:9074–9079

Fetzner S (2012) Ring-cleaving dioxygenases with a cupin fold. Appl Environ Microbiol 78:2505–2514

Finkenwirth F, Eitinger T (2019) ECF-type ABC transporters for uptake of vitamins and transition metal ions into prokaryotic cells. Res Microbiol 170:358–365

Fischer F, Robbe-Saule M, Turlin E, Mancuso F, Michel V, Richaud P, Veyrier FJ, De Reuse H, Vinella D (2016) Characterization in *Helicobacter pylori* of a nickel transporter essential for colonization that was acquired during evolution by gastric *Helicobacter* species. PLoS Pathog 12:e1006018

Flannigan R, Choi WH, Chew B, Lange D (2014) Renal struvite stones--pathogenesis, microbiology, and management strategies. Nat Rev Urol 11:333–341

Fong YH, Wong HC, Chuck CP, Chen YW, Sun H, Wong K-B (2011) Assembly of the preactivation complex for urease maturation in *Helicobacter pylori*: crystal structure of the UreF/UreH protein complex. J Biol Chem 286:43241–43249

Fong YH, Wong HC, Yuen MH, Lau PH, Chen YW, Wong K-B (2013) Structure of UreG/UreF/UreH complex reveals how urease accessory proteins facilitate maturation of *Helicobacter pylori* urease. PLoS Biol 11:e1001678

Fontecilla-Camps JC, Volbeda A, Cavazza C, Nicolet Y (2007) Structure/function relationships of [NiFe]- and [FeFe]-hydrogenases. Chem Rev 107:4273–4303

Fortin D, Southam G, Beveridge TJ (1994) Nickel sulfide, iron-nickel sulfide and iron sulfide precipitated by a newly isolated *Desulfotomaculum* species and its relation to nickel resistance. FEMS Microbiol Ecol 14:121–132

Forzi L, Sawers RG (2007) Maturation of [NiFe]-hydrogenases in *Escherichia coli*. Biometals 20: 565–578

Foster AW, Patterson CJ, Pernil R, Hess CR, Robinson NJ (2012) Cytosolic Ni(II) sensor in cyanobacterium. Nickel detection follows nickel affinity across four families of sensors. J Biol Chem 287:12142–12151

Foster AW, Pernil R, Patterson CJ, Robinson NJ (2014) Metal specificity of cyanobacterial nickel-responsive repressor InrS: cells maintain zinc and copper below the detection threshold for InrS. Mol Microbiol 92:797–812

Foster AW, Pernil R, Patterson CJ, Scott AJP, Palsson LO, Pal R, Cummins I, Chivers PT, Pohl E, Robinson NJ (2017) A light tunable range for Ni(II) sensing and buffering in cells. Nat Chem Biol 13:409–414

Fourcroy AF, Vauguelin LN (1799) Extrait d'un premier mémoire des cit. Fourcroy et Vaugueline poru servir a l'histoire naturelle, chemique et médicale de l'urine humanine, contentant quelques faits nouveaux sur son analyse et son altération spontanée. Ann Chim 31:48–71

Fritsche E, Paschos A, Beisel H-G, Böck A, Huber R (1999) Crystal structure of the hydrogenase maturating endopeptidase HydD from *Escherichia coli*. J Mol Biol 288:989–998

Fu C, Javedan S, Moshiri F, Maier RJ (1994) Bacterial genes involved in incorporation of nickel into a hydrogenase enzyme. Proc Natl Acad Sci U S A 91:5099–5103

Fu C, Olson JW, Maier RJ (1995) HypB protein of *Bradyrhizobium japonicum* is a metal-binding GTPase capable of binding 18 divalent nickel ions per dimer. Proc Natl Acad Sci U S A 92: 2333–2337

Fulkerson JF Jr, Mobley HLT (2000) Membrane topology of the NixA nickel transporter of *Helicobacter pylori*: two nickel transport-specific motifs within transmembrane helices II and III. J Bacteriol 182:1722–1730

Fulkerson JF Jr, Garner RM, Mobley HLT (1998) Conserved residues and motifs in the NixA protein of *Helicobacter pylori* are critical for the high affinity transport of nickel ions. J Biol Inorg Chem 273:235–241

Furukawa K, Ramesh A, Zhou Z, Weinberg Z, Vallery T, Winkler WC, Breaker RR (2015) Bacterial riboswitches cooperatively bind $Ni^{2+}$ or $Co^{2+}$ ions and control expression of heavy metal transporters. Mol Cell 57:1088–1098

Gadd GM, Griffiths AJ (1978) Microorganisms and heavy metal toxicity. Microb Ecol 4:303–317

Garcia-Dominguez M, Lopez-Maury L, Florencio FJ, Reyes JC (2000) A gene cluster involved in metal homeostasis in the cyanobacterium *Synechocystis* sp. strain PCC 6803. J Bacteriol 182: 1507–1514

Garcin E, Vernede X, Hatchikian EC, Volbeda A, Frey M, Fontecilla-Camps JC (1999) The crystal structure of a reduced [NiFeSe] hydrogenase provides an image of the activated catalytic center. Structure 7:557–566

Ge R, Watt RM, Sun X, Tanner JA, He Q-Y, Huang J-D, Sun H (2006a) Expression and characterization of the histidine-rich protein, Hpn: potential for nickel storage in *Helicobacter pylori*. Biochem J 393:285–293

Ge R, Zhang Y, Sun X, Watt RM, He Q-Y, Huang J-D, Wilcox DE, Sun H (2006b) Thermodynamic and kinetic aspects of metal binding properties of the histidine-rich protein, Hpn. J Am Chem Soc 128:11330–11331

Gencic S, Grahame DA (2003) Nickel in subunit b of the acetyl-CoA decarbonylase/synthase multienzyme complex in methanogens. Catalytic properties and evidence for a binuclear Ni-Ni site. J Biol Chem 278:6101–6110

Geslin C, Llanos J, Prieur D, Jeanthon C (2001) The manganese and iron superoxide dismutases protect *Escherichia coli* from heavy metal toxicity. Res Microbiol 152:901–905

Ghosh S, Sadhukhan PC, Chaudhuri J, Ghosh DK, Mandal A (1999) Purification and properties of mercuric reductase from *Azotobacter chroococcum*. J Appl Microbiol 86:7–12

Ghssein G, Brutesco C, Ouerdane L, Fojcik C, Izaute A, Wang S, Hajjar C, Lobinski R, Lemaire D, Richaud P, Voulhoux R, Espaillat A, Cava F, Pignol D, Borezée-Durant E, Arnoux P (2016) Biosynthesis of a broad-spectrum nicotianamine-like metallophore in *Staphylococcus aureus*. Science 352:1105–1109

Gilbert JV, Ramakrishna J, Sunderman FW Jr, Wright A, Plaut AG (1995) Protein Hpn: cloning and characterization of a histidine-rich metal-binding polypeptide in *Helicobacter pylori* and *Helicobacter mustelae*. Infect Immun 63:2682–2688

Glass JB, Dupont CL (2017) Oceanic nickel biogeochemistry and the evolution of nickel use. In: Zamble DB, Rowinska-Zyrek M, Kozlowski H (eds) The biological chemistry of nickel. Royal Society of Chemistry, Cambridge

Gong W, Hao B, Wei Z, Ferguson DJ Jr, Tallant T, Krzycki JA, Chan MK (2008) Structure of the $a_2e_2$ Ni-dependent CO dehydrogenase component of the *Methanosarcina barkeri* acetyl-CoA decarbonylase/synthase complex. Proc Natl Acad Sci U S A 105:9558–9563

Gourdon P, Liu X-Y, Skjorringe T, Morth JP, Moller LB, Pedersen BP, Nissen P (2011) Crystal structure of a copper-transporting PIB-type ATPase. Nature 475:59–64

Grabarse W, Mahlert F, Shima S, Thauer RK, Ermler U (2000) Comparison of three methyl-coenzyme M reductases from phylogenetically distant microorganisms: unusual amino acid modification, conservation, and adaptation. J Mol Biol 303:329–344

Grahame DA (1991) Catalysis of acetyl-CoA cleavage and tetrahydrosarcinapterin methylation by a carbon monoxide dehydrogenase-corrinoid enzyme complex. J Biol Chem 266:22227–22233

Grass G, Grobe C, Nies D (2000) Regulation of the *cnr* cobalt and nickel resistance determinant from *Ralstonia* sp. strain CH34. J Bacteriol 182:1390–1398

Grass G, Fan B, Rosen BP, Lemke K, Schlegel HG, Rensing C (2001) NreB from *Achromobacter xylosoxidans* 31A is a nickel-induced transporter conferring nickel resistance. J Bacteriol 183: 2803–2807

Greening C, Biswas A, Carere CR, Jackson CJ, Taylor MC, Stott MB, Cook GM, Morales SE (2016) Genomic and metagenomic surveys of hydrogenase distribution indicate $H_2$ is a widely utilized energy source for microbial growth and survival. ISME J 10:761–777

Gregg CM, Goetzl S, Jeong J-H, Dobbek H (2016) AcsF catalyzes the ATP-dependent insertion of nickel into the Ni,Ni-[4Fe4S] cluster of acetyl-CoA synthase. J Biol Chem 291:18129–18138

Greig N, Wyllie S, Vickers TJ, Fairlamb AH (2006) Trypanothione-dependent glyoxalase I in *Trypanosoma cruzi*. Biochem J 400:217–223

Griffith DP, Musher DM, Itin C (1976) Urease. The primary cause of infection-induced urinary stones. Investig Urol 13:346–350

Grossoehme NE, Mulrooney SB, Hausinger RP, Wilcox DE (2007) Thermodynamics of $Ni^{2+}$, $Cu^{2+}$, and $Zn^{2+}$ binding to urease metallochaperone UreE. Biochemistry 46:10506–10516

Guldan H, Sterner R, Babinger P (2008) Identification and characterization of a bacterial glycerol-1-phosphate dehydrogenase: $Ni^{2+}$-dependent AraM from *Bacillus subtilis*. Biochemistry 47: 7376–7384

Guo H, Liu H, Wu H, Cui H, Fang J, Zuo Z, Deng J, Li Y, Wang X, Zhao L (2019) Nickel carcinogenesis mechanism: DNA damage. Int J Mol Sci 20:4690

Ha N-C, Oh S-T, Sung JY, Cha KA, Lee MH, Oh B-H (2001) Supramolecular assembly and acid resistance of *Helicobacter pylori* urease. Nat Struct Biol 8:505–509

Hadj-Saïd J, Pandelia M-E, Léger C, Fourmond V, Dementin S (2015) The carbon monoxide dehydrogenase from *Desulfovibrio vulgaris*. Biochim Biophys Acta 1847:1574–1583

Hahn CJ, Laso-Pérez R, Vulcano F, Vaziourakis K-M, Stokke R, Steen IH, Teske A, Boetius A, Liebeke M, Amann R, Knittel K, Wegener G (2020) "*Candidatus* Ethanoperedens," a thermophilic genus of *archaea* mediating the anaerobic oxidation of ethane. mBio 11:e00600–e00620

Hahn CJ, Lemaire ON, Kahnt J, Engilberge S, Wegener G, Wagner T (2021) Crystal structure of a key enzyme for anaerobic ethane activation. Science 373(6550):118–121. https://doi.org/10.1126/science.abg1765

Hall DR, Leonard GA, Reed CD, Watt CI, Berry A, Hunter WN (1999) The crystal structure of *Escherichia coli* class II fructose-1, 6-bisphosphate aldolase in complex with phosphoglycolohydroxamate reveals details of mechanism and specificity. J Mol Biol 287: 383–394

Happe RP, Roseboom W, Pierik AJ, Albracht SPJ, Bagley KA (1997) Biological activation of hydrogen. Nature 385:126

Haritha A, Sagar KP, Tiwari A, Kiranmavi P, Rodrigue A, Mohan PM, Singh SS (2009) MrdH, a novel metal resistance determinant of *Pseudomonas putida* KT 2440, is flanked by metal-inducible mobile genetic elements. J Bacteriol 191:5976–5987

Hausinger RP, Orme-Johnson WH, Walsh C (1984) Nickel tetrapyrrole cofactor F430: comparison of the forms bound to methyl coenzyme M reductase and protein free in cells of *Methanobacterium thermoautotrophicum* delta H. Biochemistry 23:801–804

Hausinger RP, Desguin B, Fellner M, Rankin JA, Hu J (2018) Nickel pincer nucleotide cofactor. Curr Opin Chem Biol 47:18–23

He MM, Clugston SL, Honek JF, Matthews BW (2000) Determination of the structure of *Escherichia coli* glyoxylase I suggests a structural basis for differential metal activation. Biochemistry 39:8719–8727

Heddle J, Scott DJ, Unzai S, Park S-Y, Tame JRH (2003) Crystal structures of the liganded and unliganded nickel-binding protein NikA from *Escherichia coli*. J Biol Chem 278:50322–50329

Herr CQ, Hausinger RP (2018) Amazing diversity in biochemical roles of Fe(II)/2-oxoglutarate oxygenases. Trends Biochem Sci 43:517–532

Higgins K (2019) Nickel metalloregulators and chaperones. Inorganics 7:104

Higgins KA, Carr CE, Maroney MJ (2012a) Specific metal recognition in nickel trafficking. Biochemistry 51:7816–7832

Higgins KA, Chivers PT, Maroney MJ (2012b) Role of the N-terminus in determining metal-specific responses in the *E. coli* Ni- and Co-responsive metalloregulator, RcnR. J Am Chem Soc 134:7081–7093

Higuchi Y, Yagi T, Yasuoka N (1997) Unusual ligand structure in Ni-Fe active center and an additional Mg site in hydrogenase revealed by high resolution X-ray structure analysis. Structure 5:1671–1680

Honek JF (2015) Glyoxalase biochemistry. Biomol Concepts 6:401–414

Honek JF (2017) Nickel glyoxalase I. In: Zamble D, Rowinska-Zyrek M, Kozlowski H (eds) The biological chemistry of nickel. The Royal Society of Chemistry, Cambridge

Howlett RM, Hughes BM, Hitchcock A, Kelly DJ (2012) Hydrogenase activity in the foodborne pathogen *Campylobacter jejuni* depends upon a novel ABC-type nickel transporter (NikZYXWV) and is SlyD-independent. Microbiology 158:1645–1655

Hu HQ, Huang H-T, Maroney MJ (2018) The *Helicobacter pylori* HypA·$UreE_2$ complex contains a novel high-affinity Ni(II)-binding site. Biochemistry 57:2932–2942

Hurwitz J, Gold M, Anders M (1964) The enzymatic methylation of ribonucleic acid and deoxyribonucleic acid. IV. The properties of the soluble ribonucleic acid-methylating enzymes. J Biol Chem 239:3474–3482

Inoue M, Nakamoto I, Omae K, Oguro T, Ogata H, Yoshida T, Sako Y (2019) Structural and phylogenetic diversity of anaerobic carbon-monoxide dehydrogenases. Front Microbiol 9:3353

Iwig JS, Chivers PT (2009) DNA recognition and wrapping by *Escherichia coli* RcnR. J Mol Biol 393:514–526

Iwig JS, Chivers PT (2010) Coordinating intracellular nickel--metal-site structure-function relationships and the NikR and RcnR repressors. Nat Prod Rep 27:658–667

Iwig JS, Rowe JL, Chivers PT (2006) Nickel homeostasis in *Escherichia coli* - the *rcnR-rcnA* efflux pathway and its linkage to NikR function. Mol Microbiol 62:252–262

Iwig JS, Leitch S, Herbst RW, Maroney MJ, Chivers PT (2008) Ni(II) and Co(II) sensing by *Escherichia coli* RcnR. J Am Chem Soc 130:7592–7606

Iyaka YA (2011) Nickel in soils: a review of its distribution and impacts. Sci Res Essays 6:6774–6777

Jabri E, Karplus PA (1996) Structures of the *Klebsiella aerogenes* urease apoprotein and two active-site mutants. Biochemistry 35:10616–10626

Jabri E, Carr MB, Hausinger RP, Karplus PA (1995) The crystal structure of urease from *Klebsiella aerogenes*. Science 268:998–1004

Jacobi A, Rossman R, Böck A (1992) The *hyp* operon gene products are required for maturation of catalytically active hydrogenase isoenzymes in *Escherichia coli*. Arch Microbiol 158:444–451

Jeon WB, Cheng J, Ludden PW (2001) Purification and characterization of membrane-associated CooC protein and its functional role in the insertion of nickel into carbon monoxide dehydrogenase from *Rhodospirillum rubrum*. J Biol Chem 276:38602–38609

Jeoung J-H, Giese T, Grünwald M, Dobbek H (2009) CooC1 from *Carboxydothermus hydrogenoformans* is a nickel-binding ATPase. Biochemistry 48:11505–11513

Jeoung J-H, Giese T, Grünwald M, Dobbek H (2010) Crystal structure of the ATP-dependent maturation factor of Ni,Fe-containing carbon monoxide dehydrogenase. J Mol Biol 396:1165–1179

Jeoung J-H, Nianios D, Fetzner S, Dobbek H (2017) Quercetin 2,4-dioxygenase activates dioxygen in a side-on $O_2$-Ni complex. Angew Chem Int Ed 55:3281–3284

Jia B, Jia X, Kim KH, Jeon CO (2017) Integrative view of 2-oxoglutarate/Fe(II)-dependent oxygenase diversity and functions in bacteria. Biochim Biophys Acta 1861:323–334

Jiang D, Zhao Y, Wang X, Fan J, Heng J, Liu X, Feng W, Kang X, Huang B, Liu J, Zhang XC (2013) Structure of the YajR transporter suggests a transport mechanism based on the conserved motif A. Proc Natl Acad Sci U S A 110:14664–14669

Johnson OE, Ryan KC, Maroney MJ, Brunold TC (2010) Spectroscopic and computational investigation of three Cys-to-Ser mutants of nickel superoxide dismutase: insight into the roles played by the Cys2 and Cys6 active-site residues. J Biol Inorg Chem 15:777–793

Joho M, Inouhe M, Tohoyama H, Murayama T (1990) A possible role of histidine in a nickel resistant mechanism of *Saccharomyces cerevisiae*. FEMS Microbiol Lett 66:333–338

Joho M, Ishikawa Y, Kunikane M, Inouhe M, Tohoyama H, Murayama T (1992) The subcellular distribution of nickel in Ni-sensitive and Ni-resistant strains of *Saccharomyces cerevisiae*. Microbios 71:149–159

Jones MD, Zamble DB (2018) Acid-responsive activity of the *Helicobacter pylori* metalloregulator NikR. Proc Natl Acad Sci U S A 115:8966–8971

Jones MD, Ademi I, Yin X, Gong Y, Zamble DB (2015) Nickel-responsive regulation of two novel *Helicobacter pylori* NikR-targeted genes. Metallomics 7:662–673

Ju T, Goldsmith RB, Chai SC, Maroney MJ, Pochapsky SS, Pochapsky TC (2006) One protein, two enzymes revisited: a structural entropy switch interconverts the two isoforms of acireductone dioxygenase. J Mol Biol 393:823–834

Jubier-Maurin V, Rodrigue A, Ouahrani-Bettache S, Layssac M, Mandrand-Bethelot M-A, Köhler S, Liautard J-P (2001) Identification of the *nik* gene cluster of *Brucella suis*: regulation and contribution to urease activity. J Bacteriol 183:426–434

Kalliri E, Grzyska PK, Hausinger RP (2005) Kinetic and spectroscopic investigation of $Co^{II}$, $Ni^{II}$, and *N*-oxalylglycine inhibition of the $Fe^{II}$/a-ketoglutarate dioxygenase, TauD. Biochem Biophys Res Commun 338:191–197

Kaluarachchi H, Chan Chung KC, Zamble DB (2010) Microbial nickel proteins. Nat Prod Rep 27:681–694

Kaluarachchi H, Zhang JW, Zamble DB (2011) *Escherichia coli* SlyD, more than a Ni(II) reservoir. Biochemistry 50:10761–10763

Kasprzak KS, Salnikow K (2007) Nickel toxicity and carcinogenesis. In: Sigel A, Sigel H, Sigel RKO (eds) Metal ions in life sciences. Wiley, New York

Kerby RL, Ludden PW, Roberts GP (1997) In vivo nickel insertion into carbon monoxide dehydrogenase of *Rhodosprillum rubrum*: molecular and physiological characterization of *cooCTJ*. J Bacteriol 179:2259–2266

Kidd SP, Djoko KY, Ng J, Argente MP, Jennings MP, McEwan AG (2011) A novel nickel responsive MerR-like regulator, NimR, from *Haemophilus influenzae*. Metallomics 3:1009–1018

Kim E-J, Kim H-P, Hah YC, Roe J-H (1996) Differential expression of superoxide dismutases containing Ni and Fe/Zn in *Streptomyces coelicolor*. Eur J Biochem 214:178–185

Kim E-J, Chung H-J, Suh B, Hah YC, Roe J-H (1998a) Expression and regulation of the *sodF* gene encoding iron- and zinc-containing superoxide dismutase in *Streptomyces coelicolor* Müller. J Bacteriol 180:2014–2020

Kim E-J, Chung H-J, Suh B, Hah YC, Roe J-H (1998b) Transcriptional and post-transcriptional regulation by nickel of *sodN* gene encoding nickel-containing superoxide dismutase from *Streptomyces coelicolor* Müller. Mol Microbiol 27:187–195

Kim I-K, Yim Y-I, Kim Y-M, Lee J-W, Yim H-S, Kang S-O (2003a) CbiX-homologous protein (CbiXhp), a metal-binding protein, from *Streptomyces seoulensis* is involved in expression of nickel-containing superoxide dismutase. FEMS Microbiol Lett 228:21–26

Kim J-S, Kang S-O, Lee J-K (2003b) The protein complex composed of nickel-binding SrnQ and DNA binding motif-bearing SrnR of *Streptomyces griseus* represses *sodF* transcription in the presence of nickel ions. J Biol Chem 278:18455–18463

Kim JK, Mulrooney SB, Hausinger RP (2005) Biosynthesis of active *Bacillus subtilis* urease in the absence of known urease accessory proteins. J Bacteriol 187:7150–7154

Kim HM, Ahn B-E, Lee J-H, Roe J-H (2015) Regulation of a nickel-cobalt efflux system and nickel homeostasis in a soil actinobacterium *Streptomyces coelicolor*. Metallomics 7:702–709

King GM, Weber CF (2007) Distribution, diversity and ecology of aerobic CO-oxidizing bacteria. Nat Rev Microbiol 5:107–118

Koch D, Nies DH, Grass G (2007) The RcnRA (YohLM) system of *Escherichia coli*: a connection between nickel, cobalt, and iron homeostasis. Biometals 20:759–771

Krüger M, Meyerdierks A, Glöckner FO, Amann R, Widdel F, Kube M, Reinhardt R, Kahnt J, Böcher R, Thauer RK, Shima S (2003) A conspicuous nickel protein in microbial mats that oxidize methane anaerobically. Nature 426:878–881

Kulathila R, Kulathila R, Indic M, van den Berg B (2011) Crystal structure of *Escherichia coli* CusC, the outer membrane component of a heavy metal efflux pump. PLoS One 6:e15610

Kumar V, Mishra RK, Kaur G, Dutta D (2017) Cobalt and nickel impair DNA metabolism by the oxidative stress independent pathway. Metallomics 9:1596–1609

Kung Y, Drennan CL (2017) One-carbon chemistry of nickel-containing carbon monoxide dehydrogenase and acetyl-CoA synthase. In: Zamble D, Rowinska-Zyrek M, Kozlowski H (eds) The biological chemistry of nickel. Royal Society of Chemistry, Cambridge

Kurzer F, Sanderson PM (1956) Urea in the history of organic chemistry. J Chem Ed 33:452–459

Kusters JG, Van Vliet AHM, Kuipers EJ (2006) Pathogenesis of *Helicobacter pylori* infection. Clin Microbiol Rev 19:449–490

Kwon S, Nishitani Y, Watanabe S, Hirao Y, Imanaka T, Kanai T, Atomi H, Miki K (2016) Crystal structure of a [NiFe] hydrogenase maturation protease HybD from *Thermococcus kodakarensis* KOD1. Proteins 84:1321–1327

Kwon S, Watanabe S, Nishitani Y, Kawashima T, Kanai T, Atomi H, Miki K (2018) Crystal structures of a [NiFe] hydrogenase large subunit HyhL in an immature state in complex with a Ni chaperone HypA. Proc Natl Acad Sci U S A 115:7045–7050

Labigne A, Cussac V, Courcoux P (1991) Shuttle cloning and nucleotide sequences of *Helicobacter pylori* genes responsible for urease activity. J Bacteriol 173:1920–1931

Lacasse MJ, Zamble DB (2016) [NiFe]-hydrogenase maturation. Biochemistry 55:1689–1701

Lam R, Romanov V, Johns K, Battaile K, Wu-Brown J, Guthrie JL, Hausinger RP, Pai E, Chirgadze NY (2010) Crystal structure of a truncated urease accessory protein UreF from *Helicobacter pylori*. Proteins 78:2839–2848

Laso-Pérez R, Wegener G, Knittel K, Widdel F, Harding KJ, Krukenberg V, Meier DV, Richter M, Tegetmeyer HE, Riedel D, Richnow H-H, Adrian L, Reemtsma T, Lechtenfeld OJ, Musat F (2016) Thermophilic archaea activate butane via alkyl-coenzyme M formation. Nature 539: 396–401

Laso-Pérez R, Hahn C, van Vliet DM, Tegetmeyer HE, Schubotz F, Smit NT, Pape T, Sahling H, Bohrmann G, Boetius A, Knittel K, Wegener G (2019) Anaerobic degradation of non-methane alkanes by "*Candidatus* Methanoliparia" in hydrocarbon seeps of the gulf of Mexico. mBio 10: e01814–e01819

Leach MR, Zamble DB (2007) Metallocenter assembly of the hydrogenase enzymes. Curr Opin Chem Biol 11:159–165

Leach MR, Zhang JW, Zamble DB (2007) The role of complex formation between the *Escherichia coli* hydrogenase factors HypB and SlyD. J Biol Chem 282:16177–16186

Lebrette H, Iannello M, Fontecilla-Camps JC, Cavazza C (2013) The binding mode of Ni-(L-His)$_2$ in NikA revealed by X-ray crystallography. J Inorg Biochem 121:16–18

Lebrette H, Brochier-Armanet C, Zambelli B, de Reuse H, Borezée-Durant E, Ciurli S, Cavazza C (2014) Promiscuous nickel import in human pathogens: structure, thermodynamics, and evolution of extracytoplasmic nickel-binding proteins. Structure 22:1421–1432

Lebrette H, Borezee-Durant E, Martin L, Richaud P, Boeri Erba E, Cavazza C (2015) Novel insights into nickel import in *Staphylococcus aureus*: the positive role of free histidine and structural characterization of a new thiazolidine-type nickel chelator. Metallomics 7:613–621

Leclere V, Boiron P, Blondeau R (1999) Diversity of superoxide-dismutases among clinical and soil isolates of *Streptomyces* species. Curr Microbiol 39:365–368

Lee MH, Mulrooney SB, Renner MJ, Markowicz Y, Hausinger RP (1992) *Klebsiella aerogenes* urease gene cluster: sequence of *ureD* and demonstration that four accessory genes (*ureD*, *ureE*, *ureF*, and *ureG*) are involved in nickel metallocenter biosynthesis. J Bacteriol 174:4324–4330

Lee MH, Pankratz HS, Wang S, Scott RA, Finnegan MG, Johnson MK, Ippolito JA, Christianson DW, Hausinger RP (1993) Purification and characterization of *Klebsiella aerogenes* UreE protein: a nickel-binding protein that functions in urease metallocenter assembly. Protein Sci 2:1042–1052

Lee CW, Chakravorty DK, Chang F-MJ, Reyes-Caballero H, Ye Y, Merz KM Jr, Giedroc DP (2012) Solution structure of *Mycobacterium tuberculosis* NmtR in the apo state: insights into Ni (II)-mediated allostery. Biochemistry 51:2619–2629

Lemaire ON, Wagner T (2020) Gas channel rerouting in a primordial enzyme: structure insights of the carbon-monoxide dehydrogenase/acetyl-CoA synthase complex from the acetogen *Clostridium autoethanogenum*. Biochim Biophys Acta 1862:148330

Lenz O, Friedrich B (1998) A novel multicomponent regulatory system mediates $H_2$ sensing in *Alcaligenes eutrophus*. Proc Natl Acad Sci U S A 95:12474–12479

Li Y, Zamble DB (2009) Nickel homeostasis and nickel regulation: an overview. Chem Rev 109: 4617–4643

Li C, Vavra JW, Carr CE, Huang H-T, Maroney MJ, Wilmot CM (2020) Complexation of the nickel and cobalt transcriptional regulator RcnR with DNA. Acta Crystallogr F76:25–30

Liesegang H, Lemke K, Siddiqui RA, Schlegel HG (1993) Characterization of the inducible nickel and cobalt resistance determinant *cnr* from pMOL28 of *Alcaligenes eutrophus* CH34. J Bacteriol 175:767–778

Loke H-K, Lindahl PA (2003) Identification and preliminary characterization of AcsF, a putative Ni-insertase used in the biosynthesis of acetyl-CoA synthase from *Clostridium thermoaceticum*. J Inorg Biochem 93:33–40

Loke H-K, Bennett GN, Lindahl PA (2000) Active acetyl-CoA synthase from *Clostridium thermoaceticum* obtained by cloning and heterologous expression of *acsAB* in *Escherichia coli*. Proc Natl Acad Sci U S A 97:12530–12535

Long F, Su C-C, Zimmermann MT, Boyken SE, Rajashankar KR, Jernigan RL, Yu EW (2010) Crystal structures of the CusA efflux pump suggest methionine-mediated metal transport. Nature 467:484–488

Lopez-Maury L, Garcia-Dominguez M, Florencio FJ, Reyes JC (2002) A two-component signal transduction system involved in nickel sensing in the cyanobacterium *Synechocystis* sp. PCC 6803. Mol Microbiol 43:247–256

Louwrier A, Knowles CJ (1996) The purification and characterization of a novel D(−)-specific carbamoylase enzyme from *Agrobacterium* sp. Enzym Microb Technol 19:562–571

Lu M, Chai J, Fu D (2009) Structural basis for autoregulation of the zinc transporter YiiP. Nat Struct Mol Biol 16:1063–1068

Lu M, Jiang Y-L, Wang S, Jin H, Zhang R-G, Virolle M-J, Chen Y, Zhou C-Z (2014) *Streptomyces coelicolor* SCO4226 is a nickel binding protein. PLoS One 9:e109660

Lubitz W, Ogata H, Rüdiger O, Reijerse E (2014) Hydrogenases. Chem Rev 114:4081–4148

Lutz A, Jacobi A, Schlensog V, Böhm R, Sawers G, Böck A (1991) Molecular characterization of an operon (*hyp*) necessary for the activity of the three hydrogenase isoenzymes in *Escherichia coli*. Mol Microbiol 5:123–135

Lyu Z, Shao N, Chou C-W, Shi H, Patel R, Duin EC, Whitman WB (2020) Posttranslational modification of arginine in methyl coenzyme M reductase has a profound impact on both methanogenesis and growth of *Methanococcus maripaludis*. J Bacteriol 202:e00654–e00619

Macomber L, Hausinger RP (2011) Mechanisms of nickel toxicity in microorganisms. Metallomics 3:1153–1162

Macomber L, Elsey SP, Hausinger RP (2011) Fructose-1,6-bisphosphate aldolase (class II) is the primary site of nickel toxicity in *Escherichia coli*. Mol Microbiol 82:1291–1300

Maeda M, Hidaka M, Nakamura A, Masaki H, Uozumi T (1994) Cloning, sequencing, and expression of thermophilic *Bacillus* sp. strain TB-90 urease gene complex in *Escherichia coli*. J Bacteriol 176:432–442

Maillard AP, Girard E, Ziani W, Petit-Hartlein I, Kahn R, Covès J (2014) The crystal structure of the anti-s factor CnrY in complex with the s factor CnrH shows a new structural class of anti-s factors targeting extracytoplasmic function s factors. J Mol Biol 426:2313–2327

Maillard AP, Künnemann S, Grobe C, Volbeda A, Schleuder G, Petit-Hartlein I, De Rosny E, Nies D, Covès J (2015) Response of CnrX from *Cupriavidus metallidurans* CH34 to nickel binding. Metallomics 7:622–631

Manley OM, Myers PD, Toney DJ, Bolling KF, Rhodes LC, Gasparik JL, Grossoehme NE (2020) Evaluation of the regulatory model for $Ni^{2+}$ sensing by Nur from *Streptomyces coelicolor*. J Inorg Biochem 203:110859

Maratea D, Young K, Young R (1985) Deletion and fusion analysis of the phage phi X174 lysis gene E. Gene 40:39–46

Marcus EA, Scott DR (2001) Cell lysis is responsible for the appearance of extracellular urease in *Helicobacter pylori*. Helicobacter 6:93–99

Maroney MJ, Ciurli S (2014) Nonredox nickel enzymes. Chem Rev 114:4206–4228

Marques MC, Coelho R, De Lacey AI, Pereira IA, Matias PM (2010) The three-dimensional structure of [NiFeSe] hydrogenase from *Desulfovibrio vulgaris* Hildenborough: a hydrogenase without a bridging ligand in the active site in its oxidized, "as isolated" state. J Mol Biol 396: 893–907

Marrero J, Auling G, Coto O, Nies DH (2007) High-level resistance to cobalt and nickel but probably no transenvelope efflux: metal resistance in the Cuban *Serratia marcescens* strain C-1. Microb Ecol 53:123–133

Martin-Diaconescu V, Joseph C, Boer JL, Mulrooney SB, Hausinger RP, Maroney MJ (2017) Non-thiolate ligation of nickel by nucleotide-free UreG of *Klebsiella aerogenes*. J Biol Inorg Chem 22:497–503

Masetti M, Bertazzo M, Recanatini M, Ciurli S, Musiani F (2021) Probing the transport of Ni (II) ions through the internal tunnels of the Helicobacter pylori UreDFG multimeric protein complex. J Inorg Biochem 223:111554. https://doi.org/10.1016/j.jinorgbio.2021.111554

Matias PM, Soares CM, Saraiva LM, Coelho R, Morais J, Le Gall J, Carrondo MA (2001) [NiFe] hydrogenase from *Desulfovibrio desulfuricans* ATCC 27774: gene sequencing, three-dimensional structures determination and refinement at 1.8 Å and modeling studies of its interaction with the tetrahaem cytochrome *c*3. J Biol Inorg Chem 6:63–81

Maynard EL, Lindahl PA (1999) Evidence of a molecular tunnel connecting the active sites for $CO_2$ reduction and acetyl-CoA synthesis in acetyl-CoA synthase from *Clostridium thermoaceticum*. J Am Chem Soc 121:9221–9222

Mayr S, Latkoczy C, Krüger M, Günther D, Shima S, Thauer RK, Widdel F, Jaun B (2008) Structure of an F430 variant from archaea associated with anaerobic oxidation of methane. J Am Chem Soc 130:10758–10767

Mazzei L, Muslani F, Ciurli S (2020) The structure-based reaction mechanism of urease, a nickel dependent enzyme: tale of a long debate. J Biol Inorg Chem 25:829–845

Mazzei L, Musiani F, Żerko S, Koźminski W, Cianci M, Beniamino Y, Ciurli S, Zambelli B (2021) Structure, dynamics, and function of SrnR, a transcription factor for nickel-dependent gene expression. Metallomics 13(12):mfab069. https://doi.org/10.1093/mtomcs/mfab069

McLean RJC, Nickel JC, Cheng K-J, Costerton JW (1988) The ecology and pathogenicity of urease-producing bacteria in the urinary tract. Crit Rev Microbiol 16:37–79
McLean RJC, Beauchemin D, Clapham L, Beveridge TJ (1990) Metal-binding characteristics of the gamma-glutamyl capsular polymer of *Bacillus licheniformis* ATCC 9945. Appl Environ Microbiol 56:3671–3677
McMillan DJ, Mau M, Walker MJ (1998) Characterization of the urease gene cluster in *Bordetella bronchiseptica*. Gene 208:243–251
Mergeay M, Nies D, Schlegel HG, Gerits J, Charles P, van Gijsegem F (1985) *Alcaligenes eutrophus* CH34 is a facultative chemolithotroph with plasmid-bound resistance to heavy metals. J Bacteriol 162:328–334
Merloni A, Dobrovolska O, Zambelli B, Agostini F, Bazzani M, Musiani F, Ciurli S (2014) Molecular landscape of the interaction between the urease accessory proteins UreE and UreG. Biochim Biophys Acta 1844:1662–1674
Merrouch M, Benvenuti M, Lorenzi M, Léger C, Fourmond V, Dementin S (2018) Maturation of the [Ni-4Fe-4S] active site of carbon monoxide dehydrogenases. J Biol Inorg Chem 23:613–620
Meuer J, Bartoschek S, Koch J, Kunkel A, Hedderich R (1999) Purification and catalytic properties of Ech hydrogenase from *Methanosarcina barkeri*. Eur J Biochem 265:325–335
Miki K, Atomi H, Watanabe B (2020) Structural insight into [NiFe] hydrogenase maturation by transient complexes between Hyp proteins. Acc Chem Res 53:875–886
Miquel P (1890) C R Acad Sci 111:397
Miraula M, Ciurli S, Zambelli B (2015) Intrinsic disorder and metal binding in UreG proteins from Archae hyperthermophiles: GTPase enzymes involved in the activation of Ni(II) dependent urease. J Biol Inorg Chem 20:739–755
Mobley HLT, Hausinger RP (1989) Microbial ureases: significance, regulation, and molecular characterization. Microbiol Rev 53:85–108
Mobley HLT, Garner RM, Bauerfeind P (1995a) *Helicobacter pylori* nickel-transport gene *nixA*: synthesis of catalytically active urease in *Escherichia coli* independent of growth conditions. Mol Microbiol 16:97–109
Mobley HLT, Island MD, Hausinger RP (1995b) Molecular biology of microbial ureases. Microbiol Rev 59:451–480
Moncrief MBC, Hausinger RP (1996) Purification and activation properties of UreD-UreF-urease apoprotein complexes. J Bacteriol 178:5417–5421
Moncrief MBC, Hausinger RP (1997) Characterization of UreG, identification of a UreD-UreF-UreG complex, and evidence suggesting that a nucleotide-binding site in UreG is required for *in vivo* metallocenter assembly of *Klebsiella aerogenes* urease. J Bacteriol 179:4081–4086
Moore SJ, Sowa ST, Schuchardt C, Deery E, Lawrence AD, Ramos JV, Billig S, Birkemeyer C, Chivers PT, Howard MJ, Rigby SE, Layer G, Warren MJ (2017) Elucidation of the biosynthesis of the methane catalyst coenzyme $F_{430}$. Nature 543:78–82
Muller C, Bahlawane C, Aubert S, Delay CM, Schauer K, Michaud-Soret I, De Reuse H (2011) Hierarchical regulation of the NikR-mediated nickel response in *Helicobacter pylori*. Nucleic Acids Res 39:7564–7575
Mulrooney SB, Hausinger RP (1990) Sequence of the *Klebsiella aerogenes* urease genes and evidence for accessory proteins facilitating nickel incorporation. J Bacteriol 172:5837–5843
Mulrooney SB, Ward SK, Hausinger RP (2005) Purification and properties of the *Klebsiella aerogenes* UreE metal-binding domain, a functional metallochaperone of urease. J Bacteriol 187:3581–3585
Munkelt D, Grass G, Nies DH (2004) The chromosomally encoded cation diffusion facilitator proteins DmeF and FieF from *Wautersia metallidurans* CH34 are transporters of broad metal specificity. J Bacteriol 186:8036–8043
Muraki N, Ishii K, Uchiyama S, Itoh SG, Okumura H, Aono S (2019) Structural characterization of HypX responsible for CO biosynthesis in the maturation of NiFe-hydrogenase. Commun Biol 2: 385

Musiani F, Zambelli B, Stola M, Ciurli S (2004) Nickel trafficking: insights into the fold and function of UreE, a urease metallochaperone. J Inorg Biochem 98:803–813
Musiani F, Zambelli B, Bazzani M, Mazzei L, Ciurli S (2015) Nickel-responsive transcriptional regulators. Metallomics 7:1305–1318
Navarro C, Wu L-F, Mandrand-Berthelot M-A (1993) The *nik* operon of *Escherichia coli* encodes a periplasmic binding-protein-dependent transport system for nickel. Mol Microbiol 9:1181–1191
Nayak DD, Mahanta N, Mitchell DA, Metcalf WW (2017) Post-translational thioamidation of methyl-coenzyme M reductase, a key enzyme in methanogenic and methanotrophic archaea. elife 6:e29218
Nayak DD, Liu A, Agrawal N, Rodriquez-Carerro R, Dong S-H, Mitchell DA, Nair SK, Metcalf WW (2020) Functional interactions between posttranslationally modified amino acids of methyl-coenzyme M reductase in Methanosarcina acetivorans. PLoS Biol 18:e3000507
Nevarez JL, Turmo A, Hu J, Hausinger RP (2020) Biochemical pincer complexes. ChemCatChem 12:4242–4254
Nianios D, Thierbach S, Steimer L, Lulchev P, Klostermeier D, Fetzner S (2015) Nickel quercetinase, a "promiscuous" metalloenzyme: metal incorporation and metal ligand substitution studies. BMC Biochem 16:10
Nielubowicz GR, Mobley HLT (2010) Host-pathogen interactions in the urinary tract interaction. Nat Rev Urol 7:430–441
Nies DH, Covès J, Sawers RG (2017) Cross-talk between nickel and other metals in microbial systems. In: Zamble DB, Rowinska-Zyrek M, Kozlowski H (eds) The biological chemistry of nickel. Royal Society of Chemistry, Cambridge
Niki E, Yoshida Y, Saito Y, Noguchi N (2005) Lipid peroxidation: mechanisms, inhibition, and biological effects. Biochem Biophys Res Commun 338:668–676
Nim YS, Wong K-B (2019) The maturation pathway of nickel urease. Inorganics 7:85
Nishimura K, Igarashi K, Kakinuma Y (1998) Proton gradient-driven nickel uptake by vacuolar membrane vesicles of *Saccharomyces cerevisiae*. J Bacteriol 180:1962–1964
Noll KN, Rinehart KL Jr, Tanner RS, Wolfe RS (1986) Structure of component B (7-mercaptoheptanoylthreonine phosphate) of the methylcoenzyme M methylreductase system of *Methanobacterium thermoautotrophicum*. Proc Natl Acad Sci U S A 83:4238–4242
Norsworthy AN, Pearson MM (2017) From catheter to kidney stone: the uropathogenic lifestyle of *Proteus mirabilis*. Trends Microbiol 25:304–315
Nriagu JO (1980) Nickel in the environment. Wiley, New York
Ogata H, Kellers P, Lubitz W (2010) The crystal structure of the [NiFe] hydrogenase from the photosynthetic bacterium *Allochromatium vinosum*: characterization of the oxidized enzyme (Ni-A state). J Mol Biol 402:428–444
Ogata H, Nishikawa K, Lubitz W (2015) Hydrogens detected by subatomic resolution protein crystallography in a [NiFe] hydrogenase. Nature 520:571–574
Ogata H, Lubitz W, Higuchi Y (2016) Structure and function of [NiFe] hydrogenases. J Biochem 160:251–258
Olson JW, Maier RJ (2000) Dual roles of *Bradyrhizobium japonicum* nickelin protein in nickel storage and GTP-dependent Ni mobilization. J Bacteriol 182:1702–1705
Olson JW, Mehta NS, Maier RJ (2001) Requirement of nickel metabolism proteins HypA and HypB for full activity of both hydrogenase and urease in *Helicobacter pylori*. Mol Microbiol 39: 176–182
Outten CE, O'Halloran TV (2001) Femtomolar sensitivity of metalloregulatory proteins controlling zinc homeostasis. Science 292:2488–2492
Padmanabhan PK, Mukherjee A, Singh S, Chattopadhyaya S, Gowri VS, Myler PJ, Srinivasan N, Mahubala R (2005) Glyoxylase I from *Leishmania donovani*: a potential target for anti-parasite drug. Biochem Biophys Res Commun 337:1237–1248
Pal A, Paul AK (2010) Nickel uptake and intracellular localization in *Cupriavidus pauculus* KPS 201, native to ultramafic ecosystem. Adv Biosci Biotechnol 1:276–280
Palmgren MG, Nissen P (2011) P-type ATPases. Annu Rev Biophys 40:243–266

Palombo M, Bonucci A, Etienne E, Ciurli S, Uversky VN, Guigliarelli B, Belle V, Mileo E, Zambelli B (2017) The relationship between folding and activity in UreG, an intrinsically disordered enzyme. Sci Rep 7:5977

Paraszkiewicz K, Bernat P, Naliwajski M, Dlugonski J (2010) Lipid peroxidation in the fungus *Curvularia lunata* exposed to nickel. Arch Microbiol 192:135–141

Park I-S, Carr MB, Hausinger RP (1994) *In vitro* activation of urease apoprotein and role of UreD as a chaperone required for nickel metallocenter assembly. Proc Natl Acad Sci U S A 91:3233–3237

Park JE, Schlegel H-G, Rhie HG, Lee HS (2004) Nucleotide sequence and expression of the *ncr* nickel and cobalt resistance in *hafnia alvei* 5-5. Int Microbiol 7:27–34

Park J-S, Lee S-J, Rhie H-G, Lee H-S (2008) Characterization of a chromosomal nickel resistance determinant from *Klebsiella oxytoca* CCUG 15788. J Microbiol Biotechnol 18:1040–1043

Pasteur L (1860) De l'origine des ferments, etc. C R Acad Sci 50:849

Pearce DA, Sherman F (1999) Toxicity of copper, cobalt, and nickel salts is dependent on histidine metabolism in the yeast *Saccharomyces cerevisiae*. J Bacteriol 181:4774–4779

Pearson MA, Michel LO, Hausinger RP, Karplus PA (1997) Structure of Cys319 variants and acetohydroxamate-inhibited *Klebsiella aerogenes* urease. Biochemistry 36:8164–8172

Pennella MA, Shokes JE, Cosper NJ, Scott RA, Giedroc DP (2003) Structural elements of metal selectivity in metal sensor proteins. Proc Natl Acad Sci U S A 100:3713–3718

Peters JW, Schut GJ, Boyd ES, Mulder DW, Shepard EM, Broderick JB, King PW, Adams MWW (2015) [FeFe]- and [NiFe]-hydrogenase diversity, mechanism, and maturation. Biochim Biophys Acta 1853:1350–1369

Petkun S, Shi R, Li Y, Asinas A, Munger C, Zhang L, Waclawek M, Soboh B, Sawers RG, Cygler M (2011) Structure of hydrogenase maturation protein HypB with reaction intermediates shows two active sites. Structure 19:1773–1783

Pfaltz A, Livingston DA, Jaun B, Diekert G, Thauer RK, Eschenmoser A (1985) Factor F430 from methanogenic bacteria: on the nature of the isolation artifacts of F430, a contribution to the chemistry of F430 and the conformational stereochemistry of the ligand periphery of hydroporphinoid nickel(II) complexes. Helv Chim Acta 68:1338–1358

Pfaltz A, Kobelt A, Hüster R, Thauer RK (1987) Biosynthesis of coenzyme F430 in methanogenic bacteria. Identification of 15,17$^3$-seco-F430-17$^3$-acid as an intermediate. Eur J Biochem 170:459–467

Phillips CM, Schreiter ER, Guo Y, Wang SC, Zamble DB, Drennan CL (2008) Structural basis of the metal specificity for nickel regulatory protein NikR. Biochemistry 47:1938–1946

Phillips CM, Schreiter ER, Stultz CM, Drennan CL (2010) Structural basis of low-affinity nickel binding to the nickel-responsive transcription factor NikR from *Escherichia coli*. Biochemistry 49:7830–7838

Pierik AJ, Roseboom W, Happe RP, Bagley KA, Albracht SPJ (1999) Carbon monoxide and cyanide as intrinsic ligands to iron in the active site of [NiFe]-hydrogenases -- $NiFe(CN)_2CO$, biology's way to activate $H_2$. J Biol Chem 274:3331–3337

Pinkett HW, Lee AT, Lum P, Locher KP, Rees DC (2007) An inward-facing conformation of a putative metal-chelate-type ABC transporter. Science 315:373–377

Pinske C, Sargent F, Sawers RG (2015) SlyD-dependent nickel delivery limits maturation of [NiFe]-hydrogenases in late-stationary phase *Escherichia coli* cells. Metallomics 7:683–690

Pochapsky TC, Pochapsky SS, Ju T, Mo H, Al-Mjeni F, Maroney MJ (2002) Modeling and experiment yields the structure of acireductone dioxygenase from *Klebsiella pneumoniae*. Nat Struct Biol 9:966–972

Pochapsky SS, Sunshine JC, Pochapsky TC (2008) Completing the circuit: direct-observe $^{13}C$, $^{15}N$ double-quantum spectroscopy permits sequential resonance assignments near a paramagnetic center in acireductone dioxygenase. J Am Chem Soc 130:2156–2157

Pompidor G, Maillard AP, Girard E, Gambarelli S, Kahn R, Covès J (2008) X-ray structure of the metal-sensor CnrX in both the apo- and copper-bound forms. FEBS Lett 582:3954–3958

Quiroz-Valenzuela S, Sukuru SCK, Hausinger RP, Kuhn LA, Heller WT (2008) The structure of urease activation complexes examined by flexibility analysis, mutagenesis, and small-angle X-ray scattering. Arch Biochem Biophys 480:51–57

Ragsdale SW, Raugei S, Ginovska B, Wongnate T (2017) Biochemistry of methyl-coenzyme M reductase. In: Zamble D, Rowinska-Zyrek M, Kozlowski H (eds) The biological chemistry of nickel. Royal Society of Chemistry, Cambridge

Ragusa S, Blanquet S, Meinnel T (1998) Control of peptide deformylase activity by metal cations. J Mol Biol 280:515–523

Rai R, Saraswat VA, Dhiman RK (2015) Gut microbiota: its role in hepatic encephalopathy. J Clin Exp Hepatol 5:S29–S36

Raimunda D, Long JE, Sassetti CM, Argüello JM (2012) Role in metal homeostasis of CtpD, a $Co^{2+}$ transporting $P_{1B4}$-ATPase of *Mycobacterium smegmatis*. Mol Microbiol 84:1139–1149

Rajagopalan PT, Pei D (1998) Oxygen-mediated inactivation of peptide deformylase. J Biol Chem 273:22305–22310

Randhawa VK, Zhou F, Jin X, Nalewajko C, Kushner DJ (2001) Role of oxidative stress and thiol antioxidant enzymes in nickel toxicity and resistance in strains of the green alga *Scenedesmus acutus* f. alternans. Can J Microbiol 47:987–993

Rankin JA, Mauban RC, Fellner M, Desguin B, McCracken J, Hu J, Varganov SA, Hausinger RP (2018) Lactate racemase nickel-pincer cofactor operates by a proton-coupled hydride transfer mechanism. Biochemistry 57:3244–3251

Rankin JA, Chatterjee S, Tariq Z, Lagishetty S, Desguin B, Hu J, Hausinger RP (2021) The LarB carboxylase/hydrolase forms a transient cysteinyl-pyridine intermediate during nickel-pincer nucleotide cofactor biosynthesis. Proc Natl Acad Sci 118(39):e2106202118. https://doi.org/10.1073/pnas.2106202118

Ravichandran R, Hemaasri S, Cameotra SS, Jayaprakash NS (2015) Purification and characterization of an extracellular uricase from a new isolate of *Sphingobacterium thalpophilum* ($VITPCB_5$). Protein Expr Purif 114:136–142

Reissmann S, Hochleitner E, Wang H, Paschos A, Lottspeich F, Glass RS, Böck A (2003) Taming of a poison: biosynthesis of the NiFe-hydrogenase cyanide ligands. Science 299:1067–1070

Remaut H, Safarof N, Ciurli S, Van Beeumen J (2001) Structural basis for $Ni^{2+}$ transport and assembly of the urease active site by the metallo-chaperone UreE from *Bacillus pasteurii*. J Biol Chem 276:49365–49370

Remy L, Carriére M, Derré-Bobillot A, Martini C, Sanguinetti M, Borezée-Durant E (2013) The *Staphylococcus aureus* Opp1 ABC transporter imports nickel and cobalt in zinc-depleted conditions and contributes to virulence. Mol Microbiol 87:730–743

Reyes-Caballero H, Lee CW, Giedroc DP (2011) *Mycobacterium tuberculosis* NmtR harbors a nickel sensing site with parallels to *Escherichia coli* RcnR. Biochemistry 50:7941–7952

Righetto RD, Anton L, Adaixo R, Jakob RP, Zivanov J, Mahi M-A, Ringler P, Schwede T, Maier T, Stahlberg H (2020) High-resolution cryo-EM structure of urease from the pathogen *Yersinia enterocolitica*. Nat Commun 11:5101

Rodionov DA, Hebbeln P, Gelfand MS, Eitinger T (2006) Comparative and functional genomic analysis of prokaryotic nickel and cobalt uptake transporters: evidence for a novel group of ATP-binding cassette transporters. J Bacteriol 188:317–327

Rodionova IA, Scott DA, Grishin NV, Osterman AL, Rodionov DA (2012) Tagaturonate-fructuronate epimerase UxaE, a novel enzyme in the hexuronate catabolic network in *Thermotoga maritima*. Environ Microbiol 14:2920–2934

Rodrigue A, Effantin G, Mandrand-Bethelot M-A (2005) Identification of *rcnA* (*yohM*), a nickel and cobalt resistance gene in *Escherichia coli*. J Bacteriol 187:2912–2916

Rodrigue A, Albareda M, Mandrand-Berthelot M-A, Palacios J (2017) Nickel in microbial physiology--from single proteins to complex trafficking systems: nickel import/export. In: Zamble DB, Rowinska-Zyrek M, Kozlowski H (eds) The biological chemistry of nickel. Royal Society of Chemistry, Cambridge

Rospert S, Linder D, Ellermann J, Thauer RK (1990) Two genetically distinct methyl-coenzyme M reductases in *Methanobacterium thermoautotrophicum* strain Marburg and DH. Eur J Biochem 194:871–877

Rubio-Sanz L, Prieto RI, Imperial J, Palacios JM, Brito B (2013) Functional and expression analysis of the metal inducible *dmeRF* system from *Rhizobium leguminosarum* bv. *viciae*. Appl Environ Microbiol 79:6414–6422

Ryan KC, Johnson OE, Cabelli DE, Brunold TC, Maroney MJ (2010) Nickel superoxide dismutase: structural and functional roles of Cys2 and Cys6. J Biol Inorg Chem 15:795–807

Sachs G, Scott D, Weeks D, Melchers K (2002) The compartment buffered by the urease of *Helicobacter pylori*: cytoplasm or periplasm? Trends Microbiol 10:217–219

Saier MH Jr, Beatty JT, Goffeau A, Harley KT, Heijne WH, Huang SC, Jack DL, Jahn PS, Lew K, Liu J, Pao SS, Paulsen IT, Tseng TT, Virk PS (1999) The major facilitator superfamily. J Mol Microbiol Biotechnol 1:257–279

San Martin-Uriz P, Mirete S, Alcolea PJ, Gomez MJ, Amils R, Gonzalez-Pastor JE (2014) Nickel-resistance determinants in *Acidiphilum* sp. PM identified by genome-wide functional screening. PLoS One 9:e95041

Sar P, Kazy SK, Singh SP (2001) Intracellular nickel accumulation by *Pseudomonas aeruginosa* and its chemical nature. Lett Appl Microbiol 32:257–261

Sargent F (2016) The model [NiFe]-hydrogenases of *Escherichia coli*. Adv Microb Physiol 68: 433–507

Sasaki D, Watanabe B, Matsumi R, Shoji T, Yasukochi A, Tagashira K, Fukuda W, Kanai T, Atomi H, Imanaka T, Miki K (2013) Identification and structure of a novel archaeal HypB for [NiFe] hydrogenase maturation. J Mol Biol 425:1627–1640

Sato K, Okuba A, Yamazaki S (1998) Characterization of a multi-copper enzyme, nitrous oxide reductase, from *Rhodobacter sphaeroides* f. sp. *denitrificans*. J Biochem 124:51–54

Sawers RG, Pinske C (2017) NiFe-hydrogenase assembly. In: Johnson MK, Scott RA (eds) Encyclopedia of inorganic and bioinorganic chemistry. Wiley

Saylor Z, Maier R (2018) *Helicobacter pylori* nickel storage proteins: recognition and modulation of diverse metabolic targets. Microbiology 164:1059–1068

Schaab MR, Barney BM, Francisco WA (2006) Kinetic and spectroscopic studies on the quercetin 2,3-dioxygenase from *Bacillus subtilis*. Biochemistry 45:1009–1016

Schäfer C, Bommer M, Hennig SE, Jeoung J-H, Dobbek H, Lenz O (2016) Structure of an actinobacterial-type [NiFe]-hydrogenase reveals insight into $O_2$-tolerant $H_2$ oxidation. Structure 24:285–292

Schauer K, Gouget B, Carrière M, Labigne A, de Reuse H (2007) Novel nickel transport mechanism across the bacterial outer membrane energized by the TonB/ExbB/ExbD machinery. Mol Microbiol 63:1054–1068

Scheller S, Goenrich M, Boecher R, Thauer RK, Jaun B (2010) The key nickel enzyme of methanogenesis catalyzes the anaerobic oxidation of methane. Nature 465:606–608

Schneider J, Kaltwasser H (1984) Urease from *Arthrobacter oxydans*, a nickel-containing enzyme. Arch Microbiol 139:355–360

Schreiter ER, Sintchak MD, Guo Y, Chivers PT, Sauer RT, Drennan CL (2003) Crystal structure of the nickel-responsive transcriptional factor NikR. Nat Struct Biol 10:794–799

Schreiter ER, Wang SC, Zamble DB, Drennan CL (2006) NikR-operator complex structure and the mechanism of repressor activation by metal ions. Proc Natl Acad Sci U S A 103:13676–13681

Schulz A-C, Frielingsdorf S, Pommerening P, Lauterbach L, Bistoni G, Neese F, Oestreich M, Lenz O (2020) Formyltetrahydrofolate decarbonylase synthesizes the active site CO ligand of $O_2$-tolerant [NiFe] hydrogenase. J Am Chem Soc 142:1457–1464

Sebbane F, Mandrand-Bethelot M-A, Simonet M (2002) Genes encoding specific nickel transport systems flank the chromosomal urease locus of pathogenic Yersiniae. J Bacteriol 184: 5706–5713

Seffernick JL, McTavish H, Osbourne JP, de Souza ML, Sadowsky MJ, Wackett LP (2002) Atrazine chlorohydrolase from *pseudomonas* sp. strain ADP is a metalloenzyme. Biochemistry 41:14430–14437

Selmer T, Kahn J, Goubeaud M, Shima S, Grabarse W, Ermler U, Thauer RK (2000) The biosynthesis of methylated amino acids in the active site region of methyl-coenzyme M reductase. J Biol Chem 275:3755–3760

Senger M, Stripp ST, Soboh B (2017) Proteolytic cleavage orchestrates cofactor insertion and protein assembly in [NiFe]-hydrogenase biosynthesis. J Biol Chem 292:11670–11681

Seravalli J, Ragsdale SW (2000) Channeling of carbon monoxide during anaerobic carbon dioxide fixation. Biochemistry 39:1274–1277

Seshadri S, Benoit SL, Maier RJ (2007) Roles of His-rich Hpn and Hpn-like proteins in *Helicobacter pylori* nickel physiology. J Bacteriol 189:4120–4126

Shafaat HS, Rüdiger O, Ogata H, Lubitz W (2013) [NiFe] hydrogenases: a common active site for hydrogen metabolism under diverse conditions. Biochim Biophys Acta 1827:986–1002

Shaik MM, Cendron L, Salamina M, Ruzzene M, Zanotti G (2014) *Helicobacter pylori* periplasmic receptor CeuE (HP1561) modulates its nickel affinity via organic metallophores. Mol Microbiol 91:724–735

Sheng Y, Abreu IA, Cabelli DE, Maroney MJ, Miller A-F, Teixeira M, Valentine JS (2014) Superoxide dismutases and superoxide reductases. Chem Rev 114:3854–3918

Shi R, Munger C, Asinas A, Benoit SL, Miller E, Matte A, Maier RJ, Cygler M (2010) Crystal structures of apo and metal-bound forms of the UreE protein from *Helicobacter pylori*: role of multiple metal binding sites. Biochemistry 49:7080–7088

Shima S, Thauer RK (2005) Methyl-coenzyme M reductase and anaerobic oxidation of methane in methanotrophic archaea. Curr Opin Microbiol 8:643–648

Shima S, Krueger M, Weingert T, Demmer U, Kahnt J, Thauer RK, Ermler U (2012) Structure of a methyl-coenzyme M reductase from Black Sea mats that oxidize methane anaerobically. Nature 481:98–101

Shomura Y, Higuchi Y (2012) Structural basis for the reaction mechanism of S-carbamoylation of HypE by HypF in the maturation of [NiFe]-hydrogenases. J Biol Chem 287:28409–28419

Shomura Y, Yoon K-S, Nishihara H, Higuchi Y (2011) Structural basis for a [4Fe-3S] cluster in the oxygen-tolerant membrane-bound [NiFe]-hydrogenase. Nature 479:253–256

Shomura Y, Taketa M, Nakashima H, Tai H, Nakagawa H, Ikeda H, Ishii M, Igarashi Y, Nishihara H, Yoon K-S, Ogo S, Hirota S, Higuchi Y (2017) Structural basis of the redox switches in the $NAD^+$-reducing soluble [NiFe]-hydrogenase. Science 357:928–932

Siddiqui RA, Schlegel HG (1987) Plasmid pMOL28-mediated inducible nickel resistance in *Alcaligenes eutrophus* strain CH34. FEMS Microbiol Lett 43:9–13

Simitsopoulou M, Vafopoulou A, Choli-Papadopoulou T, Alichanidis E (1997) Purification and partial characterization of a tripeptidase from *Pediococcus pentosaceus* K9.2. Appl Environ Microbiol 63:4872–4876

Slotboom DJ (2014) Structural and mechanistic insights into prokaryotic energy-coupling factor transporters. Nat Rev Microbiol 12:79–87

Smith DH (1967) R factors mediate resistance to mercury, nickel and cobalt. Science 156:1114–1116

Snavely MD, Gravina SA, Cheung TT, Miller CG, Maguire ME (1991) Magnesium transport in *Salmonella typhimurium*. Regulation of *mgtA* and *mgtB* expression. J Biol Chem 266:824–829

Snow ET, Xu LS, Kinney PL (1993) Effects of nickel ions on polymerase activity and fidelity during DNA replication in vitro. Chem Biol Interact 88:155–173

Song HK, Mulrooney SB, Huber R, Hausinger RP (2001) Crystal structure of *Klebsiella aerogenes* UreE, a nickel-binding metallochaperone for urease activation. J Biol Chem 276:49359–49364

Song L, Zhang Y, Chen W, Gu T, Zhang S-Y, Ji Q (2018) Mechanistic insights into staphylopine-mediated metal acquisition. Proc Natl Acad Sci U S A 115:3942–3947

Soriano A, Hausinger RP (1999) GTP-dependent activation of urease apoprotein in complex with the UreD, UreF, and UreG accessory proteins. Proc Natl Acad Sci U S A 96:11140–11144

Soriano A, Colpas GJ, Hausinger RP (2000) UreE stimulation of GTP-dependent urease activation in the UreD-UreF-UreG-urease apoprotein complex. Biochemistry 39:12435–12440

Stähler FN, Odenbreit S, Haas R, Wilrich J, Van Vliet AH, Kusters JG, Kist M, Bereswill S (2006) The novel *Helicobacter pylori* CznABC metal efflux pump is required for cadmium, zinc, and nickel resistance, urease modulation, and gastric colonization. Infect Immun 74:3845–3852

Stoof J, Kuipers EJ, Klaver G, van Vliet AH (2010a) An ABC transporter and a TonB ortholog contribute to *Helicobacter mustelae* nickel and cobalt acquisition. Infect Immun 78:4261–4267

Stoof J, Kuipers EJ, van Vliet AHM (2010b) Characterization of NikR-responsive promoters of urease and metal transport genes of *Helicobacter mustelae*. Biometals 23:145–159

Su C-C, Long F, Zimmermann MT, Rajashankar KR, Jernigan RL, Yu EW (2011) Crystal structure of the CusBA heavy-metal efflux complex of *Escherichia coli*. Nature 470:558–562

Sukdeo N, Clugston SL, Daub E, Honek JF (2004) Distinct classes of glyoxylase I: metal specificity of the *Yersinia pestis*, *Pseudomonas aeruginosa* and *Neisseria meningitidis* enzymes. Biochem J 384:111–117

Sumner JB (1926) The isolation and crystallization of the enzyme urease. J Biol Chem 69:435–441

Suttisansanee U, Honek JF (2019) Preliminary characterization of a $Ni^{2+}$-activated and mycothiol-dependent glyoxalase I enzyme from *Streptomyces coelicolor*. Inorganics 7:99

Suttisansanee U, Lau K, Lagishetty S, Rao KN, Swaminathan S, Sauder JM, Burley SK, Honek JF (2011) Structural variation in bacterial glyoxylase I enzymes. Investigation of the metalloenzyme glyoxalase I from *Clostridium acetobutylicum*. J Biol Chem 286:38367–38374

Svetlitchnyi V, Dobbek H, Meyer-Klaucke W, Meins T, Thiele B, Römer P, Huber R, Meyer O (2004) A functional Ni-Ni-[4Fe-4S] cluster in the monomeric acetyl-CoA synthase from *Carboxydothermus hydrogenoformans*. Proc Natl Acad Sci U S A 101:446–451

Symmonds MF, Marshall RL, Bavro VN (2015) Architecture and roles of periplasmic adaptor proteins in tripartite efflux assemblies. Front Microbiol 6:513

Takeuchi T (1909) On the occurrence of urease in higher plants. J Coll Agric Imp Univ Tokyo i:1

Tamagnini P, Leitao E, Oliveira P, Ferreira D, Pinto F, Harris DJ, Heidorn T, Lindblad P (2007) Cyanobacterial hydrogenases: diversity, regulation and applications. FEMS Microbiol Rev 31: 692–720

Tatum EL, Peterson WH, Fred EB (1936) CCLXVI. Enzymic racemization of optically active lactic acid. Biochem J 30:1892–1897

Taylor CD, Wolfe RS (1974) Structure and methylation of coenzyme M ($HSCH_2CH_2SO_3$). J Biol Chem 249:4879–4885

Techtmann SM, Lebedinsky AV, Colman AS, Sokolova TG, Woyke T, Goodwin L, Robb FT (2012) Evidence for horizontal gene transfer of anaeobic carbon monoxide dehydrogenases. Front Microbiol 3:132

Terlesky KC, Nelson MJ, Ferry JG (1986) Isolation of an enzyme complex with carbon monoxide dehydrogenase activity containing corrinoid and nickel from acetate-grown *Methanosarcina thermophila*. J Bacteriol 168:1053–1058

Thauer RK (1998) Biochemistry of methanogenesis: a tribute to Marjory Stephenson. Microbiology 144:2377–2406

Thauer RK (2019) Methyl (alkyl)-coenzyme M reductases: nickel F-430-containing enzymes involved in anaerobic methane formation and in anaerobic oxidation of methane or of short chain alkanes. Biochemistry 58:5198–5220

Thauer RK, Bonacker LG (1994) Biosynthesis of coenzyme F430, a nickel porphinoid involved in methanogenesis. Ciba Found Symp 180:210–227

Thauer RK, Kaster A-K, Goenrich M, Schick M, Hiromoto T, Shima S (2010) Hydrogenases from methanogenic archaea, nickel, a novel cofactor, and $H_2$ storage. Annu Rev Biochem 79: 507–536

Tian J, Wu N, Li J, Liu Y, Guo J, Yao B, Fan Y (2007) Nickel-resistant determinant from *Leptospirillum ferriphilum*. Appl Environ Microbiol 73:2364–2368

Tibazarwa C, Wuertz S, Mergeay M, Wyns L, van der Lelie D (2000) Regulation of the *cnr* cobalt and nickel resistance determinant of *Ralstonia eutropha* (*Alcaligenes eutrophus*) CH34. J Bacteriol 182:1399–1409

Timm J, Brochier-Armanet C, Perard J, Zambelli B, Ollganier-de-Choudens S, Ciurli S, Cavazza C (2017) The CO dehydrogenase accessory protein CooT is a novel nickel-binding protein. Metallomics 9:575–583

Tominaga T, Watanabe S, Matsumi R, Atomi H, Imanaka T, Miki K (2012) Structure of the [NiFe]-hydrogenase maturation protein HypF from *Thermococcus kodakarensis*. Acta Crystallogr F68: 1153–1157

Tominaga T, Watanabe S, Matsumi R, Atomi H, Imanaka T, Miki K (2013) Crystal structures of the carbamoylated and cyanated forms of HypE for [NiFe] hydrogenase maturation. Proc Natl Acad Sci U S A 110:20485–20490

Trepreau J, de Rosny E, Duboc C, Sarret G, Petit-Hartlein I, Maillard AP, Imberty A, Proux O, Covès J (2011a) Spectroscopic characterization of the metal-binding sites in the periplasmic metal-sensor domain of CnrX from *Cupriavidus metallidurans* CH34. Biochemistry 50:9036–9045

Trepreau J, Girard E, Maillard AP, de Rosny E, Petit-Hartlein I, Kahn R, Covès J (2011b) Structural basis for metal sensing by CnrX. J Mol Biol 408:766–779

Tripathi VN, Srivastava S (2006) Extracytoplasmid storage as the nickel resistance mechanism in a natural isolate of *Pseudomonas putida* S4. Can J Microbiol 52:287–292

Tsang KL, Wong KB (2022) Moving nickel along the hydrogenase-urease maturation pathway. Metallomics. https://doi.org/10.1093/mtomcs/mfac003

Turmo A, Hu J, Hausinger RP (2022) Characterization of the nickel-inserting cyclometallase LarC from *Moorella thermoacetica* and identification of a CMPylated reaction intermediate. Metallomics. https://doi.org/10.1093/mtomcs/mfac014

Valko M, Morris H, Cronin MT (2005) Metals, toxicity and oxidative stress. Curr Med Chem 12: 1161–1208

Van der Linden P, Burgdorf T, Bernhard M, Belijlevens B, Friedrich B, Albracht SPJ (2004) The soluble [NiFe]-hydrogenase from *Ralstonia eutropha* contains four cyanides in its active site, one of which is responsible for the insensitivity towards oxygen. J Biol Inorg Chem 9:616–626

Van Nostrand JD, Arthur JM, Kilpatrick LE, Neely BA, Bertsch PM, Morris PJ (2008) Changes in protein expression in *Burkholderia vietnamiensis* PR1 301 at pH 5 and 7 with and without nickel. Microbiology 154:3813–3824

van Tieghem PEL (1984) Recherches sur la fermentation de l'urée. C R Acad Sci 58:40

van Vliet AHM, Poppelaars SW, Davies BJ, Stoof J, Bereswill S, Kist M, Penn CW, Kuipers EJ, Kusters JG (2002) NikR mediates nickel-responsive transcriptional induction of urease expression in *Helicobacter pylori*. Infect Immun 70:2846–2852

van Vliet AHM, Ernst FD, Kusters JG (2004) NikR-mediated regulation of *Helicobacter pylori* acid adaptation. Trends Microbiol 12:489–494

Vannini A, Pinatel E, Constantini PE, Roncarati D, Puccio S, De Bellis G, Peano C, Danielli A (2017) Comprehensive mapping of the *Helicobacter pylori* NikR regulon provides new insights in bacterial responses. Sci Rep 7:45458

Vickers TJ, Greig N, Fairlamb AH (2004) A trypanothione-dependent glyoxalase I with a prokaryotic ancestry in *Leishmania major*. Proc Natl Acad Sci U S A 101:13186–13191

Vignais PM, Billoud B (2007) Occurrence, classification, and biological function of hydrogenases: an overview. Chem Rev 107:4206–4272

Vignais PM, Billoud B, Meyer J (2001) Classification and phylogeny of hydrogenases. FEMS Microbiol Rev 25:455–501

Vinella D, Fischer F, Vorontsov E, Gallaud J, Malosse C, Michel V, Cavazza C, Robbe-Saule M, Richaud P, Chamot-Rooke J, Brochier-Armanet C, De Reuse H (2015) Evolution of *Helicobacter*: acquisition by gastric species of two histidine-rich proteins essential for colonization. PLoS Pathog 11:e1005312

Vitt S, Ma K, Warkentin E, Moll J, Pierik AJ, Shima S, Ermler U (2014) The $F_{420}$-reducing [NiFe]-hydrogenase complex from *Methanothermobacter marburgensis*, the first X-ray structure of a group 3 family member. J Mol Biol 426:2813–2826

Volbeda A, Fontecilla-Camps JC (2017) Crystallographic analyses of the active site chemistry and oxygen sensitivity of [NiFe(Se)]-hydrogenases. In: Zamble D, Rowinska-Zyrek M, Kozlowski H (eds) The biological chemistry of nickel. Royal Society of Chemistry, London

Volbeda A, Charon M-H, Piras C, Hatchikian EC, Frey M, Fontecilla-Camps JC (1995) Crystal structure of the nickel-iron hydrogenase from *Desulfovibrio gigas*. Nature 373:580–587

Volbeda A, Garcin E, Piras C, de Lacey AL, Fernandez VM, Hatchikian EC, Frey M, Fontecilla-Camps JC (1996) Structure of the [NiFe] hydrogenase active site: evidence for biologically uncommon Fe ligands. J Am Chem Soc 118:12989–12996

Volbeda A, Martin L, Cavazza C, Matho M, Faber BW, Rosebloom W, Albracht SPJ, Garcia E, Rousset M, Fontecilla-Camps JC (2005) Structural differences between the ready and unready oxidized states of [NiFe] hydrogenases. J Biol Inorg Chem 10:239–249

Volbeda A, Amara P, Darnault C, Mouesca J-M, Parkin A, Roessler MM, Armstrong FA, Fontecilla-Camps JC (2012) X-ray crystallographic and computational studies of the $O_2$-tolerant [NiFe]-hydrogenase 1 from *Escherichia coli*. Proc Natl Acad Sci U S A 109: 5305–5310

Volbeda A, Darnault C, Parkin A, Sargent F, Armstrong FA, Fontecilla-Camps JC (2013) Crystal structure of the $O_2$-tolerant membrane-bound hydrogenase 1 from *Escherichia coli* in complex with its cognate cytochrome *b*. Structure 21:184–190

Voordouw G (2002) Carbon monoxide cycling by *Desulfovibrio vulgaris* Hildenborough. J Bacteriol 184:5903–5911

Wang WC, Hsu WH, Chien FT, Chen CY (2001) Crystal structure and site-directed mutagenesis studies of N-carbamoyl-D-amino-acid amidohydrolase from *Agrobacterium radiobacter* reveals a homotetramer and insight into a catalytic cleft. J Mol Biol 306:251–261

Wang SC, Dias AV, Bloom SL, Zamble DB (2004) The selectivity of metal binding and the metal-induced stability of *Escherichia coli* NikR. Biochemistry 43:10018–10028

Wang SC, Li Y, Ho MY, Bernal M-E, Sydor AM, Kagzi WR, Zamble DB (2010a) The response of *Escherichia coli* NikR to nickel: a second nickel-binding site. Biochemistry 49:6635–6645

Wang SC, Li Y, Robinson CV, Zamble DB (2010b) Potassium is critical for the Ni(II)-responsive DNA-binding activity of *Escherichia coli* NikR. J Am Chem Soc 132:1506–1507

Wang S, Wu Y, Outten FW (2011) Fur and the novel regulator YqjI control transcription of the ferric reductase gene *yqjH* in *Escherichia coli*. J Bacteriol 193:563–574

Wang S, Blahut M, Wu Y, Philipkosky KE, Outten FW (2014) Communication between binding sites is required for YqjI regulation of target promoters within the *yqjH-yqjI* intergenic region. J Bacteriol 196:3199–3207

Wang Y, Branicky R, Noë A, Hekimi S (2018) Superoxide dismutases: dual roles in controlling ROS damage and regulating ROS signaling. J Cell Biol 217:1915–1928

Wang Y, Wegener G, Hou J, Wang J, Xiao X (2019) Expanding anaerobic alkane metabolism in the domain of archaea. Nat Microbiol 4:595–602

Wang Y, Wegener G, Ruff SE, Wang F (2020) Methyl/alkyl-coenzyme M reductase-based anaerobic alkane oxidation in archae. Environ Microbiol 23:530–541

Watanabe S, Matsumi R, Arai T, Atomi H, Imanaka T, Miki K (2007) Crystal structures of [NiFe] hydrogenase maturation proteins HypC, HypD, and HypE: insights into cyanation reaction by thiol redox signaling. Mol Cell 27:29–40

Watanabe S, Arai T, Matsumi R, Atomi H, Imanaka T, Miki K (2009) Crystal structure of HypA, a nickel-binding metallochaperone for [NiFe] hydrogenase maturation. J Mol Biol 394:448–459

Watanabe S, Matsumi R, Atomi H, Imanaka T, Miki K (2012) Crystal structures of the HypCD complex and the HypCDE ternary complex: transient intermediate complexes during [NiFe] hydrogenase maturation. Structure 20:2124–2137

Watanabe S, Kawashima T, Nishitani Y, Kanai T, Wada T, Inaba K, Atomi H, Imanaka T, Miki K (2015) Structural basis of a Ni acquisition cycle for [NiFe] hydrogenase by Ni-metallochaperone HypA and its enhancer. Proc Natl Acad Sci U S A 112:7701–7706

Watt RK, Ludden PW (1998) The identification, purification, and characterization of CooJ. A nickel-binding protein that is co-regulated with the Ni-containing CO dehydrogenase from *Rhodospirillum rubrum*. J Biol Chem 273:10019–10025

Weeks DL, Eskandar S, Scott DR, Sachs G (2000) A $H^+$-gated urea channel: the link between *Helicobacter pylori* urease and gastric colonization. Science 287:482–485

Weimer PJ, Moen GN (2013) Quantitative analysis of growth and volatile fatty acid production by the anaerobic ruminal bacterium *Megasphaera elsdenii* T81. Appl Microbiol Biotechnol 97: 4075–4081

West AL, St John F, Lopes PEM, MacKerell AD Jr, Pozharski E, Michel SLJ (2010) Holo-Ni(II) *Hp*NikR is an asymmetric tetramer containing two different nickel-binding sites. J Am Chem Soc 132:14447–14456

Willecke K, Gries E-M, Oehr P (1973) Coupled transport of citrate and magnesium in *Bacillus subtilis*. J Bacteriol 218:807–814

Wittenborn EC, Merrouch M, Ueda C, Fradale L, Léger C, Fourmond V, Pandelia M-E, Dementin S, Drennan CL (2018) Redoxdependent rearrangements of the NiFeS cluster of carbon monoxide dehydrogenase elife 7:e39451

Wittenborn EC, Cohen SE, Merrouch M, Léger C, Fourmond V, Dementin S, Drennan CL (2019) Structural insight into the metallocofactor maturation in carbon monoxide dehydrogenase. J Biol Chem 294:13017–13026

Wittenborn EC, Guendon C, Merrouch M, Benvenuti M, Fourmond V, Léger C, Drennan CL, Dementin S (2020) The solvent-exposed Fe-S D-cluster contributes to oxygen-resistance in *Desulfovibrio vulgaris* Ni-Fe carbon monoxide dehydrogenase. ACS Catal 10:7328–7335

Wöhler F (1828) Ueber künstliche bildung des harnstoffs (On the artificial formation of urea). Annalen der Physik (Berlin) 12:253–256

Wolfram L, Bauerfeind P (2002) Conserved low-affinity nickel-binding amino acids are essential for the function of the nickel permease NixA of *Helicobacter pylori*. J Bacteriol 184:1438–1443

Wolfram L, Haas E, Bauerfeind P (2006) Nickel represses the synthesis of the nickel permease NixA of *Helicobacter pylori*. J Bacteriol 188:1245–1250

Wray JW, Abeles RH (1993) A bacterial enzyme that catalyzes formation of carbon monoxide. J Biol Chem 268:21466–21469

Wroblewski LE, Peek RM Jr, Wilson KT (2010) *Helicobacter pylori* and gastric cancer: factors that modulate disease risk. Clin Microbiol Rev 23:713–739

Wu M, Ren Q, Durkin AS, Daugherty SC, Brinkac LM, Dodson RJ, Madupu R, Sullivan SA, Kolonay JF, Haft DH, Nelson WC, Tallon LJ, Jones KM, Ulrich LE, Gonzalez JM, Zhulin IB, Robb FT, Eisen JA (2005) Life in hot carbon monoxide: the complete genome sequence of *Carboxydothermus hydrogenoformans* Z-2901. PLoS Genet 1:e65

Wuerges J, Lee J-W, Yim Y-I, Kang SO, Carugo KD (2004) Crystal structure of nickel-containing superoxide dismutase reveals another type of active site. Proc Natl Acad Sci U S A 101:8569–8574

Wülfing C, Lombardero J, Plückthun A (1994) An *Escherichia coli* protein consisting of a domain homologous to FK506-binding proteins (FKBP) and a new metal binding motif. J Biol Chem 269:2895–2901

Xu J, Cotruvo JA Jr (2020) The *czcD* (NiCo) riboswitch responds to iron(II). Biochemistry 59: 1508–1516

Yang F, Hu W, Xu H, Li C, Xia B, Jin C (2006) Structure and backbone dynamics of an endopeptidase HycI from *Escherichia coli*: implications for mechanism of the [NiFe] hydrogenase maturation. J Biol Chem 282:3856–3863

Yang X, Li H, Cheng T, Xia W, Lai Y-T, Sun H (2014) Nickel translocation between metallochaperones HypA and UreE in *Helicobacter pylori*. Metallomics 6:1731–1736

Yang X, Li H, Lai T-P, Sun H (2015) UreE-UreG complex facilitates nickel transfer and preactivates GTPase of UreG in *Helicobacter pylori*. J Biol Chem 290:12474–12485

Youn H-D, Kim E-J, Roe J-H, Hah YC, Kang S-O (1996a) A novel nickel-containing superoxide dismutase from *Streptomyces* spp. Biochem J 318:889–896

Youn H-D, Youn H, Lee J-W, Yim Y-I, Lee JK, Hah YC, Kang S-O (1996b) Unique isoenzymes of superoxide dismutase in *Streptomyces griseus*. Arch Biochem Biophys 334:341–348

Yu Y, Zhou M, Kirsch F, Xu C, Zhang L, Wang Y, Jiang Z, Wang N, Li J, Eitinger T, Yang M (2014) Planar substrate-binding site dictates the specificity of ECF-type nickel/cobalt transporters. Cell Res 24:267–277

Yuen MH, Fong YH, Nim YS, Lau PH, Wong K-B (2017) Structural insights into how GTP-dependent conformational changes in a metallochaperone UreG facilitate urease maturation. Proc Natl Acad Sci U S A 114:E10890–E10898

Zadvornyy OA, Allen M, Brumfield SK, Varpness Z, Boyd ES, Zorin NA, Serebriakova L, Douglas T, Peters JW (2010) Hydrogen enhances nickel tolerance in the purple sulfur bacterium *Thiocapsa roseopersicina*. Environ Sci Technol 44:834–840

Zambelli B, Stola M, Musiani F, De Vriendt K, Samyn B, Devreese B, Van Beeumen J, Dikiy A, Bryant DA, Ciurli S (2005) UreG, a chaperone in the urease assembly process, is an intrinsically unstructured GTPase that specifically binds $Zn^{2+}$. J Biol Chem 280:4684–4695

Zambelli B, Bellucci M, Danielli A, Scarlato V, Ciurli S (2007a) The $Ni^{2+}$ binding properties of *Helicobacter pylori* NikR. Chem Commun 3649–3651

Zambelli B, Musiani F, Savini M, Tucker P, Ciurli S (2007b) Biochemical studies on *Mycobacterium tuberculosis* UreG and comparative modeling reveal structural and functional conservation among the bacterial UreG family. Biochemistry 46:3171–3182

Zambelli B, Turano P, Musiani F, Neyroz P, Ciurli S (2009) $Zn^{2+}$-linked dimerization of UreG from *Helicobacter pylori*, a chaperone involved in nickel trafficking and urease activation. Proteins 74:222–239

Zambelli B, Cremades N, Neyroz P, Turano P, Uversky VN, Ciurli S (2012) Insights in the (un)structural organization of *Bacillus pasteurii* UreG, an intrinsically disordered GTPase enzyme. Mol BioSyst 8:220–228

Zambelli B, Banaszak K, Merloni A, Kiliszek A, Rypniewski W, Ciurli S (2013) Selectivity of Ni (II) and Zn(II) binding to *Sporosarcina pasteurii* UreE, a metallochaperone in the urease assembly: a calorimetric and crystallographic study. J Biol Inorg Chem 18:1005–1017

Zamble D, Rowinska-Zyrek M, Kozlowski H (2017) The biological chemistry of nickel. Royal Society of Chemistry, Cambridge

Zeer-Wanklyn CJ, Zamble DB (2017) Microbial nickel: cellular uptake and delivery to enzyme centers. Curr Opin Chem Biol 37:80–88

Zeng Y-B, Zhang D-M, Li H, Sun H (2008) Binding of $Ni^{2+}$ to a histidine- and glutamine-rich protein, Hpn-like. J Biol Inorg Chem 13:1121–1131

Zeng Y-B, Yang N, Sun H (2011) Metal-binding properties of an Hpn-like histidine-rich protein. Chem Eur J 17:5852–5860

Zhan G, Li D, Zhang L (2012) Aerobic bioreduction of nickel(II) to elemental nickel with concomitant biomineralization. Appl Microbiol Biotechnol 96:273–281

Zhang JW, Butland G, Greenblatt JF, Emili A, Zamble DB (2005) A role for SlyD in the *Escherichia coli* hydrogenase biosynthetic pathway. J Biol Chem 280:4360–4366

Zhu T, Tian J, Zhang S, Wu N, Fan Y (2011) Identification of the transcriptional regulator NcrB in the nickel resistance determinant of *Leptospirillum ferriphilum* UBK03. PLoS One 6:e17367

Ziani W, Maillard AP, Petit-Hartlein I, Garnier N, Crouzy S, Girard E, Covès J (2014) The X-ray structure of NccX from *Cupriavidus metallidurans* 31A illustrates potential dangers of detergent solubilization when generating and interpreting crystal structures of membrane proteins. J Biol Chem 289:31160–31172

Zielazinski EL, Gonzalez-Guerrero M, Subramanian P, Stemmler TL, Argüello JM, Rosenzweig AC (2013) *Sinorhizobium meliloti* Nia is a P-ATPase expressed in the nodule during plant symbiosis and is involved in Ni and Fe transport. Metallomics 5:1614–1623